1-2013

Investigation of the Mechanical Behavior of I-Shaped Steel Beams Strengthened By Mechanically-Fastened FRP Laminates

Hothifa Nayef Rojob

جامعة الإمارات العربية المتحدة
United Arab Emirates University

UAEU

Master Program of Civil Engineering
Department of Civil and Environmental Engineering
College of Engineering
United Arab Emirates University

Investigation of the Mechanical Behavior of I-Shaped Steel Beams Strengthened by Mechanically-Fastened FRP Laminates

Author's Name:
Hothifa Nayef Rojob

Principal Supervisor:
Dr. Khaled Mahmoud El-Sawy
Associate Professor of Structural Engineering
Department of Civil and Environmental Engineering
College of Engineering
United Arab Emirates University

Co–Supervisor:
Dr. Amr Mahmoud Sweedan
Associate Professor of Structural Engineering
Department of Civil and Environmental Engineering
College of Engineering
United Arab Emirates University

جامعة الإمارات العربية المتحدة
United Arab Emirates University

UAEU

The MSc thesis by
Hothifa Nayef Rojob

Entitled:

Investigation of the Mechanical Behavior of I-Shaped Steel Beams Strengthened by Mechanically-Fastened FRP Laminates

is approved

Examination Committee

Dr. Michael J. Tait (External Examiner) .....
Associate Professor of Structural Engineering
Department of Civil Engineering
McMaster University
Hamilton, Ontario, Canada

Dr. Samir A. Emam (Internal Examiner) .....
Associate Professor of Mechanical Engineering
Department of Mechanical Engineering
College of Engineering
United Arab Emirates University
Al-Ain, Abu Dhabi, UAE.

Dr. Khaled El-Sawy (Principal Supervisor) .....
Associate Professor of Structural Engineering
Department of Civil & Environmental Engineering
College of Engineering
United Arab Emirates University
Al-Ain, Abu Dhabi, UAE.

Dr. Amr Sweedan (Co-Supervisor) .....

Associate Professor of Structural Engineering
Department of Civil & Environmental Engineering
College of Engineering
United Arab Emirates University
Al-Ain, Abu Dhabi, UAE.

January 2013

application of mechanically fastened FRP (MF-FRP) to RC elements has shown promising results in terms of installation efficiency, level of strengthening achieved, and, more importantly, preventing FRP delamination prior of concrete crushing. As such, a high potential exists for achieving a successful and efficient strengthening scheme when utilizing the MF-FRP laminates to strengthen steel beams. A unique study on the application of MF-FRP to steel beams was conducted by Alhadid (2011). The study revealed that MF-FRP leads to ductile response of the strengthened system provided that adequate number and strength of anchoring fasteners are used. Insufficient FRP length-to-span ratio or insufficient number of steel fasteners will result in unfavorable brittle mode of failure by shear rupture of the fasteners or tensile rupture in the FRP laminate.

The driving force behind the current research study stems from the need to gain a better understanding of the mechanical behavior of steel beams strengthened with MF-FRP laminates. The research is conducted numerically and analytically. Three-dimensional (3D) finite element (FE) analysis using the general purpose software package ANSYS is conducted in the numerical phase of the study. The 3D FE model developed in this study accounts for the effect of both material and geometrical nonlinearities in addition to the interfacial slip between the FRP laminates and the steel beam. The FE model is validated against the experimental results reported by Alhadid (2011), and excellent agreement is found. The validated FE model is then used to study the behavior of the composite steel-FRP beam parameters including the force distribution in anchoring steel fasteners, the stress distribution and spread of yielding in the steel section and the corresponding stress distribution in the FRP laminates. Furthermore, the FE model is utilized to investigate

ABSTRACT

Retrofitting and strengthening of steel structures have gained significant importance due to the highly increasing number of deteriorated steel structures in many places around the globe. The conventional methods of retrofitting or strengthening of steel structures by replacing steel members or attaching additional external steel plates are usually time-consuming, corrodible, and a cumbersome task. Many of the drawbacks of the conventional retrofitting systems can be overcome through the use of Fiber Reinforced Polymers (FRP) due to their high strength-to-weight ratio. Furthermore, FRP materials are corrosion resistant, which makes them more durable especially when environmental deterioration is a concern. In recent years, the application of FRP in the strengthening of existing structures has increased considerably. A significant amount of research studies has been conducted to explore the effectiveness of implementing externally bonded FRP to strengthen reinforced concrete (RC) structures. Following the successful introduction of FRP in the strengthening of RC beams and columns, researchers started to explore the concept of using the FRP materials in the strengthening of steel elements. Although this idea was initially rejected by many researchers because of the significantly low elastic modulus of the FRP relative to steel, the idea started to float to the surface again when high-modulus FRP were successfully produced. The elastic modulus of such FRP approaches and even, in some cases, exceeds the elastic modulus of steel. Similar to the case of RC, researchers initially focused on the application of externally bonded FRP (EB-FRP) for flexural strengthening of steel beams. The research outcomes revealed that steel beams strengthened with EB-FRP strips exhibit unfavorable brittle failure mechanism due to debonding of the FRP. More recently, research work on the

Increasing the thickness of the FRP laminate significantly improves the load-carrying capacity of composite steel-FRP beams. Provided that a sufficient number of fasteners is provided to avoid shear failure at the interface, increasing the number of steel fasteners, or reducing the pitch distance does not increase the load-carrying capacity significantly. However, it will ensure a ductile failure mode of the composite steel-FRP beams.

The analytical solution used in the current study provides a convenient, but accurate, tool that can be used to calculate the deflection of the composite beam while taking interfacial slip into consideration. The solution can also be used to estimate the load that initiates yielding in the steel component of the composite beam and finding the distribution of the shear forces induced in the steel fasteners.

Keywords: steel beams, strengthening, rehabilitation, fiber reinforced polymer, flexural behavior, numerical analysis, finite element method, analytical solution, composite, partially composite, load-slip

the effect of different parameters on the mechanical behavior of the strengthened beams namely; the steel section height; length, thickness and stiffness of FRP laminates; and distribution and configuration of the steel fasteners. For the analytical analysis, a closed-form analytical model is derived to predict the elastic behavior of the steel-FRP composite beams taking into consideration the slip at the steel-FRP interface. The analytical model is then utilized to evaluate the deflection, the first yielding load of the steel-FRP system and the distribution of shear forces induced in the steel fasteners.

The current study concludes that the contribution of the FRP in reducing mid-span deflection and load-carrying capacity in the elastic stage (i.e., when all materials are still elastic) increases if the elastic modulus of FRP is close to- or higher than that of the steel section. As the length of the FRP increases, the index of elastic composite action increases indicating higher efficiency of the FRP laminate, especially at low fastener stiffness. After yielding in the extreme fibers of the bottom steel flange, the FRP laminate contributes significantly in carrying the mid-span loads because the FRP laminate remains elastic and contributes significantly in carrying the tensile stresses.

The study also shows that the steel beam with deeper cross-section and strengthened with MF-FRP at the bottom flange exhibits higher improvement in its flexural capacity relative to the beam with shallow section with almost the same stiffness. This is because the shear forces carried by the steel fasteners cause a bending moment in the steel beam that is proportional to the section height, and counteracts the bending moment due to the applied mid-span load.

TABLE OF CONTENTS

ACKNOWLEDGEMENTS

Foremost, I would like to express my truly thanks to the almighty God, Allah, for showering us with his countless favors, endless kindness and vast mercy. Without his right and straightforward guidance, this study would never be produced.

I would like also to express my sincere gratitude and gratefulness to my thesis supervisors, Dr. Khaled El-Sawy and Dr. Amr Sweedan, for their endless support throughout my graduate studies and research, and for their patience, motivation, enthusiasm, and immense knowledge.

Particular thanks are due to UAE University community, in large, and the faculty and staff members of the Civil and Environmental Engineering Department, in particular, for their support and encouragement. I would like also to extend my thanks to my colleague graduate students, the international students in particular, for providing support and friendship that I really needed during the course of my study.

I am very much indebted to my family, grandparents, brothers (Yousef, Mohammad, and Mahmoud) and sisters (Sujoud, Sumayya, Saja and beloved Jana) for their continuous encouragement during this study. Special thanks are also due to my uncle Jibril Rajoub for his immeasurable support.

Finally, I take this opportunity to express the profound gratitude from my deep heart to my beloved parents for their love and continuous support. I am truly thankful for their untold blessings which have always been the source of motivation in achieving any success in my life.

LIST OF FIGURES

LIST OF TABLES

EB-FRP	Externally Bonded Fiber Reinforced Polymer
EI_∞	Flexural stiffness of the fully composite section (N.mm^2)
EI_o	Flexural stiffness of the non-composite section (N.mm^2)
E_t	Tangential modulus (N/mm^2)
F	Point load (N)
FE	Finite Element
FEA	Finite Element Analysis
FEM	Finite Element Method
$F_{fastener}$	Shear force carried by the steel fastener (N)
FRP	Fiber Reinforced Polymer
F_{shear}	The maximum shear force that can be carried by one fastener (N)
F_u	Ultimate stress (N/mm^2)
F_y	Yield stress (N/mm^2)
GFRP	Glass Fiber Reinforced Polymers
h	Beam total height (mm)
h_w	Web height (mm)
i	Iteration index
I	Moment of inertia (mm^4)
K	Uniformly distributed slip modulus (N/mm^2)
$K_{fastener}$	Elastic slip modulus of the steel fastener (N/mm)
L	Distance between supports (Beam span) (mm)
L_{comp}	Level of composite action
L_f	Length of FRP laminate (mm)
LM-FRP	Low modulus FRP
LSD	Limit State Design

NOMENCLATURE

$[K]$	Total stiffness matrix of the structure (N/mm)
$[K_E]$	Constant elastic small–strain stiffness matrix (N/mm)
$[K_T]$	Tangent stiffness matrix (N/mm)
$[K_T]_1$	New tangent stiffness matrix of iteration 1 (N/mm)
$[K_T]_I$	Tangent stiffness matrix of iteration i (N/mm)
$[K_T]_o$	Tangent stiffness matrix at the end of the previous load increment (N/mm)
$\{R_1\}$	Residual forces vector of iteration index 1 (N)
$\{u_{n,i}\}$	The total incremental deformation at the end of iteration (i) (mm)
$\{u_n\}$	The total deformation vector at the end of the n^{th} load increment (mm)
$\|\|\{R_i\}\|\|$	Norm of the residual forces (N)
$\|\|\delta\{u_i\}\|\|$	Norm of the iterative deformation (mm)
α	Composite action parameter (mm^{-1})
A	Cross sectional area (mm^2)
ASCE	American Society of Civil Engineers
b_f	Flange width (mm)
b_{frp}	Width of FRP laminate (mm)
CFRP	Carbon Fiber Reinforced Polymers
2D	Two Dimensional
3D	Three Dimensional
dF	Change in nodal forces
du	Change in nodal displacements
E	Elastic Young's modulus (N/mm^2)

V	Shear force acting on the full composite beam segment (N)
V_1	Shear force acting on subcomponent number 1 (N)
V_s	The slip force acting at the steel-FRP interface (N/mm)
v	Poisson's ratio
w	Beam deflection (mm)
WSD	Working Stress Design
Z_{xx}	Plastic section modulus of the steel beam (mm^3)
$\delta\{u_1\}$	First iterative solution for the deformations (mm)
θ	Rotation of the beam.
σ_y	Yield stress of steel (N/mm^2)

LTB	Lateral Torsional Buckling
LVDT	Linear Variable Displacement Transducer
M	Shear force acting on the full composite beam segment (N.mm)
M_1	Moment acting on subcomponent number 1 (N.mm)
MF-FRP	Mechanically Fastened Fiber Reinforced Polymer
n	Increment index or counter
N_1	Normal force acting on subcomponent number 1 (N)
P	Longitudinal distance between fasteners (Pitch size) (mm)
$q(x)$	Distributed transverse load (N/mm)
r	The distance between the centroids of the cross-sections of the top and bottom subcomponents (mm)
RC	Reinforced Concrete
S	First moment of area (mm^3)
s	The relative slip at the steel-FRP interface (mm)
S_{xx}	Elastic section modulus of the steel beam (mm^3)
τ	Longitudinal shear flow between the steel beam and FRP laminate (N/mm)
t_f	Flange thickness (mm)
t_{frp}	Thickness of FRP laminate (mm)
t_s	Stiffener plates thickness (mm)
t_w	Web thickness (mm)
u_{frp}	Deformation in the FRP (mm)
UHM-FRP	Ultra high modulus FRP
U_x	Lateral displacements (mm)
U_y	Vertical displacements (mm)
U_z	Longitudinal displacements (mm)

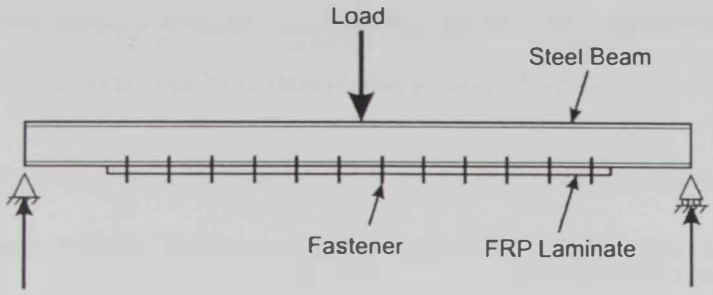

Figure 1.1: Sketch of a Typical Mechanically Fastened Steel-FRP Beam Tested Experimentally by Alhadid (2011)

During the last two decades, many researchers have studied the behavior of steel beams strengthened with FRP strips. However, the research focused on steel beams with externally bonded FRP strips (EB-FRP). The research outcomes revealed that steel beams strengthened with externally bonded FRP strips exhibit unfavorable brittle failure mechanism due to debonding of the FRP strips. Recently, Alhadid (2011) studied experimentally the flexural behavior of steel beams strengthened with mechanically fastened FRP (MF-FRP) laminates (Fig. 1.1). The study revealed that MF-FRP leads to ductile response of the strengthened system provided that adequate number and strength of anchoring fasteners are used. The driving force behind the current research study stems from the need to gain better understanding of the mechanical behavior of steel beams strengthened with MF-FRP laminates. Finite element analysis and closed-form analytical solution are employed in the current investigation.

In this introductory chapter, the problem statement is presented first, followed by the objective of the current study, the scope of the conducted work and the adopted

CHAPTER 1

INTRODUCTION

Retrofitting and strengthening of steel structures have gained significant importance due to the highly increasing number of deteriorated steel structures in many places around the globe. For example, about 143,889 highway bridges have been classified as structural deficient or functionally obsolete within highway bridge network in the USA as of December 2011. This represents about 24% of the total inventory of highway bridges. About 48% of these bridges have steel as the main carrying structural element (FHWA, Bridge Programs, National Bridge Inventory NBI 2012). Therefore, an efficient, practical and cost-effective rehabilitation technique is needed to assist in mitigating such deficiency.

The conventional methods of retrofitting or strengthening existing steel structures by replacing steel members or attaching external steel plates are usually time-consuming. In addition, this method requires lifting heavy steel items that are corrodible and difficult to fix. Many of the drawbacks of the conventional retrofitting systems can be overcome through the use of Fiber Reinforced Polymers (FRP) due to their high strength-to-weight ratio. Furthermore, FRP materials are corrosion resistant, which makes them more durable especially when environmental deterioration is a concern.

behavior of the steel-FRP system was shown provided that adequate anchorage is implemented.

The promising results obtained by Alhadid (2011), suggests more investigation about the efficiency of MF-FRP strengthening technique. As a contribution to fulfill this need, a three-dimensional (3D) nonlinear finite element simulation is employed to gain more in-depth understanding of the behavior of the steel-FRP assembly. An analytical model is also derived to investigate the elastic flexural behavior of steel beams strengthened with MF-FRP laminates.

1.2 Objectives and Scope of the Study

The main objective of this research is to examine the mechanical behavior of steel beams strengthened with MF-FRP laminates. A three dimensional (3D) nonlinear finite element model is developed and used to carry out this study. The developed finite element model is first validated against the available experimental results reported by Alhadid (2011). Then, the validated finite element model is employed to perform a numerical investigation consisting of two phases. The first phase investigates the mechanical behavior of the composite steel-FRP beams in the context of the experimental study conducted earlier by Alhadid (2011). This phase studies different issues including the interfacial shear force distribution in anchoring steel fasteners, the stress distribution and spread of yielding in the steel section, and the stress distribution in the FRP laminates. Additionally, the second phase investigates the effect of various strengthening parameters on the mechanical behavior of the steel-FRP composite beams such as the

solution methodology. Finally, the structure of the thesis is described followed by the contribution of this study to the area of rehabilitation of steel structures.

1.1 Problem Statement

Recently, following the successful use of FRP in strengthening reinforced concrete structures, researchers started to investigate the effectiveness of this material in strengthening steel structures. Although this approach was initially rejected by many researchers due to the low stiffness of FRP materials compared to steel, it was revived when high-modulus Fiber Reinforced Polymers (FRP) were successfully produced and became available commercially. The elastic modulus of such FRPs approaches and even, in sometimes, exceeds the elastic modulus of structural steel. Relevant research was directed to strengthening steel beams using externally bonded fiber reinforced polymer (EB-FRP). The research conducted in this area revealed a significant improvement in the load-carrying capacity of the strengthened steel beams. However, it was also indicated by many researchers that the steel beams strengthened with EB-FRP exhibited premature brittle failure mode due to the debonding of the FRP strips. The promising results of using Mechanically Fastened FRP (MF-FRP) strips in enhancing the flexural capacity of reinforced concrete beams with maintaining the ductile behavior of those beams have established a potential interest in achieving a successful and efficient strengthening scheme when utilizing the MF-FRP laminates to strengthen steel beams. Alhadid (2011) studied experimentally the effectiveness of strengthening steel beams with MF-FRP. A significant improvement in the flexural capacity was revealed. Additionally, a ductile

the main design parameters on the stiffness and load-carrying capacity of steel-FRP composite beams.

Meanwhile, the analytical approach is utilized to calculate the elastic deflection of simply supported steel-FRP composite beams loaded by a mid-span point load. The derived analytical model takes into consideration the partial composite action associated with the relative steel-FRP interfacial slip. The model is used to predict the first yielding load at the compression flange of the simply supported steel-FRP composite beam. The obtained analytical results are also validated by comparison with relevant finite element predictions.

1.4 Organization of the Thesis

The current research thesis consists of six chapters. In this section, a brief description of the contents of each chapter is presented.

In Chapter 1, the problem statement is discussed, followed by presentation of the objectives of the research, scope of the numerical and analytical studies and the methodologies adopted in executing the research. Finally the organization of the report chapters is presented.

Chapter 2 provides an overview of the literature review of previously published research work in the area of strengthening of reinforced concrete and steel beams. The chapter discusses experimental, analytical and numerical research related to strengthening of both reinforced concrete and steel beams using EB-FRP and MF-FRP schemes.

steel section dimensions, length and thickness of the FRP laminates, and connection configuration.

Furthermore, a closed-form analytical model is also developed to predict the elastic behavior of the steel-FRP composite beams taking into consideration the slip at the steel-FRP interface. The analytical phase of the study utilizes the partial action analytical model developed by Girhammar and Gopu (1993). The results obtained from the analytical study are validated against corresponding finite element predictions. Then, the analytical model is utilized to evaluate the deflection, and the load that initiates yielding in the compression flange of the steel beams steel-FRP.

1.3 Methodology and Approach

The current study includes implementation of numerical and analytical modeling approaches. The numerical approach involves the use of the general purpose finite element software (ANSYS, release 13) to build a detailed 3D nonlinear displacement-controlled finite element model for simply supported I-shaped steel beams strengthened with MF-FRP laminates. The finite element model takes into account both the material and geometrical nonlinearities, and accounts for the relative slip at the steel-FRP interface. The load-deflection results of the simulated beams are validated with their experimental counterparts. The validated finite element model is utilized for in-depth investigation of the distribution of stresses and forces in the different components of the steel-FRP composite system. A parametric study is conducted to investigate the effect of

Finally, Chapter 6 presents conclusions regarding the outcomes of the numerical and analytical research work. In addition, recommendations regarding future research are provided.

1.5 Study Contribution

The outcomes of the current study contribute to the field of rehabilitation of steel structures by enriching the knowledge and understanding of the mechanical behavior of steel beams strengthened with mechanically fastened FRP laminates. The parametric analyses that address a wide range of parameters is expected to help designers in producing safe and economic strengthening schemes. The analytical model is also useful for simple and accurate control of the system deflection and the calculation of the load that initiates yielding in the steel section. The recommendations of the study are expected to help in developing design provisions for mechanically fastened strengthening systems for steel beams.

Chapter 3 focuses on the development of the finite element model and its verification. The chapter provides a brief background about the finite element modeling technique. Detailed description of the 3D finite element model is also presented. Verification of the accuracy of the developed finite element model by comparison with relevant experimental results is presented at the end of the chapter.

Chapter 4 discusses the detailed numerical investigation of the mechanical behavior of the strengthened steel beams. A brief description of previous experimental research in strengthening steel beams with MF-FRP is presented. A parametric study of the mechanical behavior of the steel-FRP composite beams is provided along with detailed presentation and discussion of the corresponding distribution of forces and stresses. The effect of various design parameters on the load capacity and stiffness of steel-FRP composite beams is also presented and discussed.

Chapter 5 reports on the analytical solution of the differential equations governing the flexural behavior of the elastic steel-FRP composite beams. The chapter starts with a brief background about the partial interaction theory of composite beams. The solution of the differential equations governing the behavior of steel beams strengthened with MF-FRP laminates partially covering the bottom flange of the beam is presented. The analytical model is then used to calculate the deflection and the load at which first yielding of the steel section occurs. The analytical model is also used to find the distribution of the shear forces developed in the steel fasteners. The chapter concludes with a comparison between the analytical results and the corresponding finite element predictions.

beams is outlined. Finally, research investigations on strengthening of steel beams with FRP laminates are discussed.

2.2 Externally Bonded FRP for Strengthening of RC Beams

Externally bonded FRP system has been used to strengthen concrete structures in many places around the world since mid-1980s. The first structural engineering application of the externally bonded FRP system for flexural strengthening of reinforced concrete bridges was carried out in Switzerland in 1987 [CRC (2002)]. Since 1982, carbon fiber reinforced epoxy resin composites have been employed at the Swiss Federal Laboratories for Materials Testing and Research (EMPA) for the post-strengthening of RC beams where seventy flexural beams, having spans between 2.0 and 7.0 meters, have been tested in one of their experimental studies. Later in 1993, and based on large scale research projects undertaken in USA and in Canada in the area of repair/strengthening of RC beams using FRP, the applicability of such material in construction has been confirmed [Meier (1995)].

Rahimi and Hutchinson (2001) studied the structural behavior of RC beams strengthened with externally bonded plates made of three different materials; namely Carbon Fiber Reinforced Polymers (CFRP), Glass Fiber Reinforced Polymers (GFRP), and steel. Around thirty one beams were experimentally loaded in four-point bending while being simply supported over a span of 2100 mm. The test variables included the amount of internal steel reinforcement bars and also the type and amount of external reinforcement (i.e., CFRP, GFRP, or steel plates). The beams were 2300 mm long, 200

CHAPTER 2

LITERATURE REVIEW

2.1 Introduction

Extending the life span of existing steel structures represents a major challenge for civil engineers. It is well known that corrosion of steel structures reduces the effective cross-sectional area of the steel members, and consequently causes elevated stresses at the corroded areas. Moreover, the increase in population also participates in increasing the service loads on steel structures such as bridges. Therefore, the need for economical, fast, and reliable techniques in repairing and retrofitting of steel structures reflects the importance of using fiber reinforced polymers (FRP) as a strengthening material with high strength-to-weight ratio and corrosion resistivity. Over the last two decades, there has been significant growth in the experimental and theoretical research work studying the mechanical behavior of steel-FRP composite beams, and the effect of different parameters on their behavior.

In this chapter, the experimental, analytical and numerical research studies that have been carried out to investigate the behavior of steel and reinforced concrete (RC) beams strengthened with FRP are outlined. Firstly, research studies on strengthening of reinforced concrete beams with externally bonded FRP strips are presented. Then, research work on the use of mechanically fastened FRP to strengthen reinforced concrete

observed four modes of failures; flexural failure, ripping of concrete cover, shear failure, and hybrid mode of shear failure and ripping of concrete cover. It was found that the before brittle failure, the composite action of the strengthened beam could be divided into three distinct zones based on the distribution of the strain along the CFRP plate. The distressed zone was identified at the end of the plate, the bond development zone where strains increased linearly, and the fully composite zone at the midspan of the beam. An analytical model was developed to predict the ripping failure load based on the composite action theory in combination with the strain limit. A simple formulation to predict the bond development length was also presented.

Buyle-Bodin *et al.* (2002) used finite element method (FEM) to study the flexural behavior of the RC beams strengthened with externally bonded CFRP laminates. They investigated two parameters; the number of CFRP layers and the influence of initial damage. An experimental study was carried out to validate the nonlinear FE model, where seven prismatic 150x300 mm RC beams with span of 2800 mm were tested in four-point bending setup. Six of the RC beams were strengthen by one or more externally bonded CFRP laminates. Each CFRP laminate was 50 mm wide and 1.2 mm thick and had a tensile strength of 2400 MPa and modulus of elasticity of 150 GPa. One of the beams was used as the control beam, while two beams were strengthened with one layer of CFRP and two beams were strengthened with two layers of CFRP. The other two beams were first loaded to a percentage of the ultimate load measured for the control beam before applying the CFRP laminates; one of them with one layer and the other one with two layers. The FE model was prepared using the French Code CASTEM-2000 developed by the French Nuclear Research Center. The FE model is a 2D plane stress

mm wide and 150 mm deep. The externally bonded plates were 1930 mm long. The thickness of the CFRP laminates varied from 0.4 mm (2-ply) to 1.2 mm (6-ply), while the chosen thickness for GFRP was 1.8 mm (12-ply). It was noted that the strength of beams strengthened with composite plates were substantially increased. The ultimate load-carrying capacity of the beams increased by about 230% over their non-strengthened counterparts. The concrete beams that had been preloaded up to 80% of its ultimate load before bonding had an equivalent performance to the other beams. This indicates the effectiveness of this repair technique in practical implementation. The amount of improvement in the strength of the considered beams is influenced by the amount and strength of the composite plates. Rahimi and Hutchinson (2001) also developed a two-dimensional (2D) nonlinear model using the Finite Element Analysis System LUSAS. The smeared crack concept was implemented to predict the propagation of cracks in the RC beam. The finite element (FE) model was validated against the experimental results.

Nguyen *et al.* (2001) examined the performance of RC beams with externally bonded CFRP plates. They studied the effect of plate length, the reinforcement steel ratio and the thickness of concrete cover on the behavior of the beams with more emphasis on the brittle failure mode of concrete ripping. A total of 10 RC beams of 120x150 mm cross-section and 1500 mm length were tested with nine beams strengthened with CFRP laminates. The RC beams were overdesigned in shear to prevent shear failure. The CFRP laminates had an ultimate tensile strength of 3140 MPa, and an elastic modulus of 181 GPa, while the adhesive has an elastic modulus of 12.8 GPa. Strain gauges were attached to the concrete surface, steel bars and along the CFRP plates. The beams were tested in four-point bending after two weeks of attaching the CFRP laminates. The researchers

anchorage bond is provided [Barners Ra, *et al.* (1999)]. A number of researchers have proposed analytical models to analyze debonding in structural members strengthened with externally bonded reinforcements. They followed approaches that can be classified as strength or fracture. The strength approach involves the calculation of stress distribution along the interfacial connection in the strengthened members based on elastic material properties [Reperts (1989), El-Mihilmy (2001)]. On the other hand, the fracture models utilize the elastic and fracture material properties. Hamoush *et al.* (1990) used linear elastic fracture mechanism and finite element method to model debonding in steel plated concrete beams. Buyukozturk *et al.* (2004) has suggested that proper characterization of debonding problems and their inclusion in the design code is essential for common use of the technique. Research in the area of externally bonded CFRP has revealed that this technique can't utilize the full tensile strength of FRP materials due to their premature debonding [ACI committee 440 (2002)].

Abdel Baky *et al.* (2007) used FEM to simulate the flexural and interfacial behavior of RC beams strengthened with externally bonded CFRP laminates. The nonlinear FE model was developed using the ADINA (2004) and was capable of predicting the various failure modes, including debonding of the CFRP laminate at plate end and at intermediate cracks. The concrete was assigned a nonlinear stress-strain relationship, while the steel was modeled as bilinear elastic-plastic material with a tangent modulus in the strain hardening regime of 1% of the elastic modulus. The FRP was assumed to behave elastically in a linear manner up to failure. Two models (nonlinear and bilinear models) for the concrete-CFRP interfacial connection were used as proposed by Lu *et al.* (2005). The FE model was validated against experimental data

model in which 1.0 mm thick bond elements were used to model the glue between the CFRP laminate and the concrete. The FE model was capable to account for opening and closure of crack in the case of cyclic loading. The beams strengthened with 1 layer of CFRP (1.2 mm thick) have gained 51 to 58% improvement in the load-carrying capacity over the control beam, while the beams strengthened with 2 layers of CFRP (2.4 mm thick) have gained 73 to 77% improvement. The repaired beams show increase in the ultimate load-carrying capacity in the same range of strengthened beams, but the improvement in stiffness was reduced. All the strengthened beams exhibit brittle failure mode by horizontal crack in the concrete cover. A good correlation was found between the FE model and the experimental results, where the maximum difference between the FE and the experimental results was 12%.

Buyukozturk *et al.* (2004) conducted a review of the progress achieved in the area of debonding problem in RC members strengthened using FRP composites. According to the researcher, the majority of the debonding failures reported in the literature took place in concrete substrate. However, depending on the concrete material and geometric properties, other possible failure mechanisms for the RC structures are concrete crushing before yielding of the reinforced steel, steel yielding followed by FRP rupture, steel yielding followed by concrete crushing, and FRP debonding. Debonding failure behavior of strengthened beams was found to be highly dependent on the amount of steel reinforcements and the amount of external FRP reinforcement [Garden *et al.* (1997), Maalej *et al.* (2001)]. Moreover, Saadatmanesh *et al.* (1990) showed that inappropriate choice of bonding material caused premature debonding in the retrofitted member. Debonding problem may become significant under fatigue loading unless adequate

Sayed-Ahmed *et al.* (2009) conducted an intensive review on the CFRP-Concrete bond strength. The review showed that Bizindavyi *et al.* (1999) and Chajes *et al.* (1996) had reported that the bond is significantly influenced by the surface preparation and quality of concrete. The surface preparation was achieved by roughening the surface and exposing small or medium size aggregate. According to Spadea *et al.* (1998), the degree and type of external anchorage was found to be important in maintaining the composite behavior. Bakay (2003) showed that for traditional RC beams strengthened with externally bonded CFRP strips with no additional anchorage, composite action halted at about 85% of the ultimate load of the beam. Meanwhile, for beams with additional anchorage, composite behavior was maintained up to almost 99% of the ultimate load. The review also showed that according to experimental studies by Chen *et al.* (2001), Udea *et al.* (2003), Yuan *et al.* (2004) and Lue *et al.* (2005), the major factors affecting bond-slip and composite action between the CFRP and concrete were the concrete compressive strength, effective bond length, CFRP laminate axial stiffness, CFRP to concrete width ratio, adhesive axial stiffness and adhesive compressive stiffness. In addition, the research carried out by Shahawy *et al.* (1996), Arduini *et al.* (1997), Maalej *et al.* (2001), Rahimi *et al.* (2001), Sayed-Ahmad *et al.* (2004), Lu *et al.* (2005), Hosny *et al.* (2006) and Esfahani *et al.* (2007) revealed that the failure mode of RC beams strengthened with externally bonded FRP can be separated in two categories based on the duration of composite action between the materials. When the composite action is maintained until the ultimate load is reached, failure can occur in one of three modes based on the reinforcement ratio and the shear strength of the beam. Those failure modes are the concrete crushing prior-to or following yielding of steel reinforcement, tensile

for 25 specimens tested by Brena *et al.* (2003), the comparison showed a good agreement. Numerical simulation of Abdel Baky *et al.* (2007) revealed that the maximum interfacial shear stress is dependent on the steel reinforcement ratio. With an increase in the steel reinforcement ratio from 0.46 to 3.3%, the maximum shear stress at the same load level was reduced by 60%. It was also found that it is useful to use intermediate anchorage along the FRP strengthened beams to mitigate debonding.

Kotynia *et al.* (2008) studied experimentally and numerically the flexural behavior of the RC beams strengthened with various externally bonded CFRP configurations. The objective of the experimental study was to delay the intermediate crack debonding and to increase both the load-carrying capacity and the CFRP utilization ratio. Ten rectangular RC beams with span of 4200 mm and 150x300 mm cross-section were tested in four point bending setup. According to Kotynia, all the beams failed by intermediate debonding crack between the CFRP strip and concrete. It was found that attaching two layers of CFRP sheets with an extra U-shaped laminate along the soffit of the beam produced the most effective enhancement in the flexural capacity. The width of the CFRP strip was shown to have an influence in the debonding behavior. The debonding was noticed few millimeters in the concrete cover in the case of narrow strips, while in the case of wide strips, the debonding was along the internal bottom steel reinforcements. A nonlinear bond stress-slip model was adopted in a 3D nonlinear FE model to characterize the interfacial elements between the FRP and concrete. The FE model showed a good agreement with the experimental results.

externally bonded FRP laminates. Lamanna *et al.* (2001) found that the use of multiple small fasteners, as opposed to large diameter bolts, distributes the load equally over the composite strip and doesn't cause premature failure due to excessive stress concentration at the holes in the composite strip. The test specimens were divided into two target concrete design strengths; namely 21 and 42 MPa concrete. The beams were 1220 mm long and had a cross-section of 153x153 mm. For the 21 MPa group, all the beams failed due to crushing in the concrete at the compression zone. The increase in the yield moment over the control (unstrengthened) beam ranged from 19 to 37%. On the other hand, some beams in the 42 MPa group failed by shear in the steel fasteners, initiating at the edge of FRP-concrete connection. The associated increase in the yield moment over the control beam ranged from 8 to 18%. The beams exhibited initial cracking during fastening in the case of high charge or large diameter fasteners used to attach the FRP laminates. The investigators clarified that those cracks are related to the edge distance from the concrete free surface which was increased in larger beams.

Lamanna *et al.* (2002) conducted an extension of his previous work [Lamanna *et al.* (2001)]. They tested nine RC beams of T cross-section with cross-sectional dimensions of 1524 mm, 203 mm, 305 mm and 762 mm for flange width, flange height, web width and total height, respectively. They reported that increasing the thickness of the mechanically fastened FRP strip resulted in significant improvement in the yield and ultimate moment capacities. The beam strengthened with one strip showed an increase of 8.0 % in yield moment and 14.4 % in the bending moment at a mid-span deflection of 63.5 mm (2.5 in.). The beam strengthened with two strips showed an increase of 11.7 % in yield moment, and an increase of 27.2 % in the ultimate moment. Lamanna *et al.*

rupture of the CFRP, and shear failure of the concrete beam. However, when the composite action is not maintained until the ultimate load is reached, premature failure resulting from debonding of FRP occurs.

2.3 Mechanically Fastened FRP for Strengthening of RC Beams

As shown earlier, many researchers reported that strengthening of RC beams with externally bonded FRP laminates requires difficult surface preparation to provide adequate bond strength between the FRP laminates and concrete substrate. Furthermore, it was found by many researchers that RC beams strengthened with externally bonded FRP laminates encountered brittle failure mode due to the debonding of the FRP laminate. The study by Bonnaci and Maalej (2001) showed that up to 69% of the surveyed RC beams externally bonded with FRP failed by debonding of the FRP strips. An alternative technique to strengthen the reinforced concrete beams is the mechanically fastened system, where the FRP laminate is attached to the soffit of the RC beam using fasteners. In this section, the main research reported in the literature about the mechanically fastened FRP in strengthening RC beams in flexure is outlined.

Lamanna *et al.* (2001) have used off-the-shelf powder-actuated fasteners to attach pultruded FRP strips to the soffit of RC beams. Those RC beams strengthened with mechanically fastened fiber reinforced polymers (MF-FRP) gained 65 to 75% increase in the load-carrying capacity of similar beams strengthened using externally bonded FRP laminates. However, the fastening method is extremely rapid and the failure modes of the beams strengthened by the MF method were more ductile than those strengthened with

An analytical model to predict the mechanical behavior of RC beams strengthened using MF-FRP strips was discussed by Bank *et al.* (2007). The model utilized the strain compatibility, equilibrium and constitutive relations of the materials. It was capable of predicting the ultimate strength and failure modes of RC beams strengthened by MF-FRP. The procedure proposed by Bank *et al.* (2007) was used to proportion strengthening systems for large-scale beams (7300 mm long and cross-section 510x150 mm) which were tested and their results were used to verify the analytical model. The analytical model showed a good agreement with the experimental results where the percentage errors ranged from 6.5% to 22.6%

More research on the influence of fasteners' arrangement pattern and spacing on the flexural performance of the MF RC beams was conducted by Martin *et al.* (2008). Six RC beams with 3350 mm span and square cross-section with side length of 304.8 mm were tested in four-point loading setup. The FRP laminates used in the experiment were fabricated of both carbon and glass fibers in veinylester resin. A significant improvement in the ultimate capacity of the strengthened beams was obtained by 12% to 39% increase over the control beam (i.e., unstrengthened beam) with a negligible loss in their ductility. It was also found that the distribution pattern of the fasteners has an influence on the flexural performance of the MF-FRP concrete beams with same number of fasteners.

Lee *et al.* (2009) proposed a method to estimate the nominal moment capacity of RC beams strengthened with MF-FRP system pointing the significance of nail rotation associated with flexural cracking, and based on a strain reduction factor of 24%. The proposed method was verified with experimental study conducted on twelve small-size

(2002) developed an analytical model to predict the response of strengthened RC beams. The model was capable of predicting the results with a 7% maximum percentage error relative to the experimental outcomes.

Lammana *et al.* (2004) studied the effects of three different strip moduli, different fastener lengths and layouts, and the effect of predrilling on the flexural capacity of RC beams strengthened with MF-FRP laminates. Fifteen RC beams, 3658 mm long, with a cross-section of 304.8x304.8 mm were tested in three-point loading. The measured concrete compressive strength at 28 days was 28 MPa. The unstrengthened beams were designed in accordance with ACI 318-99 (ACI, 1999) to behave in a ductile fashion. Primary tension steel was provided by two #8 grade 60 deformed bars with a reinforcement ratio of 1.56%. Shear reinforcements were provided in the form of closed stirrups of #4 grade 60 deformed bars spaced at 102 mm. The moduli of the FRP strips were 5.6, 26.3, and 57.0 GPa and a cross-sectional dimension of 102x3.2 mm. The fastening system used was a Hilti DX A41 powder-actuated fastening system. Increases in yield and ultimate moments of up to 21.6 and 20.1%, respectively, were achieved. In case of long fasteners used in conjunction with predrilled holes, the strengthened beams showed ductility similar to the control beams. The failure mode of most of the beams was a typical ultimate failure mode of a RC flexural member; concrete crushing in the top of the beam except for the beams without predrilling, with high strip modulus tended to fail by strip detachment. Predrilling pilot holes reduces the amount of visible initial cracking and allows greater penetration of the fasteners, resulting in a better overall strength and ductility. Three of the beams were strengthened with MF-FRP strips showed strength comparable to the beams strengthened with bonded FRP strips.

ductility. For better utilization of the FRP strip strength, the researcher suggested to extend the length of FRP strip to a sufficient development length.

A numerical approach developed by Nardone *et al.* (2011) was used to predict the fundamental behavior of RC beams strengthened by MF-FRP in terms of ultimate and serviceability limit states. The model accounts for the equilibrium, compatibility, constitutive relationships, and the slip between the FRP and concrete. Knowing the load-slip relationship of the fasteners is essential in order to apply the proposed model. The results obtained by the iterative solution were compared with those of experimental results found in the literature showing a good agreement. The model is also capable of predicting three modes of failure for the reinforced concrete beams strengthened with MF-FRP strips; namely, bearing failure, net tension failure, and concrete crushing.

2.4 Externally Bonded FRP for Strengthening of Steel Beams

Following the successful use of externally bonded FRP laminates in strengthening reinforced concrete beams, researchers started applying the same techniques to steel beams. Sen *et al.* (2001) conducted an experimental study to explore the applicability of using CFRP laminates in retrofitting steel bridge members. The experimental work included testing six composite steel wide flange beams (W8x24) made of grade A36 steel with span of 6100 mm. The top flange of each beam was attached to a 114x710 mm reinforced concrete slab connected by 36 shear connectors. The specimens were loaded in four-point loading setup until they become severely distressed. After that the CFRP laminates with different thicknesses were bonded to the bottom flange of the beams. The

MF-FRP beams and two control unstrengthened beams. A previous analytical model developed by [Lammana (2002), Bank *et al.* (2004), Bank *et al.* (2007)] agreed with the experimental results in terms of load capacity. However, the model predicted mid-span deflections were not in agreement with the experimental results.

Lee *et al.* (2009) aimed to improve the prediction of the flexural behavior of RC beams strengthened by MF-FRP. They took into account the slip between the FRP and concrete caused by bearing in the FRP and rotation of the fasteners. A pull-off test was conducted to investigate the behavior of the FRP concrete connection. The dominant failure mode of the tested RC beam strengthened by MF-FRP, was yielding of the primary steel reinforcement followed by concrete crushing with progressive delamination of FRP strip. It was found that the fasteners acted as crack initiators.

Ebead (2011) used a hybrid MF-FRP laminates in strengthening RC beams in addition to a normal MF-FRP system. The hybrid system differs from the normal MF-FRP system by the epoxy that had been injected in the holes in order to enhance the attachment of the laminate and to prevent the probable corrosion that might affect the fasteners. Twenty one beams were tested in four-point loading setup. The beams had a clear span of 2250 mm and rectangular cross-section of 250 depth and 150 mm width. The beams were strengthened with different lengths of FRP strips, and the fasteners were placed in different distribution patterns. The specimens strengthened with hybrid MF-FRP system gained a higher ultimate flexural capacity than their counterparts strengthened with the traditional MF-FRP system. However, they experienced less

El Damatty *et al.* (2003a) studied the flexural performance of I-shaped steel beams strengthened with GFRP laminates externally bonded to their flanges. The study included the test of three W150x37 steel beams, one control beam and two rehabilitated beams with a span of 2800 mm. The yield stress and modulus of elasticity of the steel beams were 363 MPa and 200 GPa, respectively. The GFRP laminates were 2400 mm long, 19 mm thick, and 154 wide. The values of 206.85 MPa for tensile strength and 17.2 GPa for modulus of elasticity were obtained from a tensile test conducted for the GFRP laminates. Methacrylate adhesive systems (A0420) was used to attach the GFRP laminates to the bottom and top flanges of the steel beams. According to El Damatty *et al.* (2003b), the average values of the linear continuous springs simulating the shear and peel stiffness of the adhesive per unit area were equal to 21.79 N/mm^3 and 2.26 N/mm^3, respectively. The experimental results revealed an increase of 17%, 23% and 78% in the initial stiffness, yield moment and ultimate moment of the rehabilitated beams over the control beam, respectively. The rehabilitated beams failed by a tensile rupture in the GFRP laminates, while no failure was observed at the interface between the GFRP and the steel interface, which indicates a good performance of the adhesive. The researchers also developed a closed form analytical model that can predict the yield moment capacity of the rehabilitated steel beam. The model also provides an estimate of the stress induced in the adhesive, the steel, and the GFRP laminates within the range of elastic behavior. The study also included the use of the finite element software ANSYS to simulate the rehabilitated beam numerically. The three dimensional FE model was developed using eight node solid elements to simulate the steel section and GFRP laminates, while the adhesive was simulated using three dimensional continuous spring elements located at

main contribution of CFRP laminates was noticed at the post-yielding stage due to the low modulus of elasticity of the CFRP relative to that of the steel material. The beams retrofitted with thicker CFRP laminates gained higher stiffness and experienced less deflection. The researchers suggested using steel bolts to assist in transferring the load especially with thicker CFRP laminates.

Analytical and numerical procedures were developed by Deng *et al.* (2004) to calculate the stresses in steel beams strengthened with externally bonded CFRP laminates. The material was assumed to be linear elastic and shear deformations were neglected. The closed-form solution for the governing differential equations was presented, where the interfacial stresses in the steel composite beams could be evaluated. The finite element modeling technique was used to calculate the stresses in the steel composite beams for the case of CFRP plates with a tapered end. The FE model was used to conduct a parametric study to investigate the effect of different parameters on the mechanical behavior of the beams; namely tapered-end CFRP, length of taper, thickness of CFRP, thickness and modulus of adhesive, and the elastic modulus of CFRP plates. The parametric study showed that the maximum shear and normal stresses in the adhesive layer at the free end of adhesively bonded plates decrease as the thickness of the adhesive increases. The decrease in the elastic modulus of the CFRP plate reduces the maximum shear stress, but has little influence on the normal stress. The maximum shear and normal stresses decrease as the thickness of the end of the taper decreases and the length of the taper increases.

used were 6.4 mm thick and 38.1 mm in width. The ultimate capacity of the tested girders was increased by 17% to 25% over the predicted capacities of the unstrengthened specimens. Additionally, Liu *et al.* (2001) studied the efficiency of CFRP laminates in strengthening artificially notched steel girders. The study revealed an increase of 45% to 60% in the inelastic load capacities. Furthermore, Tavakkolizadeh *et al.* (2003a) examined eight S5x10 steel beams with 1300 mm span. The specimens were notched in the tension flange at different depths. Different CFRP lengths were used for the different notches depths. The results indicated a significant increase in the ultimate load-carrying capacity. The beams with deep notches exhibited significant deflection compared to those with shallow notches. In another study, Edberg *et al.* (1996) examined the effectiveness of four different schemes of attaching the FRP laminates to the tension flange of W8x10 steel beams of 1372 mm span. The FRP laminates were applied over the central 1219 mm of each beam. The first scheme consisted of a 4.6 mm thick CFRP plate, bonded directly to the tension flange, where the second reinforcement scheme utilized a similar CFRP plate, but was attached to an aluminum honeycomb structure to position the CFRP plate further away from the steel section to increase the moment of inertia of the section. In the third scheme, a foam core was attached to the tension flange, followed by wrapping the whole assembly by a GFRP sheet. The fourth scheme utilized a GFRP pultruded channel, which was both adhesively bonded and mechanically connected to the tension flange with self-tapping screws. The specimens were tested in four-point bending setup. The increase in stiffness was 20%, 30%, 11% and 23% for the schemes from one to four, respectively. while the increase in the strength was 42%, 71%, 41%, and 37% for the same schemes. Tavakkolizadeh *et al.* (2003b) conducted an experimental study on three steel-concrete

the interface between the steel and the GFRP. The comparison between the experimental, numerical and analytical showed an excellent agreement.

El Damatty *et al.* (2005) studied the use of Glass Fiber Reinforced Polymers in enhancing the flexural capacity of steel bridges. A detailed nonlinear numerical model was developed for the bridge before and after attaching GFRP sheets to the bottom flange of its steel girders. The analysis of nonlinear moving load was conducted to determine the critical truck locations that led to maximum GFRP axial stresses, and maximum adhesive shear and peel stresses. The bridge steel girders had a span of 24.85 m. The girders height, web thickness, flange width, and flange thickness were 910 mm, 12 mm, 307 mm, and 20 mm, respectively. An increase in the truck weight carrying capacity of the girders of about 25% was achieved using this retrofitting scheme without suffering from premature failure in the concrete, GFRP or adhesive.

An extensive review on retrofitting steel beams using externally bonded FRP laminates was conducted by Shaat *et al.* (2004). The review showed that researchers discussed the different approaches used to examine the feasibility and efficiency of retrofit of steel girders; namely, repair of naturally deteriorated steel girders, repair of an artificially notched girder, strengthening of an intact section to increase the flexural strength and stiffness, and retrofit of steel girders in composite action with a concrete deck. The review showed that Gillespie *et al.* (1996) investigated the performance of four full-scale beams removed from a deteriorated steel bridge. The four corroded bridge girders were 9754 mm in length, 610 mm deep, and had a flange width of 229 mm. The tension flanges were retrofitted with one layer of CFRP laminates, where the CFRP strips

steel beams with span of 1800 mm strengthened with different lengths of CFRP laminates were tested in four-point loading setup. The CFRP laminates were 50 mm wide and 1.4 mm thick. Extra steel plates were welded to the compression flanges of the beams to prevent failure due to compressive yielding. Increasing the CFRP laminates length resulted in a significant increase in the flexural capacity of the strengthened beams. However, the failure mode of the beams of longer laminates was due laminate rupture at mid-span. Meanwhile, the beams strengthened with shorter laminates failed due to debonding of the CFRP laminates.

The static behavior of the H-shaped steel beams strengthened with CFRP laminates was studied experimentally, analytically and numerically by Colombi *et al.* (2006). Three identical 2500 mm long HEA 140 steel beams were strengthened by attaching one or two layers of CFRP strips to the bottom flange of the steel beams using two different epoxy adhesives (Sikadur 30 and Sikadur 330). One more beam was tested as a control beam to provide reference results. The CFRP strips had a length of 2000 mm, width of 60 mm, thickness of 1.4 mm, and a Young's modulus of 200 GPa. The beams were tested in three-point bending setup. At 20 mm mid-span deflection, the revealed results showed an increase in the strength of about 10% and 23% for beams strengthened with one layer and two layers, respectively. On the other hand, no significant difference was observed between the two types of adhesive. Two different analytical models were used to predict strains in the CFRP strips. The first model involves a strength approach to evaluate the interfacial and adherent stress distributions and is based on the assumption of elastic material behavior. The second one uses the standard transformed section method to evaluate the stress in the CFRP strips. A finite element model was developed using the

composite girders using W355x13.5 steel beams with a 75 mm thick by 910 mm wide concrete slab. The CFRP laminates were 75 mm wide 1.27 mm thick and were applied in different number of layers. The results indicated increase in the ultimate load-carrying capacity of 44%, 51%, and 76% for the beams retrofitted with one, three, and five layers of CFRP, respectively.

The failure modes controlling the response of steel beams retrofitted with externally bonded FRP laminates were summarized by Buyukozturk *et al.* (2003). The possible failure modes are top flange buckling in compression, web buckling in shear, FRP rupture and FRP debonding. The researchers empathized the need to consider all possible failure modes in the design process.

High modulus CFRP laminates were used by Schnerch (2005) to strengthen composite steel-concrete bridge girders. The research first investigated the efficiency of bond adhesive by testing small-scale beams strengthened with CFRP using different types of adhesive. The optimal adhesive was then selected to be used in large-scale steel-concrete girders. The influence of using CFRP laminates with intermediate and high modulus was investigated by testing the large-scale beams. The results revealed that the high modulus CFRP was more efficient in increasing the stiffness and the ultimate strength of the strengthened beams by a percentage increase of 36% and 45%, respectively, over the control beam. The investigation showed also that prestressing the CFRP laminates improved the performance of the strengthened beams.

Lenwari *et al.* (2005) investigated the flexural behavior of rolled steel beams strengthened with partial-length, externally bonded CFRP laminates. Seven W100x17.2

modulus of elasticity, and strain-hardening ratio of the steel beams were 400 MPa, 200 GPa, and 0.01 respectively. The tensile strength, compressive strength, and modulus of elasticity of the FRP sheets were 135 MPa, 165 MPa, and 12.4 GPa, respectively. The experimental results were used in verifying the accuracy of the analytical model which was able to predict the peel and shear behavior of the adhesive material. An excellent agreement was shown between the experimental measurements and the results obtained from the analytical model. It was indicated that the tensile stress in the GFRP strip increased from zero at the GFRP edge to the maximum value at the mid-span. The adhesive peel stress reached 37% of its expected capacity.

Benachour *et al.* (2008) studied the shear and normal interfacial stress in simply supported beams strengthened with bonded prestressed composite laminates analytically. The linear elastic analytical model was able to adapt different loading schemes; uniform distributed load, arbitrary positioned single point load, and two symmetric point loads. The model did not account for slippage between the steel and FRP laminate as a perfect bond was assumed. Increasing percentage of fiber aligned in the beam's longitudinal direction resulted in increasing the effective modulus of the externally prestressed bonded FRP plate. It was found that laminates with higher elastic modulus produce a lower concentration of stress at the edge of steel-FRP interfacial connection. Using more flexible adhesives resulted in a more uniform distribution of interfacial stress and reduced the value of maximum critical interfacial stress at the ends of the laminate. The study recommended using mechanical anchorage devices at the end of prestressed laminates in order to avoid premature failure of the strengthening scheme and ensure sufficient anchorage capacity at the ends of the laminates.

general purpose FE software ABAQUS to evaluate the stresses in the strengthened beams. The beam was modeled using standard two nodes beam elements while the adhesive layers and the CFRP strips were modeled by standard eight nodes plane stress elements. The results of both analytical and FE models showed good agreement with the experimental outcomes.

An experimental study to investigate the effectiveness of ultra-high modulus and high modulus pre-preg CFRP in strengthening artificially degraded rectangular hollow steel sections was carried out by Photiou (2006). Four beams were upgraded, two utilizing U-shaped pre-preg FRP units, which extended up the vertical sides of the beam to the neutral axis height, whereas the other two beams used a flat pre-preg FRP plate bonded to the tension flange of the beams. For each of the geometrical shapes either an ultra-high modulus or a high modulus CFRP was used. The beams of were tested under four-point loading setup. The results showed that the beams strengthened with ultra-high modulus pre-preg CFRP experienced a brittle failure mode due to fiber breakage, while the beams strengthened with high modulus pre-preg CFRP failed in a ductile mode. The results showed also that the use of u-shaped pre-preg CFRP prevented the debonding at high loading values.

Youssef (2006) developed an analytical model to predict the linear and non-linear behavior of steel beam strengthened with externally bonded GFRP sheets. Simply supported W150x37 steel beams, strengthened by bonded 19 mm GFRP sheets to the top and bottom flanges were tested in four-point loading setup. The beams had a length of 2800 mm while the GFRP sheet was 2400 mm long and 152 mm wide. The yield stress,

An intensive review on the strengthening of steel structures with externally bonded FRP composites was conducted by Teng *et al.* (2012). The researchers classified the structural use of FRP with steel in two categories. The first category is the bond-critical applications, where the interfacial shear stress transfer function of the adhesive layer that bonds the steel and the FRP together is crucial to the performance of the structure. The externally bonded FRP for flexural strengthening of steel beams is part of this category. The second category is the contact-critical applications, where the steel and FRP should remain in contact to ensure the effective interfacial normal stress transfer. An example of the second category is the confinement of concrete-filled steel tubular with FRP jackets. Accordingly, the investigation revealed that the possible interfacial failure modes in the steel beams strengthened with externally bonded FRP are the failure within the adhesive layer (i.e. cohesion failure), and failure at the material interfaces (adhesion failure) between the adhesive and steel or between the adhesive and FRP. The debonding failure modes for a simply supported steel beam strengthened in flexure with externally bonded FRP are the intermediate debonding and plate-end debonding. The intermediate debonding occurs away from the FRP plate ends and at a defect or at a location where high interfacial shear stress arise due to local yielding of steel section. While the end-plate debonding mode occurs when the debonding initiates at the FRP plate end due to high interfacial shear stress and peeling stress. The researchers raised several issues which didn't receive sufficient investigations and should be given attention in future research like the durability of the bonding adhesive, fire resistance of FRP-strengthened structures, strengthening of steel structures against blast and impact loading, and the use of external FRP reinforcement for both strengthening and corrosion resistance.

Saleem *et al.* (2010) developed a nonlinear 3D FE model, using the general purpose finite element program ABAQUS, to investigate the mode of failure and flexural behavior of both steel and steel–concrete composite beams strengthened by different lengths of CFRP plates. The developed 3D FE model accounted for the geometric and material nonlinearities. An eight-node brick element was employed to model the concrete slab, steel beam, adhesive layer, and CFRP plate. The FE results were validated against a previous experimental study. The researchers concluded that the growth of intermediate debonding leading to a complete debonding failure was prevented by splices near the supports of the beam. Reverse tapered splice plate ends did not suffer from the peak shear stress as the traditional one. So, this geometry has a higher resistance to debonding failure.

Recently the effect of CFRP laminate length on the mechanical behavior of continuous steel beams was investigated numerically by Kadhim (2011). The finite element analysis was carried out using the general purpose finite element software ANSYS. The results obtained from the 3D FE analysis were validated against results from a previous experimental work. Brick elements were used to simulate the steel beam, while shell elements were used to simulate the CFRP laminates. The steel material was assigned a bilinear stress-strain relation, while the CFRP was modeled as a linear elastic material. The 3D FE model was employed to five small-scale beams similar to those tested experimentally by Jun (2007). The Finite element analysis showed that when the length of CFRP laminate reached 40% of span length in sagging region and 60% of beam length in hanging region, insignificant increase in the ultimate load-carrying capacity occurs.

post-yield modulus of steel. More details about the outcomes of Alhadid's study are presented, wherever applicable, in Chapters 3 and 4.

2.6 Conclusions

According to the preceding literature review related to strengthening reinforced concrete, steel and composite beams using FRP materials, it can be seen that there is only one experimental research study that investigated strengthening of steel beams with mechanically fastened FRP (MF-FRP). However, some researchers [eg. Edberg *et al.* (1996)] used steel fasteners to prevent debonding of FRP laminates externally bonded to the tension flange of the steel beams. The experimental work done by Alhadid (2011) on the mechanical behavior of steel beams strengthened with mechanically fastened FRP laminates was limited to investigate few parameters related to the considered length and thickness of FRP laminates experimentally. Therefore, the need to understand more about the characteristics of the MF-FRP system in strengthening steel beams was the driving force behind this current study.

2.5 Mechanically Fastened FRP for Strengthening of Steel Beams

To the author's knowledge in 2013, the first attempt for using mechanically fastened fiber reinforced polymer strips in strengthening steel beams was carried out by Alhadid (2011). The study investigated the performance of 24 mechanically fastened steel-FRP connections experimentally. A non-linear load-slip relationship was established based on the experimental findings. The interfacial load-slip relationship was incorporated in a 3D FE analysis to examine the influence of various design parameters on the connection behavior. Additionally, Alhadid tested eight beams strengthened with FRP laminates of different lengths and thicknesses. The FRP laminates lengths were 1200, 1800 and 2200 mm, the beams where strengthened with one and two layers of FRP laminates. The typical FRP laminate was 100 mm wide and 3.175 mm thick. Three steel beams (with no FRP) were also tested and used as control specimens. The base steel section in all of these beams was UB 203x102x23 with total length of 3000 mm and span of 2750 mm. The strengthened beams exhibited ductile failure mode accompanied by bearing in the FRP laminate when sufficient number of fasteners were used. On the contrary, the strengthened beams with insufficient fasteners failed in a brittle manner by sudden shear failure in the fasteners. The experimental results also revealed that increasing the thickness and length of FRP results in a slight improvement in the yield moment (i.e., moment at first yield in the steel section) but a significant enhancement in the ultimate flexural capacity of the strengthened beams. The investigation showed that the contribution of the FRP laminates becomes noticeable after the initiation of yielding of the bottom steel flange where the elastic modulus of the FRP becomes higher than the

beams. Then, the FE model of the composite beams is validated against the experimental results reported in the research work by Alhadid (2011).

3.2 Finite Element Method Background

The Finite Element Analysis (FEA) is a mathematical technique used to find approximate numerical solutions for partial differential equations over complicated domains. Solving complex elasticity problems was the driving force behind establishing the FEA in civil, mechanical, and aeronautical engineering. Alexander Hrennikoff (1941) and Richard Courant (1942) have used mesh discretization of a continuous domain into a set of discrete sub-domains, usually called elements [Pelosi, G. (2007)]. In 1947 Olgierd Zienkiewicz gathered their work into what is called the Finite Element Method of today [Stein E. (2009)]. The development of the computational capabilities of computers by the early 1960s has empowered the applications of the FEM in the different engineering applications.

The Finite Element Method has been used successfully to study the elastic and inelastic behavior of various structural elements. Typically, the FEM starts with the discretization of the considered structure through creating the FE mesh where each element is connected to the adjacent elements through nodes. The solution of the partial deferential equations that govern the stress-deformation relationship is approximated at the element level. The deformation field is then approximated by piecewise deformation functions along each element (typically called shape functions). Boundary conditions are typically applied at the mesh nodes to represent forces and supports. A set of

CHAPTER 3

FINITE ELEMENT MODELING OF COMPOSITE STEEL-FRP BEAMS

3.1 Introduction

As discussed earlier, one of the objectives of this study is to investigate the mechanical behavior of composite steel-FRP beams. In this regard, two approaches may be followed; namely experimental and numerical. The experimental approach, where small-scale (or full-scale) prototypes of the beams under consideration are built and tested up to failure or excessive deflection, would result in more realistic representation of the beam behavior. However, this approach is costly and can only be adopted for a limited number of specimens. Therefore, numerical simulation would be a more affordable and risk-free approach especially if a parametric study is required to show the effects of the different geometrical and/or material parameters on the behavior of the considered beams.

The Finite Element Method (FEM) is a well-established numerical simulation technique that has been extensively used by many researchers in the area of stress analysis. The following sections report on the implementation of the FEM in studying the mechanical behavior of composite steel-FRP beams under flexural stresses. Firstly, a brief background about the FEM is provided followed by a description of the developed FE model, material properties and boundary conditions of the composite steel-FRP

stresses are required. In other words, this simple type of analysis does not require incremental application of the loads.

3.2.2 Non-linear Elasto-Plastic Finite Element Analysis

Two of the major sources of non-linearity in solids and structures are considered in the current study. The first source is the geometrical non-linearity where significant change in geometry of the solid or structure during applying the load increments is experienced. The second source arises from elasto-plastic material non-linearity where stress is non-proportional to strain and the material experiences yielding and plastic deformations. In non-linear finite element analysis, the stiffness matrix $[K]$ is no longer constant as it becomes dependent on both the geometry and the stress level in the solid/structure at the instant of load increment application. Therefore, the non-linear stiffness matrix $[K_T]$ relates the incremental loads to the corresponding incremental deformations as in the following equation

$$\{\mathrm{d}F\} = [K_T]\{\mathrm{d}u\} \tag{3.3}$$

3.2.3 Newton-Raphson Procedure for Incremental Load Application

The Newton-Raphson procedure is often used for the solution of non-linear problems. In this iterative procedure, the load is applied in increments through the application of the following constraint condition to the finite element governing equation

$$\{\mathrm{d}F\} = \{F_{n+1}\} - \{F_n\} \tag{3.4}$$

where n is the index of the load increment.

simultaneous linear equations are developed and used as an approximation of the solution of the partial differential equations of equilibrium. These equations relate the change in nodal forces $\{dF\}$ to the change in nodal displacements $\{du\}$ through a matrix called the stiffness matrix of the structure $[K]$. This can be written as:

$$\{dF\} = [K]\{du\} \tag{3.1}$$

The structural stiffness matrix $[K]$ is dependent on the geometry of the deformed structure and the stress and strain histories of the elements during incrementing the load to reach its final value. If load is applied in increments, Eqn. 3.1can be used to obtain the corresponding increments of deformations. These incremental deformations are used to obtain incremental strains which in turn define the corresponding incremental stresses through the proper material constitutive relationships. Total deformations, strains, and stresses may be obtained by summing their incremental counterparts as the applied load advances in a predefined loading scenario.

3.2.1 Linear Elastic Finite Element Analysis

This simple type of analysis applies to structures with linear elastic materials that undergo insignificant change in their initial geometry after deformation (i.e., small deformations). In this particular case, the stiffness matrix $[K]$ becomes constant $[K_E]$ and Eqn. 3.1 may be written as:

$$\{F\} = [K_E]\{u\} \tag{3.2}$$

This equation implies that the deformations are proportional to the total applied loads. As such, the loads can be applied with their full values at which deformations and

stiffness matrix $[K_T]_1$. The total incremental deformation $\{u_{n,i}\}$ at the end of iteration (i) is expressed as

$$\{u_{n,i}\} = \{u_n\} + \Delta\{u_i\} = \{u_n\} + \sum_{j=1}^{j=i} \delta\{u_j\} \tag{3.5}$$

where $\{u_n\}$ is the total deformation vector at the end of the n^{th} load increment.

The iterative procedure continues until the convergence of the equilibrium condition is achieved (i.e., norm of the residual forces $\|\{R_i\}\|$ approaches a negligible value) which is termed "*Force Convergence Criterion*" and is expressed as

$$\|\{R_i\}\| / \|d\{F\}\| < Tolerance \tag{3.6}$$

or, norm of the iterative deformation $\|\delta\{u_i\}\|$ becomes negligible which is referred to as "*Displacement Convergence Criterion*" and is given by

$$\|\delta\{u_i\}\| / \|\Delta\{u_i\}\| < Tolerance \tag{3.7}$$

The *Tolerance* is typically assigned a small value (e.g., 0.001) that is sufficiently near to zero [Gerald *et al.* (2003), Mathews and Kurtis (2004)].

Despite the rapid quadratic convergence of the Newton-Raphson procedure, it can be time consuming and inconvenient in some particular situations. This is due to the fact that the tangent stiffness matrix $[K_T]$ has to be calculated and factorized at each iteration. One way to avoid this problem is to formulate the tangent stiffness matrix only at the first one or two iterations (the Modified Newton-Raphson Method) while it is kept constant over the rest of the iterations. This would save computing time, but will slow down the convergence rate and more iterations may be required. Another drawback of both the Newton-Raphson method and its modified version is that they fail once a behavior

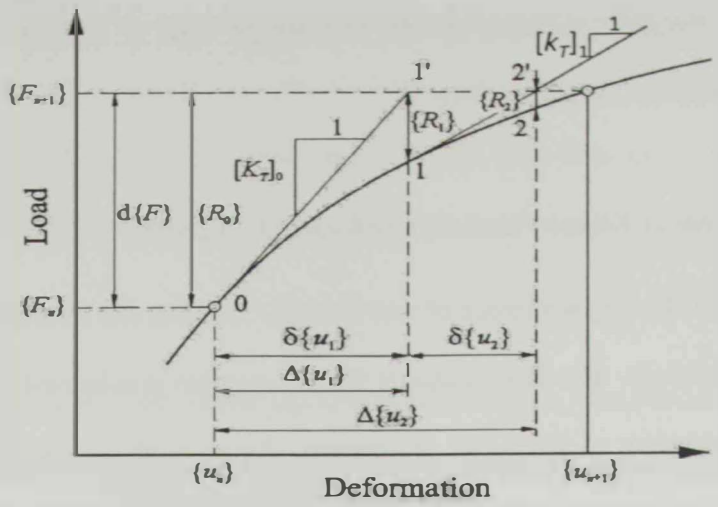

Figure 3.1: Newton-Raphson Iterative Procedure

Figure 3.1 illustrates the incremental load and associated iterative equilibrium solution approach. In this solution procedure, the stiffness matrix $[K_T]$ (called tangent stiffness matrix) is fully calculated at the start of each iteration and termed $[K_T]_i$, where i is the iteration index. The solution starts with the calculation of the tangent stiffness matrix at the end of the previous load increment (termed $[K_T]_0$). This tangent stiffness matrix along with the load increment $d\{F\}$ are used to obtain first iterative solution for the deformations $\delta\{u_1\}$ which can be used to obtain the iterative strains and stresses. The convergence or equilibrium of the first iterative solution is checked by assessing the difference between the integration of the total internal stresses over the volume and the overall external loads (not incremental ones). This difference is termed residual forces and denoted by $\{R_1\}$ where the subscript refers to the iteration index. The negative values of residual force vector, in turn, are applied to the system again with a new tangent

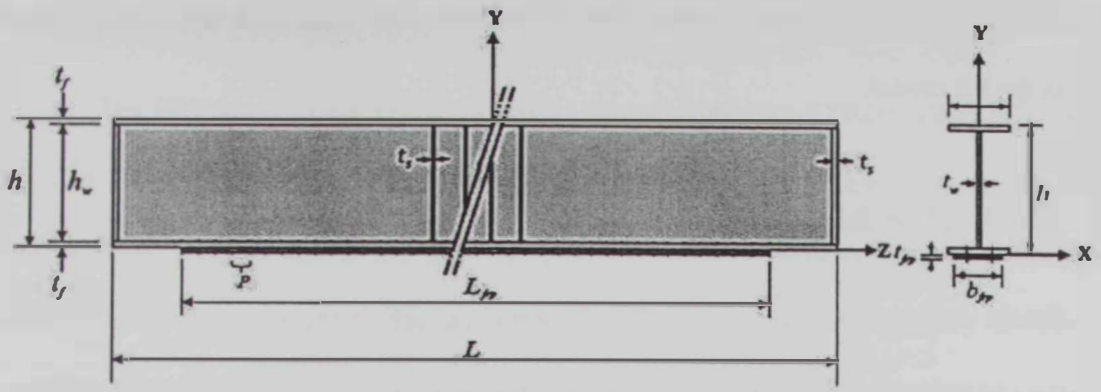

Figure 3.2: Typical Geometry of Composite Steel-FRP Beam

As indicated in Fig. 3.2, the depth of the beam is directed along the *Y*-axis while its span coincides with the *Z*-axis. The beam geometry is characterized by its span L (i.e., distance between supports), flange width b_f, flange thickness t_f, web height h_w, and web thickness t_w. The FRP laminates geometry is characterized by the length L_{frp}, thickness t_{frp} and width b_{frp}. The pitch size (longitudinal distance between fasteners) is denoted as P. The beam is simply supported at its left and right ends. Stiffener plates with thickness t_s are used at both ends of the beam to avoid web crippling due to concentrated reaction forces. Similar stiffeners are also used at (and around) the point of application of the mid-span concentrated load as shown in Fig. 3.2.

3.3.1 Description of the Finite Element Model

A three dimensional (3D) finite element model is developed using ANSYS (2011) to simulate the behavior of composite steel-FRP beams. The following sections provide

exhibiting a peak load is encountered. Thus the peak load is underestimated because a numerical, rather than structural, instability occurs. At this time, it is crucial to resort to another technique that works for peak load cases. The Arc-Length Control Method emerges as a convenient alternative for these cases [Crisfield (1981)].

In the current study the Newton-Raphson method will be used, as the structural system will be displacement-controlled, where the displacement increments will be applied at the mid span of the composite beams. This will help to overcome the instability issue encountered by Newton-Raphson at the peak load.

3.3 Finite Element Model of Composite Steel-FRP Beams

The Finite Element Method is used to model full-scale simply supported composite steel-FRP beams bent about their major flexural axis under the effect of a concentrated mid-span load. The FE model is expected to simulate the flexural behavior of the considered beams, predict the ultimate load capacities, and capture any local or global buckling modes. The general-purpose finite element software ANSYS (2011) is utilized to perform the FE simulation. The nonlinearity considered in the finite element analysis is due to both geometrical and material nonlinearities.

Figure 3.2 shows the geometry of a typical composite steel-FRP beam considered in the current study. The geometry is defined using a global Cartesian coordinate system with its origin located at the bottom of the steel cross section at the mid-span of the beam.

Fiber Reinforced Polymer (FRP):

The FRP used in the current study is manufactured by STRONGWELL®. This kind of FRP can be drilled without significantly affecting the mechanical properties of the laminate. This is due to the fact that such laminates include carbon tows that are sandwiched between layers of fiberglass mats and bonded together by a highly corrosion resistant veinylester resin. This combination of materials improves the bearing properties of the laminates that is mainly provided by the glass mat (GFRP mat) that surrounds the carbon fibers.

The FRP was modeled as a linear elastic material with different material characteristics in the various working directions. The elastic moduli, shear moduli and Poisson's ratio values are shown in Table 3.1 (Kachlakev and McCurry, 2000) for a composite FRP plate with its longitudinal fibers directed in the Z-direction.

Table 3.1: Summary of Material Properties for FRP Composites

Direction	Elastic Modulus (MPa)	Poisson's Ratio	Shear Modulus (MPa)
Out-of plane of laminate	$E_x = 4800$	$\nu_{xy} = 0.3$	$G_{xy} = 1967$
in-plane of laminate and ⊥ to fibre direction	$E_y = 4800$	$\nu_{xz} = 0.22$	$G_{xz} = 3270$
in-plane of laminate and parallel to fibre direction	$E_z = 62190$	$\nu_{yz} = 0.22$	$G_{yz} = 3270$

Load-Slip Relationship of Fasteners:

As reported by Alhadid (2011), the load-slip relationship, shown in Fig. 3.4, corresponds to a particular case of the interfacial behavior of steel-FRP connection,

details about the material models, types of elements, loads, and boundary conditions used in the FE model.

3.3.1.1 Material Models

Steel:

The steel material is known to exhibit an elasto-plastic stress-strain relationship. Figure 3.3 shows the typical uniaxial multi-linear stress-strain relationship defined by the steel's elastic Young's modulus E, tangential modulus E_t, yield stress F_y, and ultimate stress F_u. In this study, E_t is assumed to be $0.03E$ and Poisson's ratio v to be equal to 0.3. For the case of elastic steel material (i.e., no yielding), only E and v are required to be defined.

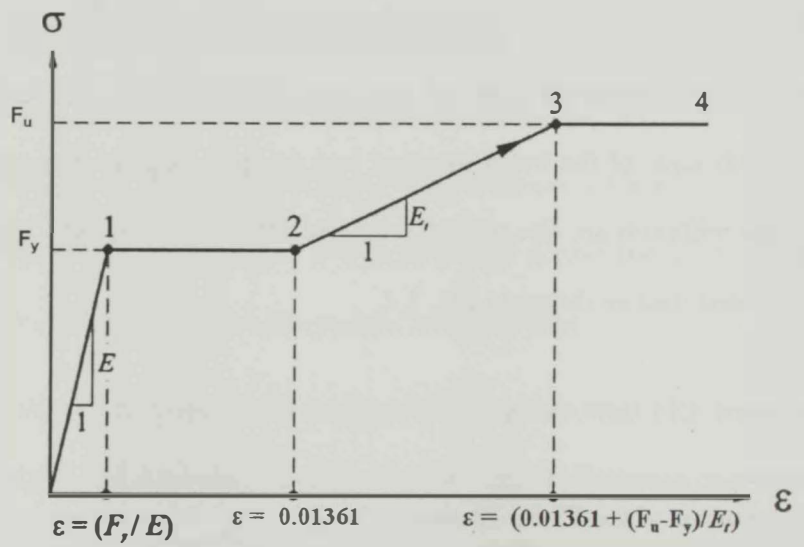

Figure 3.3: Material Model Used to Simulate the Mechanical Properties of the Steel

3.3.2 Types of Elements

An 8-node solid element, SOLID45, is used to model both the steel beam and FRP laminates. The element is defined by eight nodes each having three translational degrees of freedom in the x, y, and z directions. The general geometry and node locations for this element are shown in Fig. 3.5. The element is able to model large deformations and large strain in addition to material nonlinearities defined earlier for the steel material.

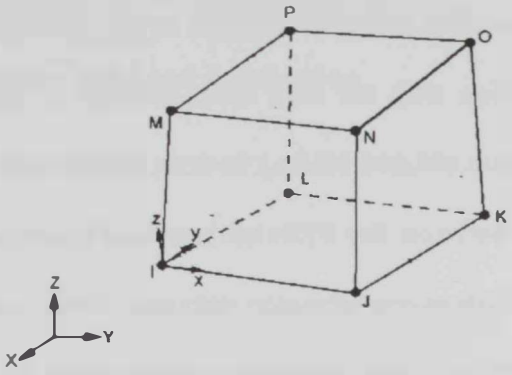

Figure 3.5: SOLID45, 3-D structural Solid Element as Defined in (ANSYS 2011)

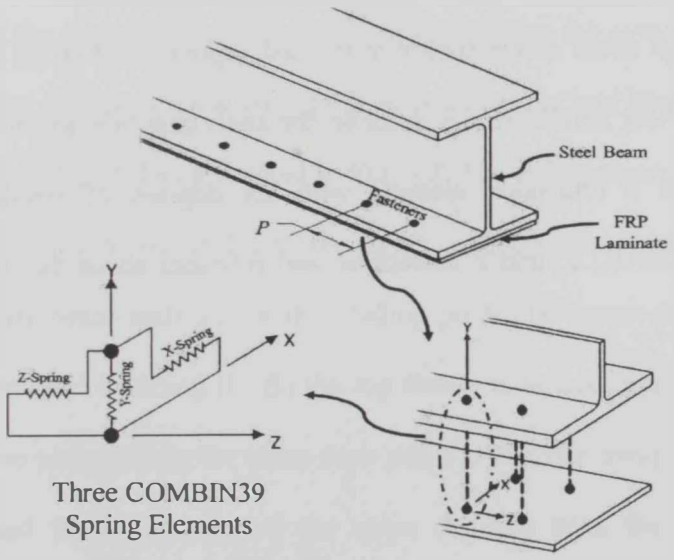

Figure 3.6: Fasteners and Spring Elements in X, Y, and Z Directions

where the SAFESTRIP FRP laminate has a thickness of 3.175 mm and the steel fastener diameter is 6-mm. The relationship is initially linear until it reaches a value of about 7.5 kN, after which small parts of the GFRP mats around the fastener holes start to rupture associated with significant increase in the slip with slight increase in the load. This response is characterized by noticeable bending in the fasteners in addition to significant bearing deformations at the bolt holes. Beyond slip of about 9-mm, the load values start to pick up again with remarkable peeling of the GFRP mats associated with folding of the washers. Once the peak load is reached at about 13-mm slip, gradual excessive bearing damage takes place leading, finally, to progressive tearing out of the FRP laminates. This damage results in failure of the connection associated with reduction in its load carrying capacity.

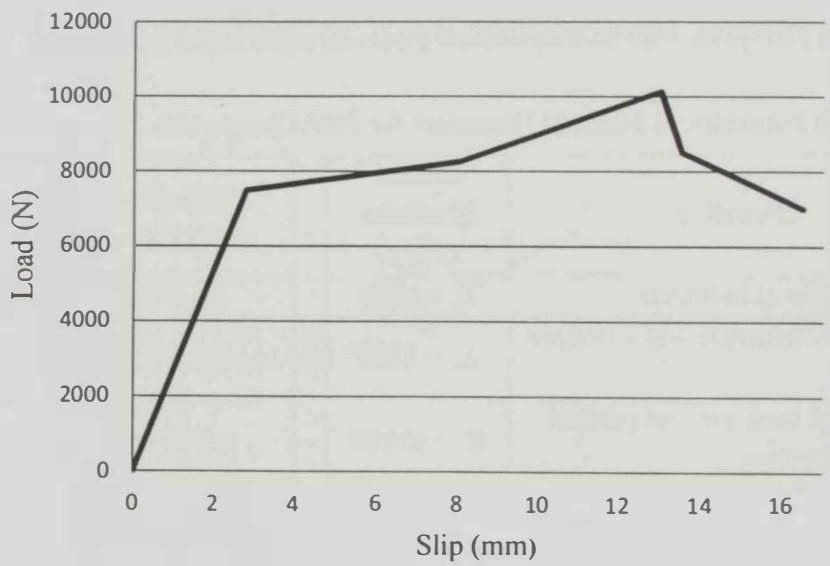

Figure 3.4: Load-Slip Relationship as Obtained Through Experimental Results [Alhadid (2011)]

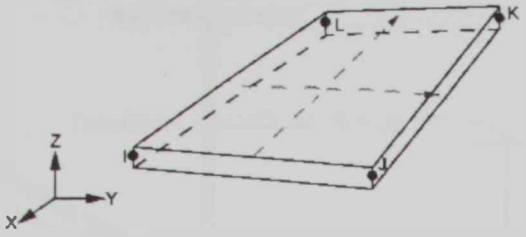

Figure 3.7: 4-Node Structural Shell Element, SHELL181, as Given by ANSYS (2011)

3.3.3 Boundary Conditions and Load Application

Figure 3.8 shows the general geometry of the composite steel-FRP beam with its applied boundary conditions. The beam is subjected to a mid-span point load and supported on rollers at its left and right ends. Accordingly, vertical displacements U_y and lateral displacement U_x are restrained at the bottom nodes of the cross section at both supported ends. Besides, the displacements in the longitudinal direction U_z are restrained at the all nodes of the cross section at the mid span to enforce the symmetry condition in the Z-direction. The stiffeners installed at both ends and at the mid span of the beam are part of the geometrical model as presented in Fig. 3.8. The stiffeners are used to eliminate the local buckling that may occur due to the stress concentration at some points on the cross-sections at the beam ends and at the loading point. To ensure that the beam will have no lateral torsional buckling (LTB) the top flange is braced in the lateral direction (i.e., $U_x = 0$) at two points along the beam (one point is 355 mm away from mid-span in the Z-direction and the other point at the same distance from the mid-span on the

In the adopted strengthening technique, mechanical fasteners are used to connect the FRP laminate to the bottom flange of the steel beam. In the developed FE model, multi-linear spring elements *COMBIN39* are used to simulate the action of fasteners. This element is defined by two (preferably coincident) node points and a generalized force-deflection relationship. Three spring elements are typically used to simulate the behavior of the real fastener in the three directions of action X, Y and Z as shown in Fig. 3.6. The idealized load-slip relationship for the spring element in the Z direction was identified experimentally by Alhadid (2011) as depicted in Fig. 3.4. The spring in the Y direction (the vertical interaction with the steel cross section) is assigned a significantly high fastener stiffness value (50,000 N/mm) in both tension and compression such that no overlapping occurs between the FRP laminate and the Steel flange. Meanwhile, the spring acting in the transverse direction although is not contributing in carrying any loads, it is assumed to have same properties as the element in the Z direction.

The 4-node shell elements *SHELL181* are used to simulate the stiffeners at the locations of high stress concentration at the end supports and at the loading point at the mid span. Element *SHELL181* is suitable for analyzing thin to moderately-thick shell structures. It is a four-node element with six degrees of freedom at each node; translations in the X, Y, and Z directions, and rotations about the X, Y, and Z-axes as shown in Fig. 3.7.

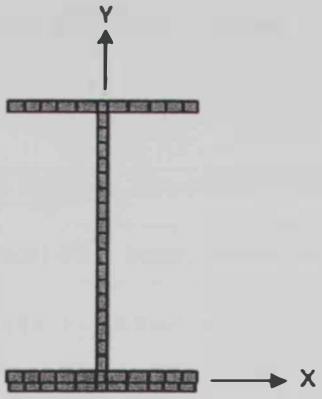

Figure 3.9: Typical Cross-Sectional View of the Mesh of the Composite Steel-FRP Beam

A convergence study is carried out to verify the adequacy of the selected element sizes. Figure 3.10 shows sample results of the convergence study in which the element sizes are changed according to the limitations mentioned above. The applied mid-span load at an arbitrary deflection value at the mid-span (120 mm in this case) are plotted for several various size configurations. Accordingly the final elements sizes are selected such that the increase in the number of elements does not result in change in the results. A typical mesh configuration is shown in Fig. 3.11 for a British universal beam UB 203x102x23 with the following dimensions (in mm): L= 2750, t_f= 9.3, b_f= 101.8, t_w = 5.4, h_w = 184.6, t_{frp}= 3.175, b_{frp}= 100.

opposite direction). Meanwhile, the rest of the nodes are left unrestrained against any kind of deformation.

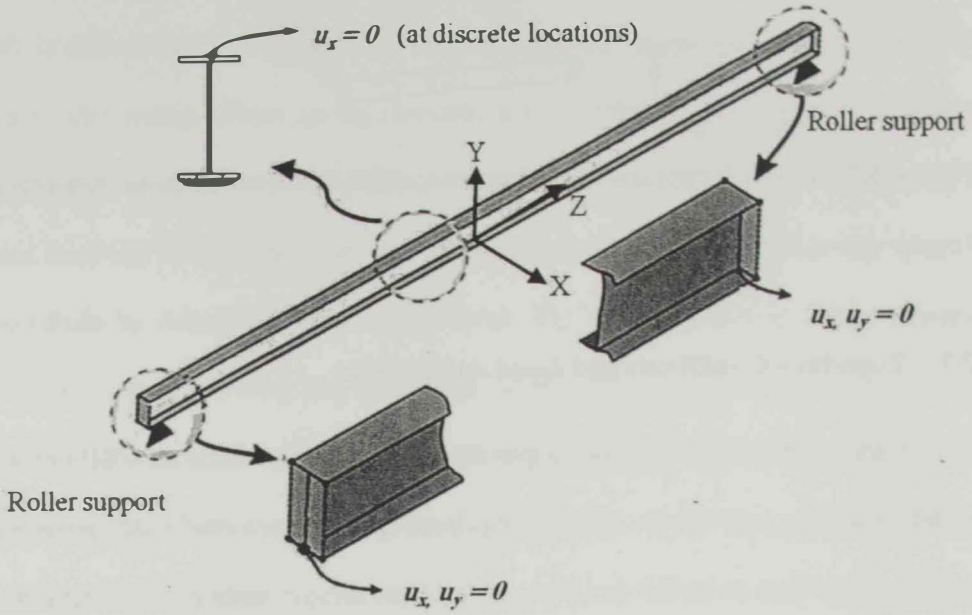

Figure 3.8: Boundary Condition for a Typical Composite Steel-FRP Beam

3.3.4 Element sizes and Meshing Considerations

As it was mentioned before, the steel beam cross section is modeled by solid elements (*SOLID45*). The side length of the element in the X and Y directions is selected not to exceed twice the thickness of the web as shown in the cross-sectional view of the composite steel-FRP beam presented in Fig. 3.9. The maximum length of the element in the Z direction is set to be four times the side length in the other two directions. The selected sizes for the elements are selected to ensure convergence of the solution within a reasonable execution time.

3.4 Validation of the Finite Element Model

To verify the performance of the developed three dimensional finite element model described in the previous sections, the model is employed to simulate the elasto-plastic behavior of composite steel-FRP beams under mid-span concentrated loads that have been studied experimentally by Alhadid (2011). The obtained mid-span load-deflection results from the FE analysis of the considered beams are compared to the experimental outcomes to validate the accuracy of the proposed model.

The experimental study investigated the enhancement in the load-carrying capacity of steel beams strengthened with FRP laminates, with different lengths and thicknesses, that are anchored to the bottom flange. The 3D FE model incorporates all the geometrical details and material models as described by Alhadid (2011) in his study. The material properties of the FRP are summarized in Table 3.1. The steel material properties are F_y = 335 MPa, F_u = 429 MPa. The cross-section of all the beams tested is UB203x102x23. Five 12-mm thick stiffeners are welded to the steel beam at mid-span. The load-slip relationship of a 6-mm diameter fastener in a 3.175-mm thick FRP laminate is given in Fig. 3.4. Since bearing deformations around the holes in the FRP laminate control the load-slip behavior [Alhadid (2011)], the loads in the load-slip relationship shown in Fig. 3.4 are scaled by (t_{frp} / 3.175 mm) for laminate thicknesses other than 3.175-mm.

Figure 3.2 shows a typical steel beam used by Alhadid (2011) with the following dimensions (in mm): L= 2750, t_f= 9.3, b_f= 101.8, t_w= 5.4, h_w= 184.6, b_{frp}= 100. Alhadid tested a group of eigth UB203x102x23 beams; three control steel beams (i.e., without

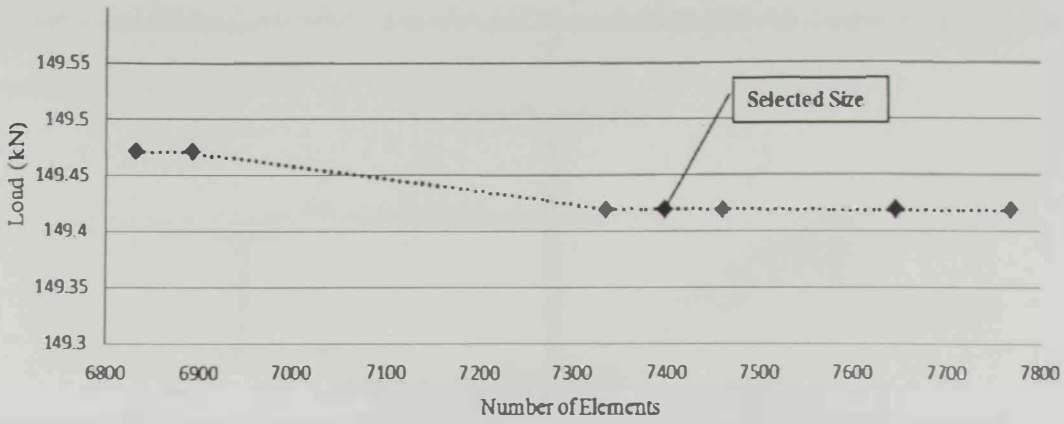

Figure 3.10: Results of Convergence Study, Mid-Span Load at 120 mm Mid-Span Deflection Versus Number of Elements for Different Mesh Sizes

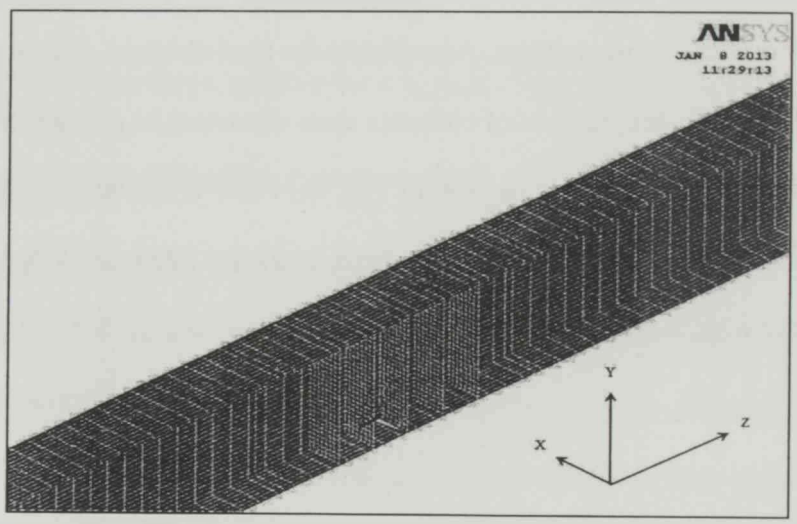

Figure 3.11: Typical Mesh Configuration for Composite Steel-FRP Beams (UB203x102x23, L = 2750 mm, t_{frp} = 3.175 mm, b_{frp} = 100 mm)

model is capable of simulating the latter failure mode only (as defined by the load-slip relationship of the fastener in Fig. 3.4).

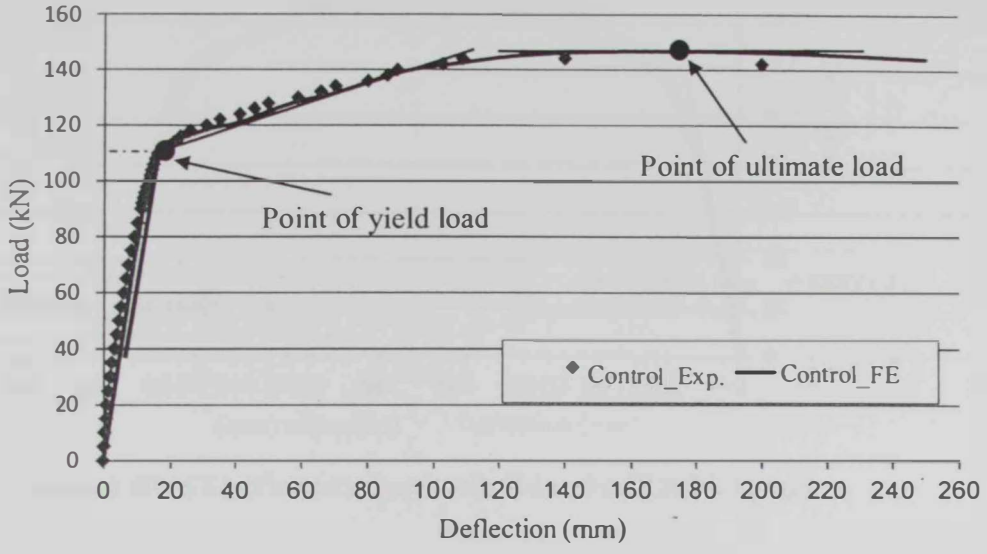

Figure 3.12: The Load-Deflection Curves of the Control Beam Specimen

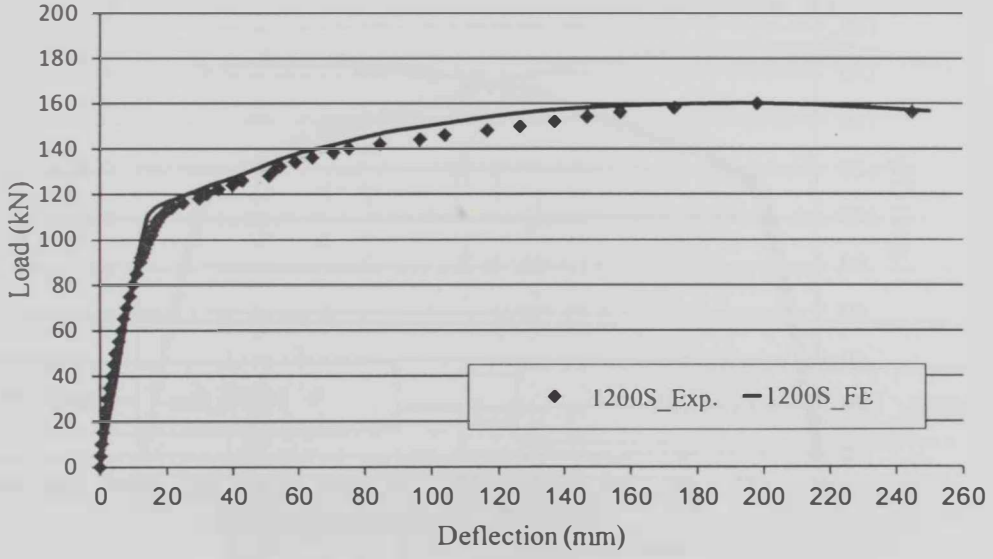

Figure 3.13: The Load-Deflection Curves of the 1200S Specimen

FRP) and five composite steel-FRP beams. The main differences between the tested beams are the FRP length (L_{frp}) and thickness (t_{frp}). The beams are labeled as xxxxS or xxxxD where "xxxx" stands for the length of FRP in mm, "S" indicates a single layer of FRP (i.e., t_{frp} = 3.175 mm), and "D" refers to double layers of FRP (i.e., t_{frp} = 6.35 mm). Table 3.2 shows the different beams used in the validation study along with their corresponding parameters.

Table 3.2: Basic Parameters of the Different Beams Used in the Validation Study

#	Beam Designation		FRP Length (mm)	Number of FRP Layers	FRP Thickness t_{frp} (mm)
	Experimental	Finite Element			
1	Control	Control_FE	--	--	--
2	1200S	1200S_FE	1200	1	3.175
3	1200D	1200D_FE	1200	2	6.35
4	1800S	1800S_FE	1800	1	3.175
5	2200S	2200S_FE	2200	1	3.175
6	2200D	2200D_FE	2200	2	6.35

The experimental mid-span load-deflection results are reported in Fig. 3.12 to Fig. 3.17 as dots while the FE predictions are shown as solid lines. A simple look at these figures show the excellent agreement between the numerical and experimental results except for the 1200D specimen as presented in Fig. 3.14. It is important to note that Alhadid (2011) reported that the failure mode of specimen 1200D was due to shear failure in the fasteners while all the other specimens failed due to bearing in FRP laminates around the fasteners holes. The deviation between the experimental results and numerical predictions of this particular specimen is attributed to the fact that the FE

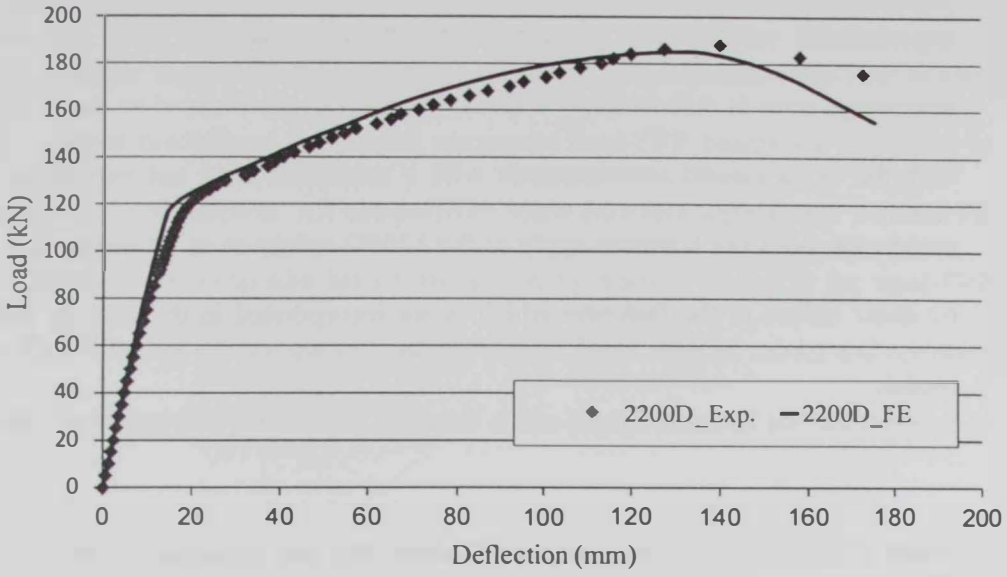

Figure 3.16: The Load-Deflection Curves of the 2200D Specimen

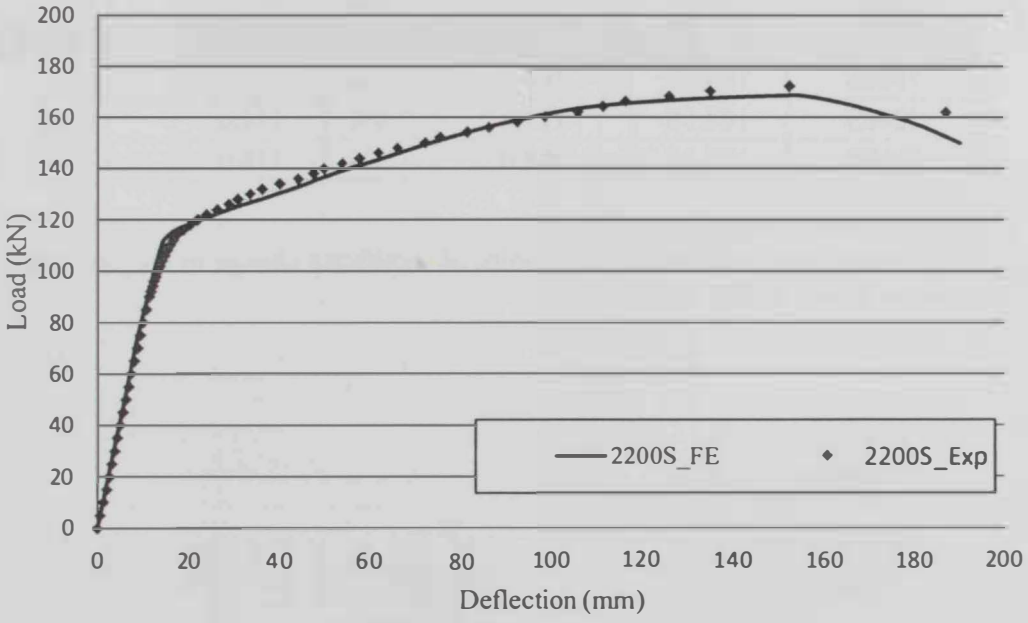

Figure 3.17: The Load-Deflection Curves of the 2200S Specimen

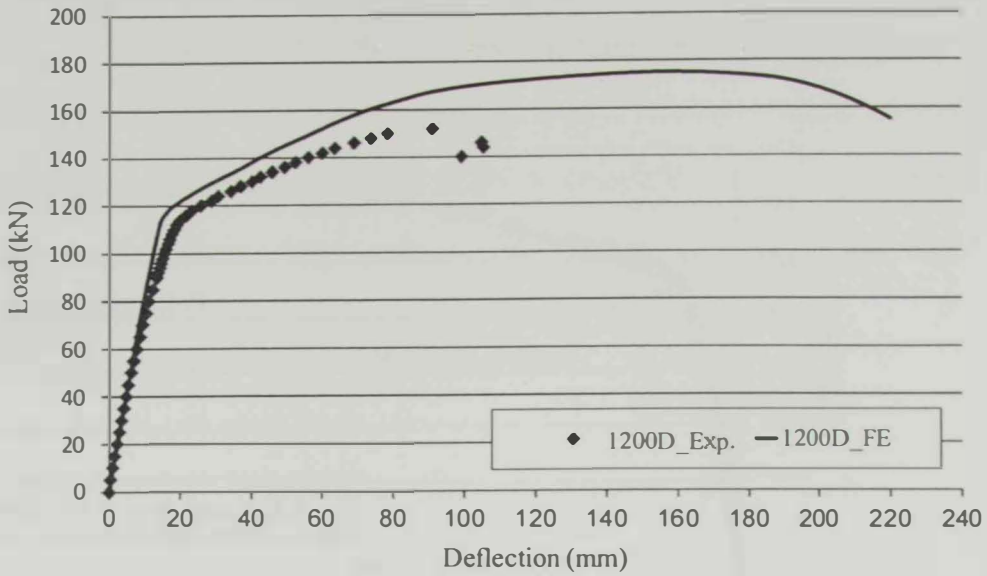

Figure 3.14: The Load-Deflection Curves of the 1200D Specimen

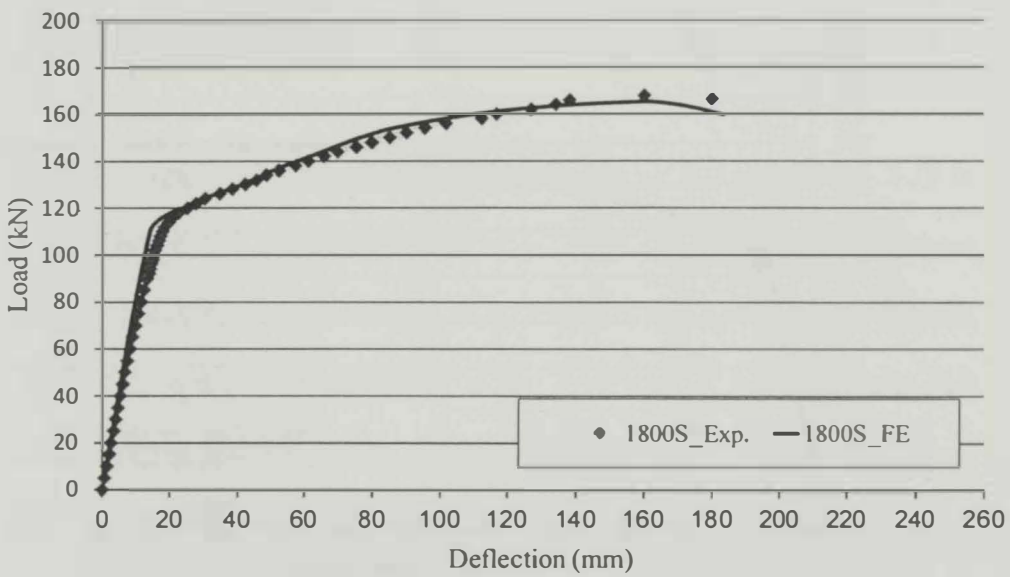

Figure 3.15: The Load-Deflection Curves of the 1800S Specimen

3.5 Conclusions

This chapter reports on finite element modeling of composite steel-FRP beams. The finite element predictions for several composite steel-FRP beams are compared to their experimental counterparts. All comparisons show excellent agreements with the FE results for behavior of composite beams dominated by bearing failure at the steel-FRP interface. This validates the accuracy of the developed finite element model and confirms its reliability to be used in performing in-depth elasto-plastic flexural studies reported in Chapter 4.

Table 3.3 shows a summary of the comparison between the FE predictions and the experimental results. The yielding and ultimate loads are both reported and the percentage error is calculated. It is clear that the FE results show an excellent agreement with the experimental measurements with a maximum error not exceeding 2.6%. This conclusion does not however apply to the 1200D specimen as its response is dominated by shear failure in the fasteners which is not incorporated in the adopted finite element model.

Table 3.3: Comparison Between the FE Model and The Experimental Results of Steel-FRP Beams

Specimen	Ultimate load (kN)		% Δ*	Yielding load (kN)**		% Δ*
	FE Model	Exp. Results		FE Model	Exp. Results	
Control	146.70	144.0	1.9%	109.0	110.0	0.9%
1200S	160.18	160.0	0.1%	110.0	112.0	1.8%
1200D	175.11	152.0	15%	112.5	114.0	1.3%
1800S	165.33	168.0	1.6%	111.0	112.0	0.9%
2200S	168.50	172.0	2.0%	114.0	117.0	2.6%
2200D	185.18	188.0	1.5%	118.0	120.0	1.7%

* % Δ = (Exp. – FE)/(FE)%.
** Yielding load is estimated at the point of significant change in the load-deflection slope as shown in Fig. 3.12.

is always realized in real life applications. In order to understand the improvement of the mechanical behavior of traditional steel beams when strengthened with FRP laminates, it is essential to estimate the internal shear forces induced in the fasteners and the corresponding relative slip at the steel-FRP interface. The work presented in this chapter aims at the understanding of the mechanical behavior of partial composite steel-FRP beams under the effect of mid-span point load.

4.1.1 Fully Composite Beams

The classical Euler–Bernoulli elastic beam theory assumes that "*any plane cross-section remains plane after deformation*" (i.e., no relative slip occurs between layers of the cross-section). This assumption simplifies the prediction of the mechanical behavior of any elastic composite beam which is termed as *fully-composite*. In this case, the shear force generated in any fastener connecting the components of a typical elastic fully-composite steel-FRP beam (Fig. 4.1) can be estimated as:

$$F_{fastener} = \tau\, p = \frac{V\, S}{I}\, p \qquad (4.1)$$

where

$F_{fastener}$: shear force in the fastener

τ: longitudinal shear flow between the steel beam and FRP laminate

V: shear force in the composite beam's cross-section

S: first moment of area of the steel beam cross-section about the centroid axis of the transformed steel-FRP section shown in Fig 4.2. Transforming the FRP area to its

CHAPTER 4

MECHANICAL BEHAVIOR AND PARAMETRIC STUDY OF STEEL-FRP BEAMS

4.1 Introduction

In a typical mechanically fastened steel-FRP composite beam system, the fasteners connect different longitudinal components of the system to ensure that the different layers at any cross-section work together to withstand bending moments and shear forces developed in the beam due to the applied loads. The fasteners in this type of composite beams carry the shear forces that develop at the interface between steel beam and FRP laminate. Therefore, it is anticipated that the mechanical behavior of such beams depends mainly on the magnitude of the shear forces induced in the fasteners. In other words, the degree of composite action (i.e., amount of strain compatibility between the connected steel flange and FRP laminates at the location of the fasteners) is influenced by the shear forces in the fasteners. If no relative slip exists between the steel and FRP at the interface, the steel-FRP system is said to have *full-composite* action otherwise *partial-composite* action exists where relative slip, small or large, occurs at the steel-FRP interface.

Although a steel-FRP beam with full-composite action is the target of any designer because of its higher strength and stiffness, there is no guarantee to achieve it within practical and economical design constraints. Therefore, a partial composite system

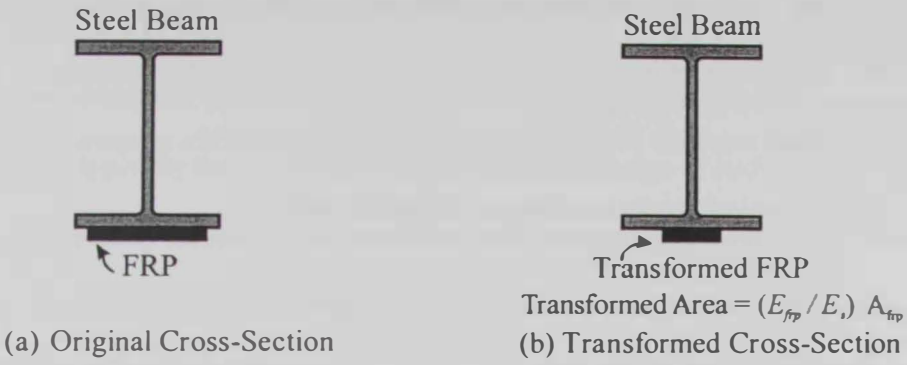

(a) Original Cross-Section (b) Transformed Cross-Section

Figure 4.2: Original and Transformed Steel-FRP Cross-Section

If the equilibrium of the steel beam is studied separately from the FRP laminate (Fig. 4.3), it is obvious that the shear forces developed in the fasteners create a bending moment in the steel beam that counteracts the bending moment due to applied load. In other words, the bending moment carried by the steel beam becomes less than the bending moment due to the applied load. The difference between the formerly mentioned bending moment values is carried internally by the developed compression in steel beam and tension in the FRP laminate. This is the main source of the strengthening effect when FRP laminate is fastened to the steel beam (Fig. 4.3).

It is also important to note that the ratio between the elastic modulus of FRP (i.e., E_{frp}) and the modulus of steel (i.e., E_s) affects the contribution of the FRP to the load-carrying capacity of the composite beam. If the FRP modulus is significantly less than that of the steel, the FRP laminate is not expected to contribute significantly in carrying the loads until the extreme fibers of the steel section starts to yield. In such a case, negligible additional resistance is provided by the yielded bottom steel flange while the FRP laminate, which is still elastic, becomes more efficient in carrying the tensile stresses. On the other hand, significant contribution of the FRP could be attained, even

equivalent steel area is achieved by multiplying the area of FRP by the ratio of its elastic modulus E_{frp}, relative to the elastic modulus of steel, E_s (i.e., E_{frp} / E_s).

I: moment of inertia of the transformed steel-FRP cross-section

p: pitch of the fasteners (spacing between fasteners)

Equation 4.1 shows that the shear force $F_{fastener}$ in any fastener is proportional to the shear force V developed in the fully-composite beam at the location of the fastener under consideration. Therefore, the distribution of the shear forces in the fasteners typically matches that of the shearing force along the beam. For example, in the case of fully composite steel-FRP beam under three-point loading scheme, the shear forces in all the fasteners are constant in magnitude and their directions are as shown in Fig. 4.1.

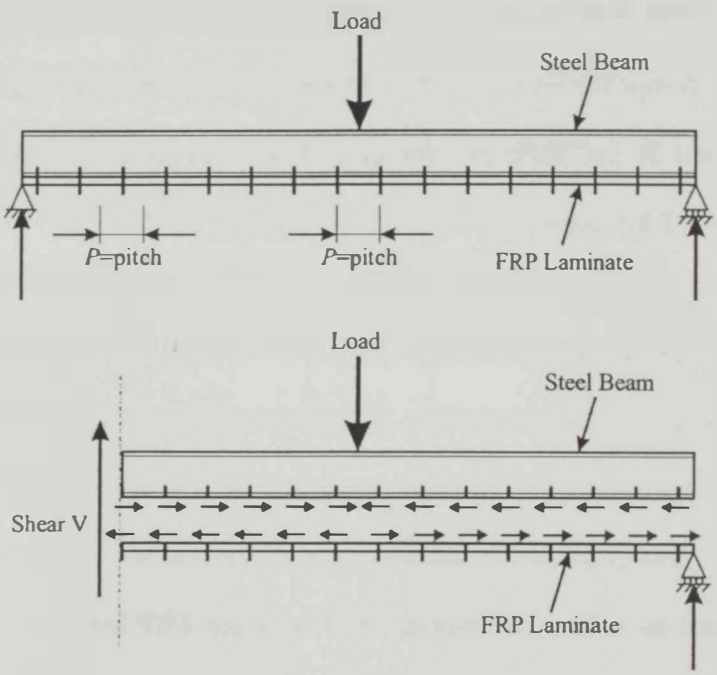

Figure 4.1: Shear Forces in Fasteners of a Typical Steel-FRP Composite Beam

4.1.2 Partially Composite Beams

The estimation of the shear forces in the fasteners of a partially composite steel-FRP beam is typically the key to an efficient structural design of such beams. These shear forces are typically related to the interfacial slip between the steel and the FRP at the fasteners. Figure 4.4 shows the longitudinal deformations u_s and u_{frp} in both the steel and the FRP at the fastener locations, respectively. The slip is defined by the difference between these two longitudinal translations (i.e., $slip = u_s - u_{frp}$). Figure 4.5 shows the slip as obtained in the experimental work of Alhadid (2011).

To simulate the slip between the steel and the FRP in a typical elastic partially composite beam, the fasteners are typically approximated by elastic springs of constant stiffness magnitude [Karam (1992), Elsayed *et al.* (2005), Achillides *et al.* (2006), Punmia *et al.* (2007), Girhammar and Pan (2007)]. Such spring stiffness depends on many factors including the stiffness of both the steel bottom flange and the FRP laminate, amount of bearing deformation per unit shear load at the fastener hole, and fastener type and diameter Alhadid (2011).

before yielding of the steel section (i.e., when steel is still elastic), if the elastic modulus of the FRP is close-to or higher than that of the steel section. An example of that is the case of ultra-high modulus FRP with tensile modulus of 440 GPa or more, which is much higher than the typical steel's modulus of about 200 GPa.

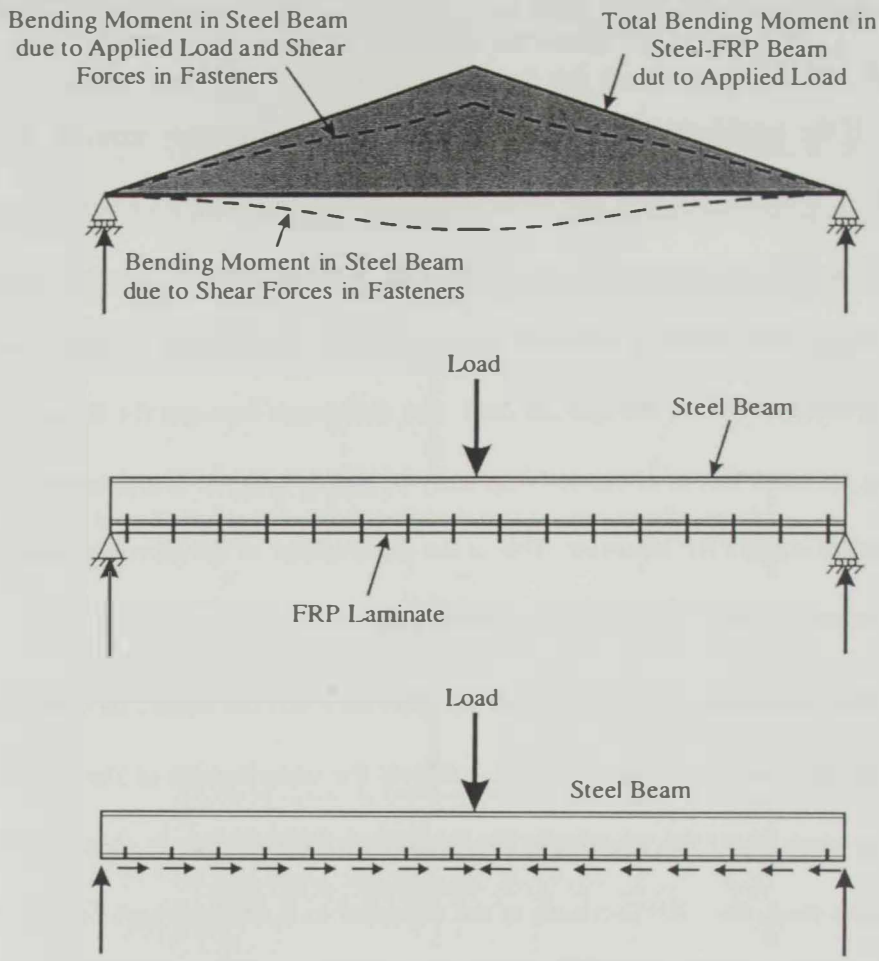

Figure 4.3: Bending Moments in Steel-FRP beam, Steel Beam, and FRP Laminate

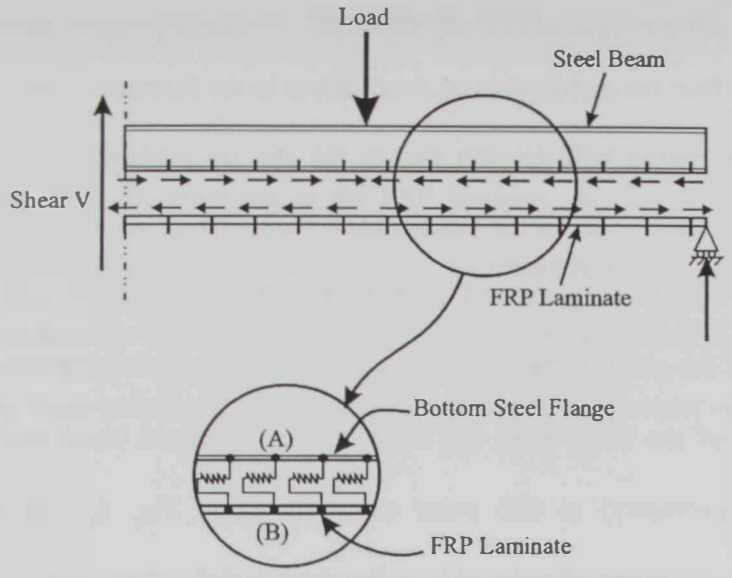

Figure 4.6: Spring Model of Fasteners in the Steel-FRP Composite Beam

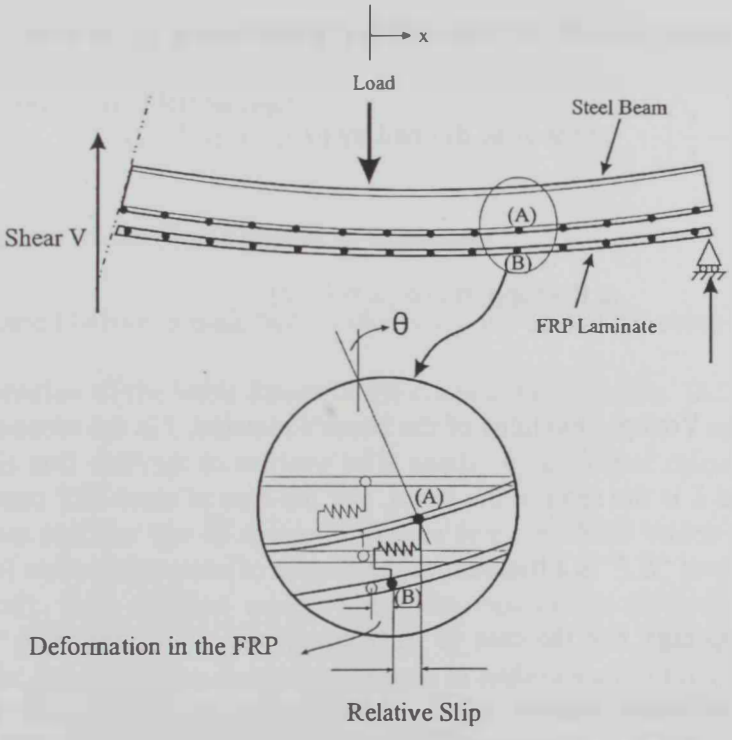

Figure 4.7: Slope of a Simply Supported Beam Under Three-Point Loading

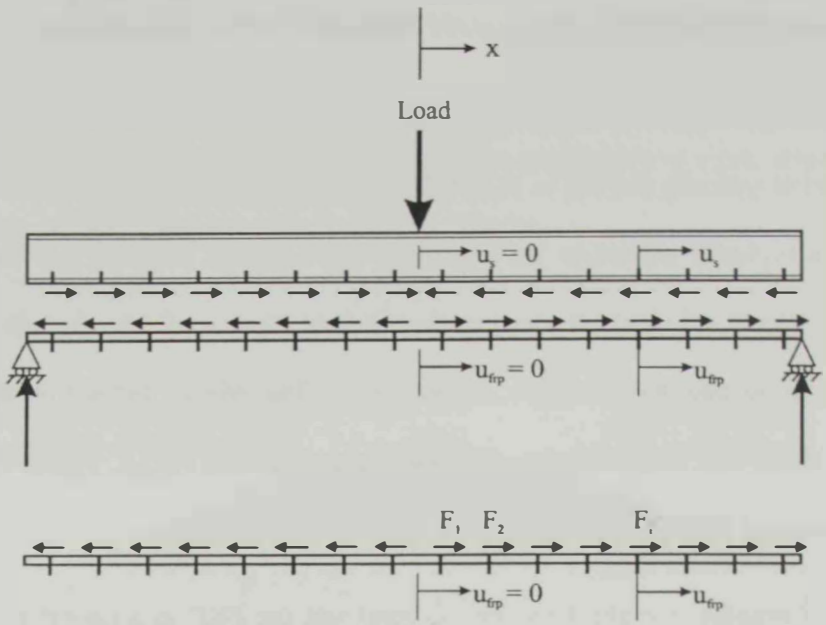

Figure 4.4: Deformations in the Steel and FRP Laminate

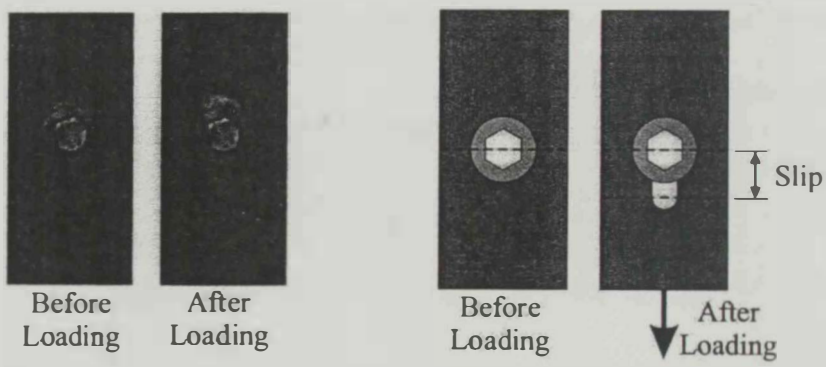

a) Physical Slip [Alhadid (2011)] b) Sketch of Slip

Figure 4.5: Physical Definition of the Slip in a Typical Steel-FRP Connection

of the points at the bottom flange, increases as the x-coordinate increases towards the support.

Meanwhile, the deformations in the FRP laminate, u_{frp}, at the locations of the fasteners are directly proportional to the shear forces transmitted from the steel beam to the FRP laminate through the fasteners. For the steel-FRP beam shown in Fig. 4.4 (steel-FRP beam under three-point loading) , the deformation at the i^{th} fastener is defined by:

$$u_{frp} = \left(\frac{1}{E_{frp}\, A_{frp}} \right) \sum_{j=1}^{j=i} F_j \; x_j \tag{4.4}$$

where x_j is the x-coordinate of the j^{th} fastener measured from mid-span, F_j is the shear force in the j^{th} fastener, E_{frp} is the Young's modulus of the FRP material, and A_{frp} is the cross-sectional area of the FRP laminate.

4.1.3 Distribution of the Shear Forces in Fasteners

As discussed before, a main task in analyzing any steel-FRP composite beam is to assess the distribution of the shear forces in the connecting fasteners. Although this task is essential, it is still difficult to achieve as it needs sophisticated calculations through digital computers and the use of special software (e.g., ANSYS which uses the Finite Element Method). Two extreme cases, where the calculation of such distribution is relatively simple, are worth the discussion to help in understanding the general behavior of the steel-FRP composite beams. The first case corresponds to a full composite action where the stiffness of the equivalent springs of the fasteners is very high (or theoretically infinity). In this case, the distribution of the fasteners' shear forces follows the same

Figure 4.6 shows a simple spring model that is presented to help in identifying the factors that affect the distribution of shear forces in the fasteners. It is clear that the shear force in each spring will develop due to the slip (or relative longitudinal movement) between two points; one on the bottom steel flange (point A) and the other on the FRP laminate (point B) as presented in Fig. 4.6. It is imperative that the longitudinal movement of the point on the steel flange is directly proportional to the counterclockwise rotation, θ, of the steel beam (or slope of the deformed beam relative to its initial unreformed geometry) at that point as presented in Fig. 4.7. In other words, the longitudinal movement of point (A) on the steel is defined by (θh / 2), where H is the total height of the steel section. For example, the slope of a simply supported elastic beam under symmetrical three-point loading shown in Fig. 4.7, is defined by:

$$\theta = \frac{F L x}{4 E I}\left(1 - \frac{x}{L}\right) \qquad \text{at the zone defined by } (0 \leq x \leq L/2) \tag{4.2}$$

$$\theta_{max} = \frac{F L^2}{16 E I} \qquad \text{at the support (i.e., } x = L/2) \tag{4.3}$$

where E is the Young's modulus of the beam's material, I is the cross-sectional moment of inertia, and L is the span of the beam. For the case of steel-FRP composite beam, the value of the term "$E I$" is a function of the degree of composite action (or the stiffness of the fastener spring). For the case of fully composite action, the term "$E I$" is obtained from the transformed section (based on Fig. 4.2) while for the case of no composite action, this term is calculated for the steel cross-section only (i.e., ignoring the FRP). Equation 4.2 shows that the beam's slope, and consequently the longitudinal translations

As discussed in Chapter 3, the FE model developed for this study is intended to simulate the flexural behavior of the steel-FRP composite beams. Therefore, steel stiffeners are added at the locations of stress concentration (i.e., at mid-span load and supports) to prevent local buckling. Additionally, lateral supports are employed at two locations along the span of the beams to prevent lateral torsional buckling. With these constraints, it is ensured that the mechanical behavior of any beam is dominated by its flexural behavior. As shown earlier by experimental research studies on flexural behavior steel and RC beams strengthened by mechanically fastened FRP [Alhadid (2011), Nardone *et al.* (2011), Ebead (2011), and Lee *et al.* (2009)] four dominant failure modes have been observed. These are (1) bearing in fastener holes in the FRP laminate, (2) shear failure in the fasteners, (3) tensile rupture in the FRP, and (4) flexural failure in the original beam (crushing in the RC beam or yielding in the steel beam). The FE model is capable of modeling the effect of bearing in fastener holes (embedded in the load-slip model as discussed earlier in Chapter 3, Fig. 3.4) and yielding in the cross-section of the steel beam (embedded in the elasto-plastic behavior of the steel material). The remaining two failure modes are identified by monitoring the longitudinal stresses in the FRP laminate and the shear force in each fastener at each loading step. Once these stresses or forces reach their maximum limiting values, failure of the composite beam is assumed and the analysis is terminated. More details about this issue is introduced within the context of the work presented in this chapter.

distribution of the beam's shear force diagram, as discussed earlier in section 4.1.1. The other extreme case is when there is negligible or no composite action (i.e., when the spring stiffness is very small or theoretically zero). In such case, the fasteners' shear forces become very small with a distribution that increases as the fastener location moves towards the support. The general case of partially composite beams lies between these two extreme cases and therefore, the distribution of the fasteners' shear forces is expected to be increasing nonlinearly towards the support.

4.2 Finite Element Analysis of Partially Composite Steel-FRP Beams

A numerical study using the Finite Element Method (FEM) is carried out to explore the effects of the different geometrical and/or material parameters on the behavior of the considered partial composite beams. The numerical study is composed of two phases. The first phase is conducted in the context of the experimental study performed by Alhadid (2011) to shed more light into the experimental results and explain them in view of the FE results. Besides, other steel-FRP beams with different fastener' stiffness and FRP lengths are considered.

The second phase considers three hypothetical case studies of simply supported partially composite steel-FRP beams having span of 7.0 m each. The beams are assumed to have different cross-sections dimensions which are intentionally selected to provide the very close plastic modulus Z_x to represent three equally possible flexural designs for the same applied bending moment.

Table 4.1 shows a summary of the tested beams along with the different characteristics related to the FRP laminates and the fasteners used. The load-deflection curves of the considered beams have been already shown in Chapter 3.

Table 4.1: Main Experimental Outcomes of Alhadid (2011) Experimental Study

Specimen ID* / No of Specimens	FRP thickness (mm)**	FRP length (mm)	Experimental Results				Yield load increase	Ultimate load increase
			P_y (kN)	M_y (kN.m)	P_u (kN)	M_u (kN.m)		
Control / 3	N/A		110.0	75.6	144.0	99.0	N/A	N/A
2200S / 2	3.175	2200	117.0	80.4	172.0	118.3	6.4%	19.4%
1800S / 2	3.175	1800	112.0	77.0	168.0	115.5	1.8%	16.7%
1200S / 2	3.175	1200	112.0	77.0	160.0	110.0	1.8%	11.1%
2200D / 1	6.350	2200	120.0	82.5	188.0	129.3	9.1%	30.6%
1200D / 1	6.350	1200	114.0	78.4	146.0	100.4	3.6%	1.4%

* S refers to single FRP laminate while D refers to double FRP laminate

** The thickness of each FRP layer is 3.175 mm

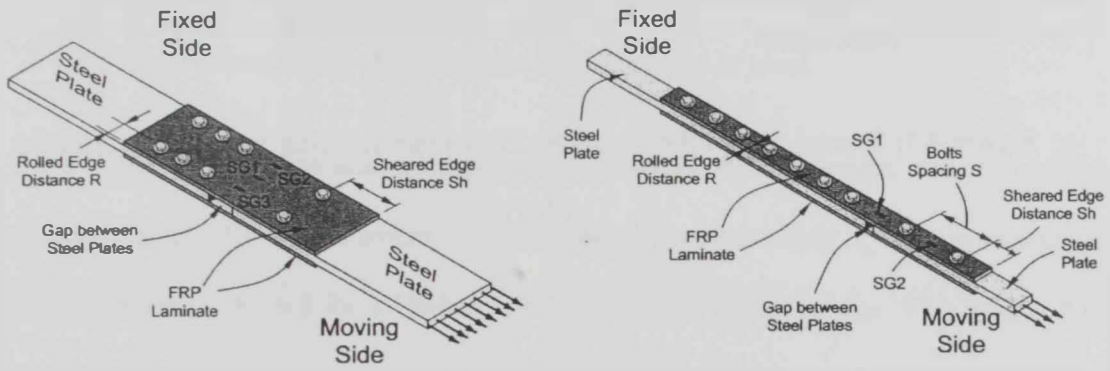

(a) Steel-FRP Short Connection

(b) Steel-FRP Long Connection

Figure 4.8: Typical Specimens for Testing Direct Shear in Steel-FRP Connections [After Alhadid (2011)]

4.3 Parametric Study – Phase I

4.3.1 Brief Description of Alhadid's Experimental Study

Recently, Alhadid (2001) conducted an experimental study that aimed at exploring the flexural behavior of I-shaped steel beams strengthened with mechanically fastened FRP laminates. The study included two main phases. The first phase of Alhadid's study targeted testing various configurations of lap steel-FRP connections in direct shear setups (Fig. 4.8) whose experimental load-slip results were used to develop a mathematical model capable of describing the interfacial load-slip behavior of the steel-FRP connections. In the second phase, eight steel I-shaped beams strengthened with mechanically fastened FRP laminates of different lengths and thicknesses (Fig. 4.9) were tested in 3-point loading setup (i.e., with mid-span load). In addition, three steel beams (with no FRP) have been tested and used as control specimens. The same steel section, UB 203x102x23, was used in all of the tested beams with total length of 3000 mm and simply supported span of 2750 mm. Strain gages were used to measure the strain at different locations of the steel section and the FRP laminates, while a linear variable displacement transducer (LVDT) was used to measure the deflection at the mid-span of the beams where the point load is applied. Steel stiffeners, 12 mm thick, were welded to each beam around the mid-span and at the supports to prevent local buckling, while lateral supports were used at two points along the span to prevent the lateral torsional buckling. The experimental mid-span load-deflection results were used to describe and compare the behavior of the different steel-FRP beams with different FRP laminate lengths, thicknesses and fasteners' arrangement.

insufficient number of fasteners started with some bearing deformations in the FRP and then failed in a brittle manner by sudden shear failure in the fasteners.

- Increasing the thickness and length of FRP laminates resulted in a slight improvement in the yield moment (i.e., moment at first yield in the steel section) in the range of 1.8% to 9.1%. Meanwhile, the results showed significant enhancement in the ultimate flexural capacity of the strengthened beams (between 11.1% to 30.6%).

- The addition of the fastened FRP laminates at the bottom flange of the steel beam delays yielding of the steel bottom flange relative to yielding of the upper flange.

- The contribution of the FRP laminate becomes noticeable after the initiation of yielding of the bottom steel flange at which point the elastic stress-strain modulus of the FRP becomes higher than the post-yield modulus of steel.

Although the experimental approach in studying the mechanical behavior of the composite Steel-FRP beams would be more realistic, unfortunately, it is more expensive and can be only adopted for a limited number of cases or specimens. This means that only few parameters can be investigated. In addition, experimental measurements are limited to deflections and strains at specific locations, which may not be sufficient to fully understand the mechanical behavior of the considered beams. On the contrary, using the finite element method enables estimating quantities that are difficult or impossible to measure experimentally such as the stress distribution in the FRP laminate and forces in the fasteners. The finite element model developed for this purpose was discussed and

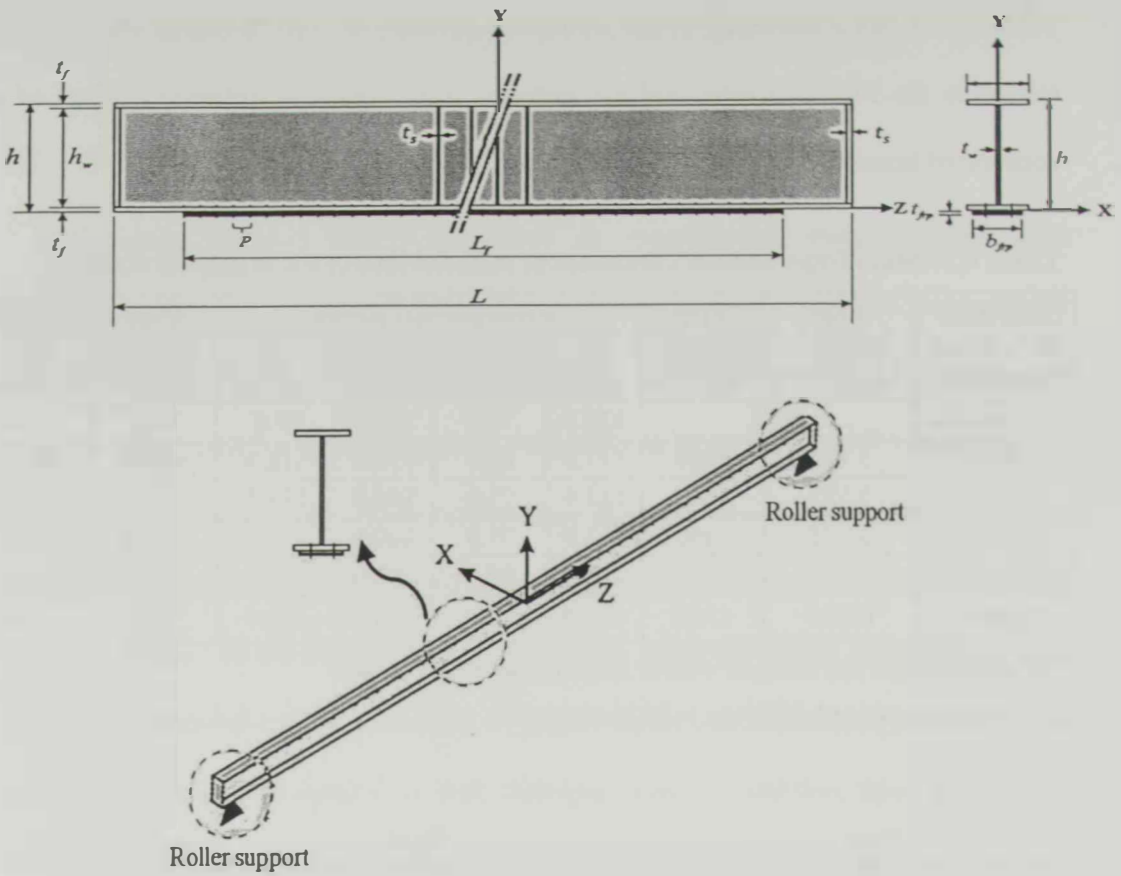

Figure 4.9: Typical Steel-FRP Specimen for 3-Point Loading Setup [After Alhadid (2011)]

The main observations of Alhadid's experimental study are summarized as follows:

- When a sufficient number of fasteners was used, the strengthened beams exhibited ductile failure mode accompanied by bearing deformations at the fasteners holes in the FRP laminate. On the contrary, the response of the strengthened beams with

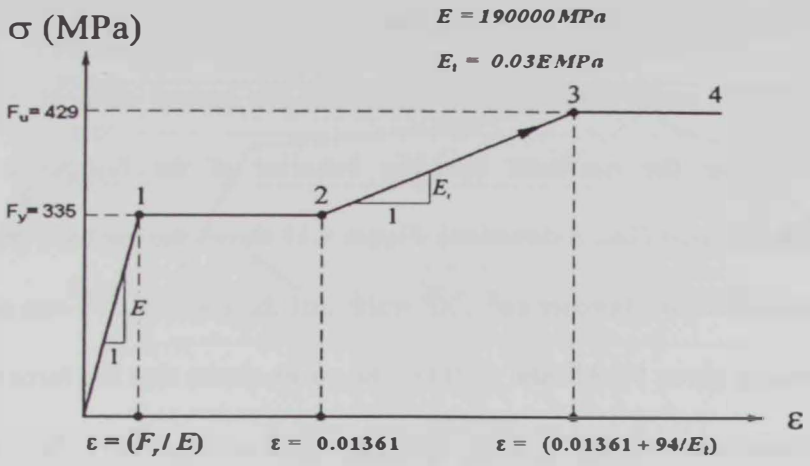

Figure 4.10: Material Model Used to Simulate Uniaxial Stress-Strain Behavior of Steel [After Alhadid (2011)]

FRP Material

The FRP was modeled as a linear elastic material with different characteristics in the different working directions (i.e., along axes X, Y, and Z shown in Fig. 4.9). The elastic modulus, shear modulus and Poisson's ratio values are provided in Table 4.2 [Kachlakev and McCurry (2000)].

Table 4.2: Material Properties of the FRP Laminates [After Alhadid (2011)]

Elastic Modulus (MPa)	Poisson's Ratio	Shear Modulus (MPa)
$E_x = 4800$	$\nu_{xy} = 0.3$	$G_{xy} = 1967$
$E_y = 4800$	$\nu_{xz} = 0.22$	$G_{xz} = 3270$
$E_z = 62190$	$\nu_{yz} = 0.22$	$G_{yz} = 3270$

validated against the main experimental results obtained by Alhadid (2011) as presented in Chapter 3. For completeness and clarity of each chapter, the model will be briefly described in the following section.

4.3.2 Description of the Finite Element Model

The three-dimensional (3D) finite element modeling of the steel-FRP beams is conducted using the general purpose finite element software package ANSYS (2011). The mechanical properties of the materials used in the model are selected in accordance with the real material properties reported by Alhadid (2011). Different types of finite elements, and suitable boundary conditions are used to accurately simulate the mechanical behavior of the steel-FRP beams under consideration.

4.3.3 Material Properties

Steel Material

Figure 4.10 shows the material model adapted to simulate the real behavior of the steel material. The steel material is assumed to be elasto-plastic with yield stress of F_y = 335 MPa with a multi-linear isotropic hardening that has initial elastic Young's modulus E = 190,000 MPa, and strain hardening modulus E_t = 0.03 E. These values have been proposed earlier by Alhadid (2011) in his experimental study.

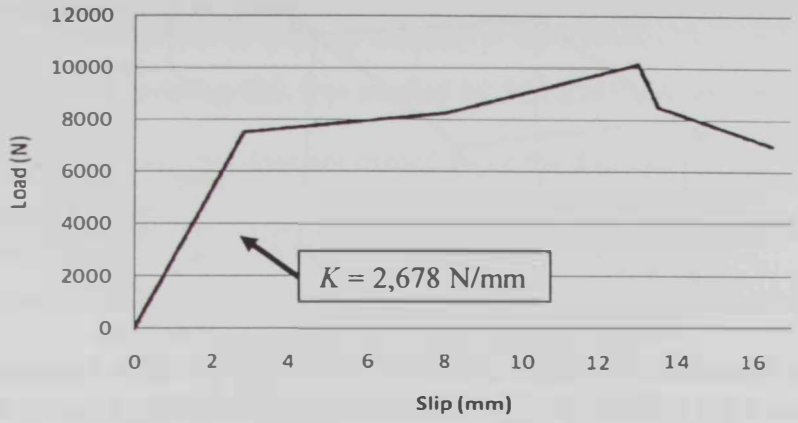

Figure 4.11: Load-Slip Model of the 6-mm Diameter Fastener in 3.175-mm Thick FRP Laminate [After Alhadid (2011)]

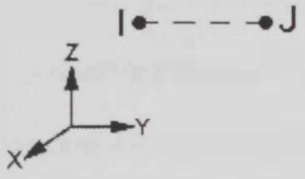

Figure 4.12: 2-Node 3D Link (or Spring) Element COMBINE39 [ANSYS (2011)]

4.3.4 Type of Elements and Mesh Size

The 8-node solid element, SOLID45, in ANSYS (Fig. 4.13) is used to model both the steel beam and FRP laminates. Each node in the element has three translational degrees of freedom in the Cartesian X, Y, and Z directions. The element is capable of modeling large deformations and large strains in addition to material nonlinearities.

Fasteners Load-Slip Model

ANSYS's multi-linear unidirectional link (or spring) element, *COMBIN39*, is used to simulate the nonlinear load-slip behavior of the fastener in the beam's longitudinal direction (i.e., Z-direction). Figure 4.11 shows the load-slip relationship of a typical 6-mm diameter fastener and FRP width and thickness of 100 mm and 3.175 mm, respectively, as given by Alhadid (2011). The curve shows that the force carried by the fastener depends on the relative slip between the steel and the FRP. This load-slip model is implemented in the FE model in the Z-direction at the location of the fastener. This element is defined by two coincident nodes (Fig. 4.12) and a Cartesian direction is added as a property of the element. One of these two nodes should lie on the steel flange and the other node is on the FRP laminate. It is important to note that the FE mesh of the lower steel flange should not essentially match the FE mesh of the FRP laminate; but their nodes at the location of the fasteners should exactly coincide in coordinates.

Another very stiff elastic spring is added along the Y-direction such that no penetration takes place between the FRP laminate and the steel section. A similar stiff elastic spring is also added along the transverse direction (i.e., X-direction) since it is not contributing significantly in carrying any loads.

4.3.5 Element Sizes and FE Mesh

The steel-FRP cross-section was meshed by SOLID45 elements with side-length in the X- and Y-directions that does not exceed twice the thickness of the web as shown in Fig.4.15. The side-length of the element in the Z-direction is set to be less than four times the element's size in the other two directions (i.e., X- and Y-directions) (Fig. 4.16). The final mentioned element sizes are realized after reaching a difference in the results between any two consecutive mesh refinements that does not exceed 2%.

Figure 4.15: Typical Mesh of the Cross-Section of the Steel-FRP Beam

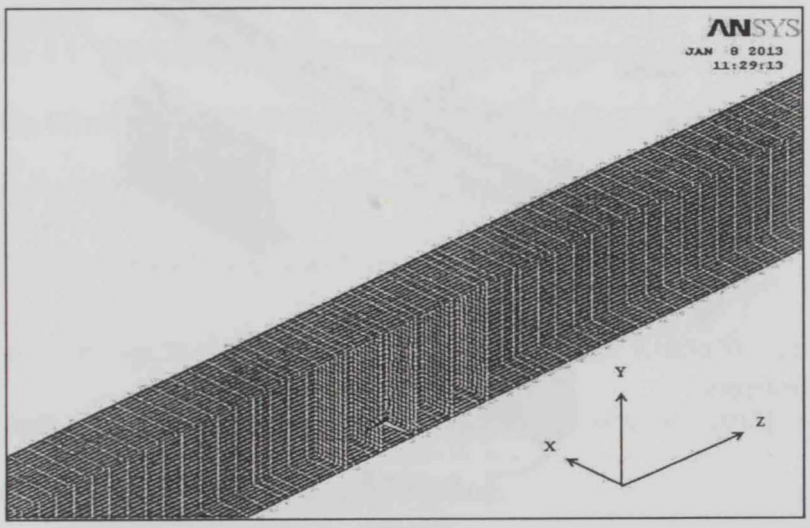

Figure 4.16: Typical Mesh Size in the Longitudinal Direction of the Steel-FRP Beam

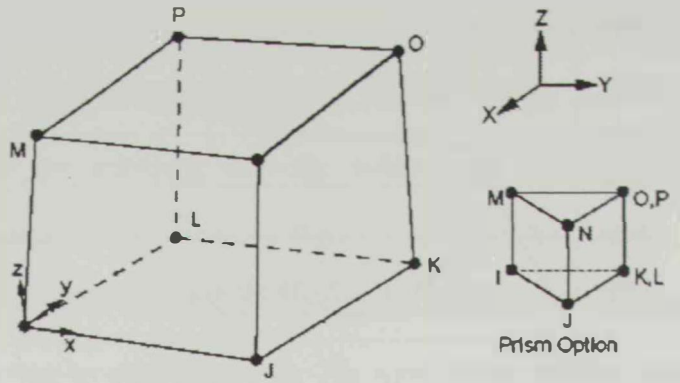

Figure 4.13: 8-Node 3D Structural Solid Element SOLID45 [ANSYS (2011)]

The 4-node 3D shell element, *SHELL181*, is used to simulate the stiffeners at the location of high stress concentration at the supports and at the loading point at the mid span. The shell element is suitable for analyzing thin to moderately-thick shell structures. Each node has six degrees of freedom; translations in the X, Y, and Z-directions, and rotations about the X, Y, and Z-axes as shown in Fig.(4.14).

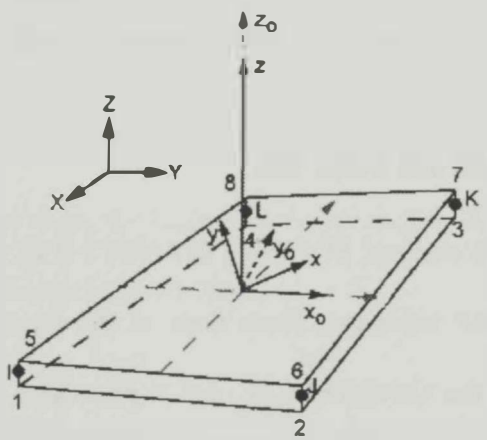

Figure 4.14: 4-Node 3D Structural Shell Element SHELL181 [ANSYS (2011)]

Beams with various geometrical parameters are analyzed under mid-span concentrated load. In spite of the symmetrical geometry and load of the problem, which suggests modeling one half of the beam, a full model of the beam is required. This full model is required to simulate the phenomena of warping of the cross-section around the Z-axis and asymmetrical torsional buckling around the X-axis.

4.3.7 Comparison Between FE Results and Alhadid's Experimental Findings

In the case of *partially composite* beam under consideration, the shear forces in a fastener are directly related to the amount of slip between the bottom steel flange and FRP laminate and on the fastener's spring stiffness. In addition, the amount of slip depends on the spring's stiffness relative to the tensile stiffness of the FRP laminate and steel flange. The FE model, described earlier in Chapter 3 and briefly in this chapter, is used to analyze the different steel-FRP beams that has been tested by Alhadid (2011) and listed in Table 4.1. The comparison between the experimental and numerically obtained load-deflection behavior of such beams has been discussed in Chapter 3 in the context of the verification of the FE model. It is shown that the FE model is capable of capturing the mechanical behavior of such beams with very good accuracy.

The shear forces in the fasteners and the longitudinal tensile stresses in the FRP laminate, which were not measured experimentally by Alhadid (2011), are the main scope of the numerical study reported in this section.

4.3.6 Boundary Conditions and Load Application

Figure 4.17 shows the general geometry of the composite Steel-FRP beam with its applied boundary conditions. The beam is roller supported at its left and right ends. Since the beam may be symmetrical or asymmetrical after deformation, the translations in the longitudinal direction U_z are restrained at the bottom nodes of the bottom steel flange at the mid span. Stiffeners are added at both ends and close to the mid span of the beam to eliminate the local buckling that may happen due to the stress concentration at the loading and reaction points. To ensure that the beams will have no lateral torsional buckling the beam was symmetrically braced in at different locations (i.e., $U_x = 0$) along the beam as shown in Fig. 4.17. Meanwhile, the rest of the nodes are left unrestrained against any kind of deformation.

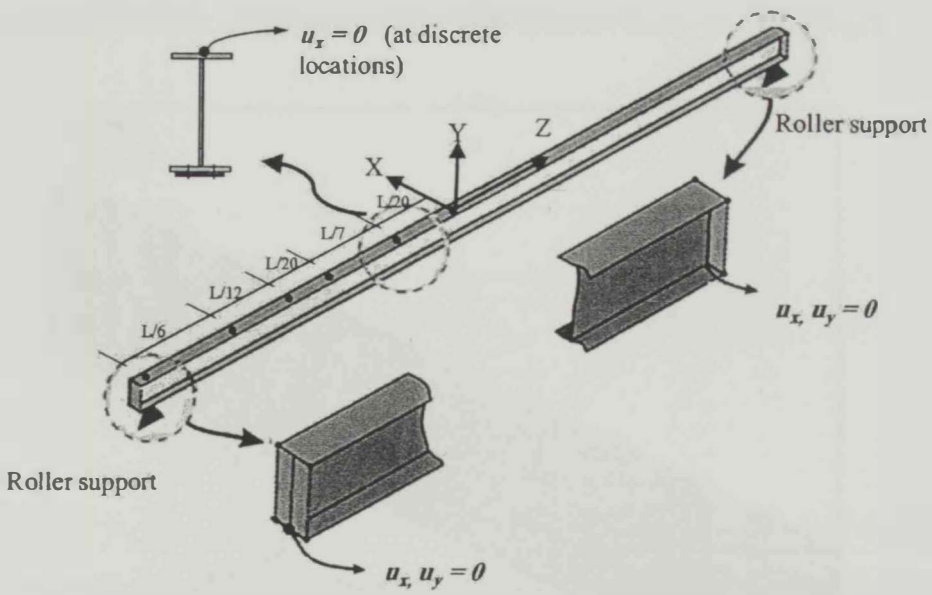

Figure 4.17: Boundary Condition for a Typical Composite Steel-FRP Beam (Symmetrical Lateral Supports are Shown for the Left-Side of the Beam Only)

100,000 N/mm). The value of 2,678 N/mm represents the value of the fasteners' modulus used by Alhadid (2011), while the other values represent different levels of the composite actions where the value of 100,000 N/mm is assumed to represent the full composite action. Under the effect of this particular mid-span load and for a fully composite steel-FRP beam, the shear force in each fastener, calculated as per Eq. 4.1, is 903.3 N. Some general observations for the elastic behavior of steel-FRP beams can be obtained from Figs. 4.19 to 4.21 as follows:

- Figures 4.19 and 4.20 reveal that zero relative slip occurs at the mid span, due to symmetry, leading to very small shear forces in the nearby fasteners. This slip increases gradually as a result of the increase in the slope of the deformed steel beam and approaches its maximum value at the fasteners close to the edges of FRP laminate. This trend has been observed for all the beams with different FRP lengths.

- In Figs. 4.19 and 4.20, as the length of the FRP decreases (e.g., beam 1200S), and consequently the number of fasteners decreases, the shear forces in the fasteners increases, even above the value 903.3 N that corresponds to the fully composite case. This is attributed to the need to distribute the maximum tensile force in the FRP at the mid-span on the total number of fasteners. On the contrary, as the length of the FRP increases (e.g. beam 2750S) , leading to a higher number of fasteners, the maximum shear force in the fasteners near to the FRP edge approaches a constant value and the distribution follows the shape of the beam's shear force diagram.

- Comparing the distributions shown in Figs. 4.19 and 4.20, it is clear that increasing the fastener stiffness from K=2,678 N/mm to 100,000 N/mm increases the shear

Elastic Behavior:

At small mid-span loading, the fasteners and the steel and FRP materials behave elastically. In this case, the fastener's spring stiffness modulus, K, takes the value of 2,678 N/mm that follows the slope of the initial branch of the spring's load-slip relationship shown in Fig. 4.11. Several steel-FRP beams have been analyzed using the FEM. The beams are denoted as 1200S, 1800S, 2200S, and 2750S where S refers to a single FRP layer of 3.175-mm thick, and 1200, 1800, 2200 and 2750 refer to the different lengths of the FRP laminate. Figure 4.18 shows a sample layout of the fasteners in beam 1200S, where the longitudinal pitch and edge distances are kept as 100-mm and 50-mm, respectively.

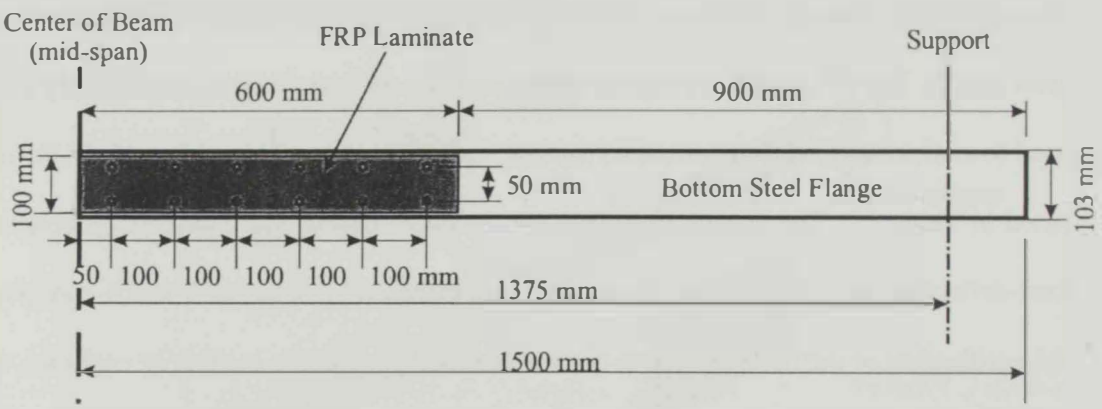

Figure 4.18: Sample Bottom View of 1200S Beam Showing the Typical Fasteners' Pitch and Edge Distance

The results of the FE analyses are presented in Figs. 4.19 to 4.21. The figures show the distribution of shear forces in the fasteners at the loading of 75.0 kN for different FRP lengths (44%, 65%, 80% and 100% of the beam's span) and different fastener moduli (namely 2,678 N/mm, 5,000 N/mm, 10,000 N/mm, 20,000 N/mm and

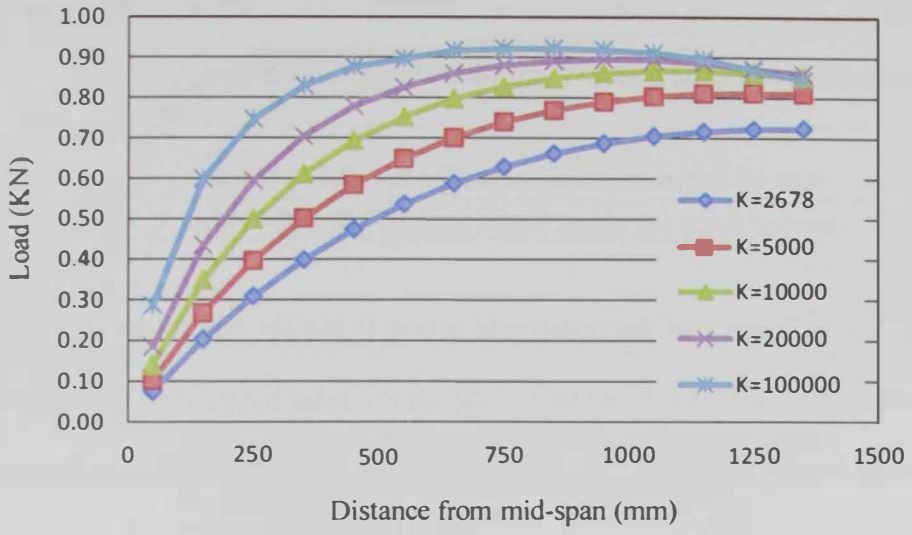

Figure 4.21: Forces in Fasteners of 2750S Steel-FRP Beam Under a Mid-span Load of 75.0 kN and Different Spring Moduli in (N/mm)

- Figure 4.21 shows that for beam 2750S (i.e., FRP covers the full length of the steel beam) and as the fastener stiffness increases, the maximum shear forces in the fasteners increases and approaches the extreme value of 903.3 N that corresponds to the case of the fully composite steel-FRP beam. In addition, the distribution tends to follow the shape of the shear force diagram of the beam especially for high stiffness of fasteners.

- To assess the level of composite action of any partially composite steel-FRP beam, it is reasonable to compare the sum of the developed shear forces in the fasteners located in the half mid-span of the partial composite steel-FRP beam (e.g., K=2,678 N/mm) with their counterpart of the nearly full composite case (i.e., K=100,000

forces in the fasteners, especially for short FRP laminates. It is also clear that the shear force in the edge fastener approaches 903.3N that corresponds to the full composite beam case.

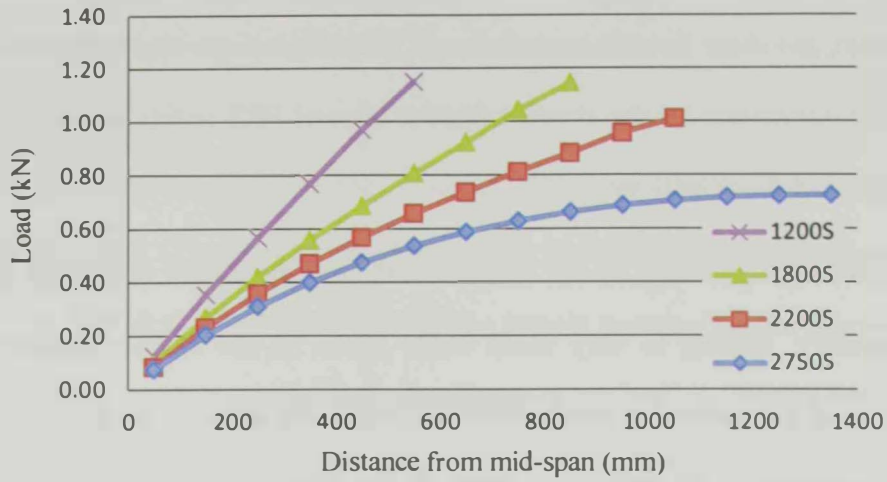

Figure 4.19: Forces in Fasteners for a Mid-span Load Of 75.0 kN and Spring Modulus of K = 2,678 N/mm

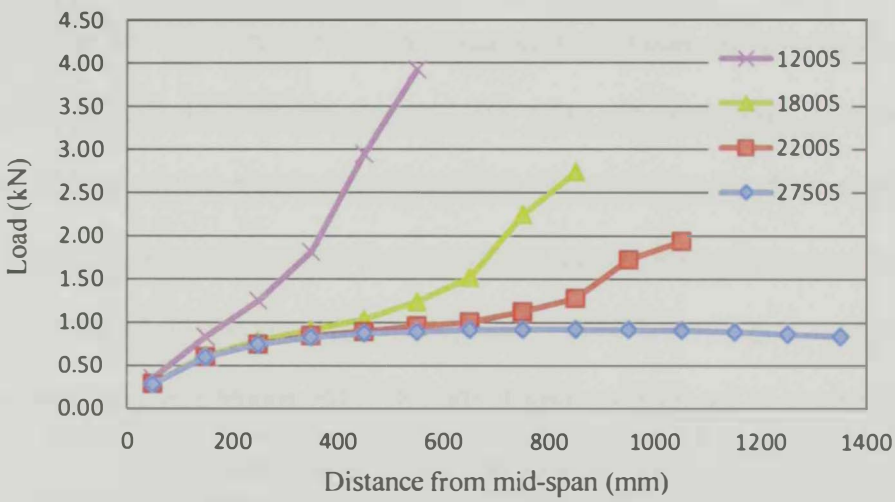

Figure 4.20: Forces in Fasteners for a Mid-span Load of 75.0 kN and Spring Modulus of 100,000 N/mm

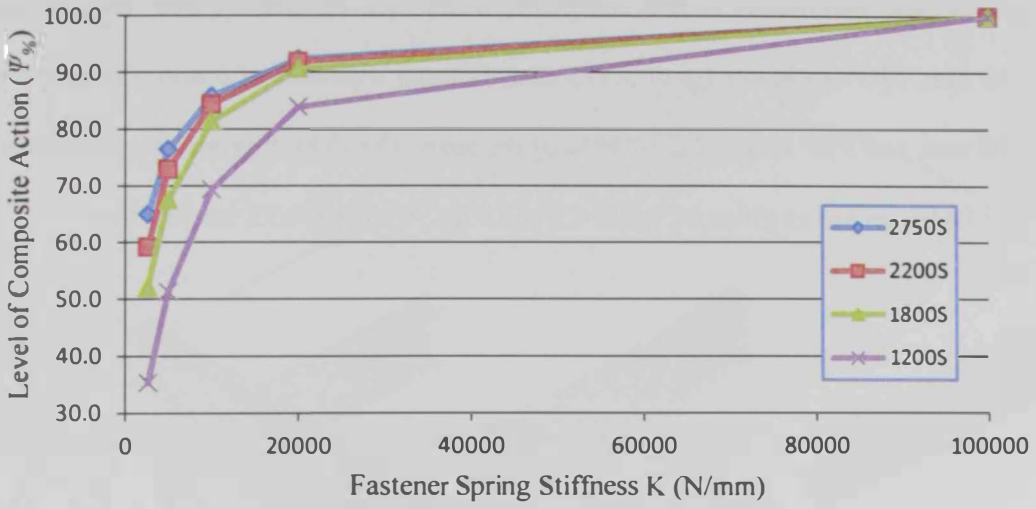

Figure 4.22: Level of Composite Action in Different Beams Due to a Mid-span Load of 75 kN

Elasto-Plastic Behavior

Figures 4.23a and 4.23b show contour plots of the Von Mises equivalent stresses in the 1200S beam due to mid-span loads of 120 kN and 160 kN, respectively. The figures show zones around the mid-span where the Von Mises stresses have reached the limiting yield value. It can be noticed that the zone enlarges and extends towards the support as the mid-span load increases from 120 kN to 160 kN. Figure 4.24 shows the propagation of the plasticity in a the composite beam 2200D at different load levels. It is clear that the plasticity in the top flange is more spread than the bottom flange due to the addition of the FRP laminate.

To shed more light on the elasto-plastic behavior, FE analyses have been conducted for composite steel-FRP beams with different lengths of the FRP laminate and different pitch sizes between the fasteners. Unless otherwise noted, the default

N/mm). Performing such simple comparison for the beam 1200S gives an index of the level of composite action Ψ_{comp} which is calculated as:

$$\Psi_{comp} = \frac{\text{sum of fasteners' shear forces for K = 2,678 N/mm}}{\text{sum of fasteners' shear forces for K = 100,000 N/mm}} = 35.4\%$$

The low efficiency of the composite action is mainly due to the small value of the elastic spring stiffness K relative to the elastic axial longitudinal stiffness of the steel bottom flange ($E_s A_{flange} / pitch$) or that of the FRP laminate ($E_{frp} A_{frp} / pitch$).

- Figure 4.22 shows the effect of the fastener stiffness, K, on the composite action index (Ψ_{comp}), for steel-FRP beams with different FRP lengths; namely 1200S, 1800S, 2200S, and 2750S. The figure shows that as the length of the FRP increases, the index of composite action increases indicating higher efficiency of the FRP laminate, especially at low fastener stiffness. As the fastener stiffness increases and becomes very high (e.g., above 20,000 N/mm), the effect of the FRP length becomes less significant.

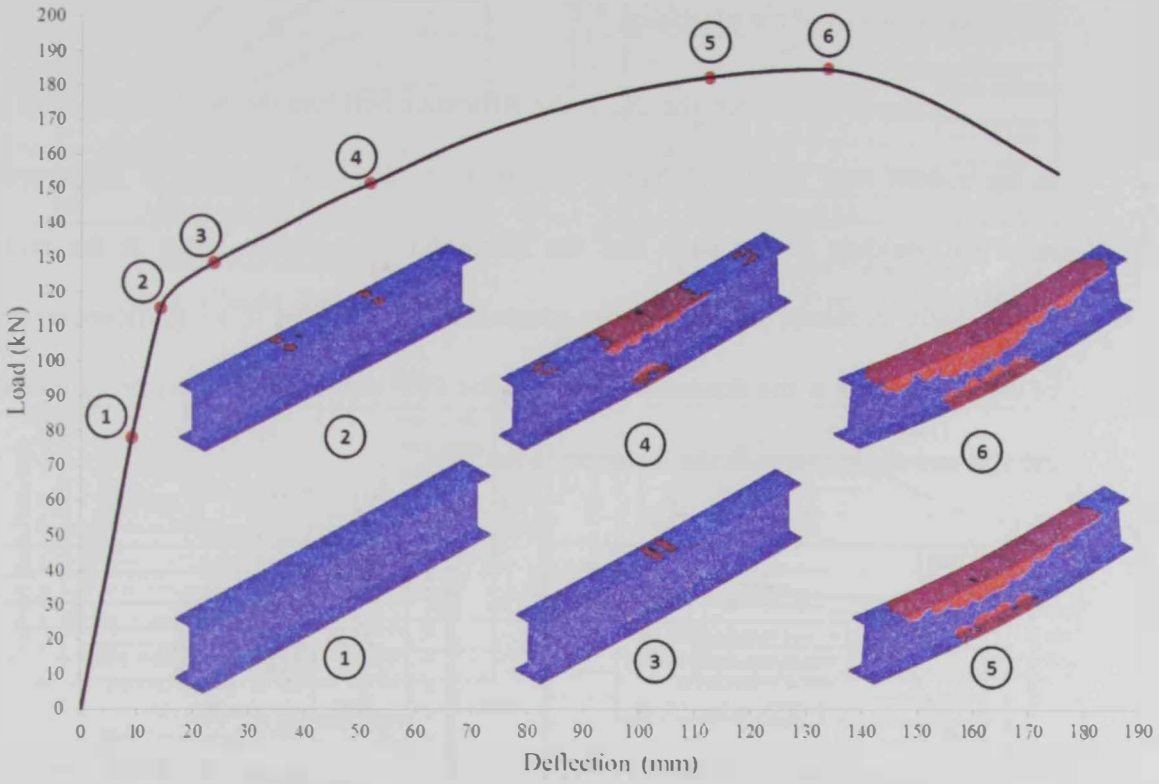

Figure 4.24: Yielded Zones at Different Loading Levels on the 2200D Composite Beam

Figure 4.25 shows the forces carried by fasteners in the different steel-FRP beams at different mid-span load levels. Four levels of the mid-span load are considered; namely load of 75 kN in the elastic behavior zone, load at first yield in the steel, load of 145 kN in the post-yield zone, and peak or ultimate load. The figure shows that the distributions of the fasteners' shear forces in the elastic zone and at first yield are similar for each of the considered beams with different FRP lengths. This indicates no significant change in the mechanical behavior until the steel reaches its first yield. On the other hand, the figure clearly shows that after first yield there is a significant increase and change in the distribution pattern of the fasteners' shear forces for all of the considered FRP lengths.

geometrical parameters of the composite beams are defined by FRP laminate width of 100 mm, FRP thickness t_{frp} of 3.175 mm, fastener diameter of 6 mm, fastener pitch P of 100 mm, and FRP length L_{frp} of 85% of the span. The default properties of the steel, FRP, and fasteners are as given in Table 4.2 and Figs. 4.10 and 4.11, respectively.

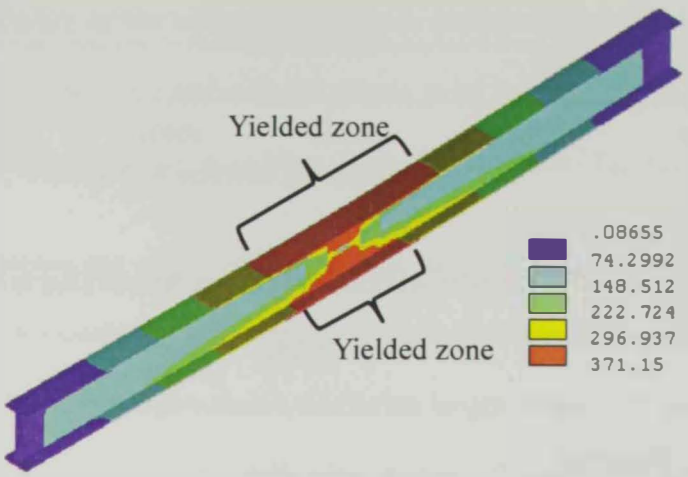

a) Mid-span Load = 120 kN

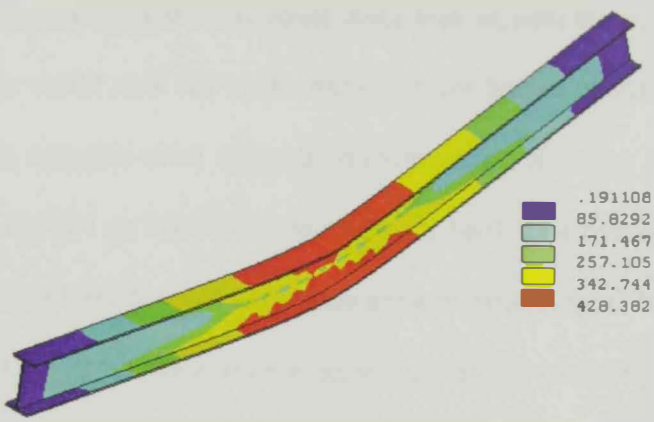

b) Mid-span Load = 160 kN

Figure 4.23: Contour Plots of Von Mises Stresses (in MPa) Due to a mid-Span Load Acting on Beam 1200S

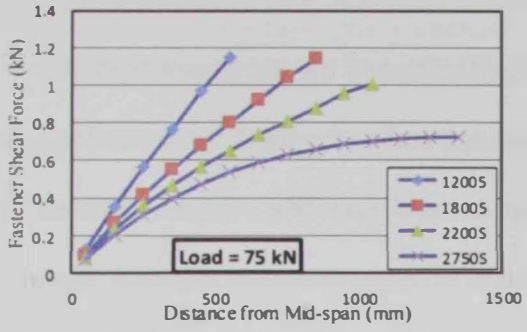

(a) at Elastic Zone = 75 kN

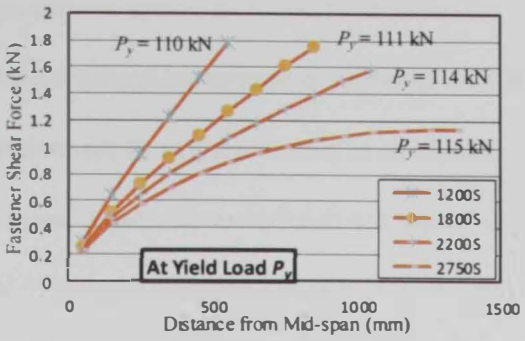

(b) at First Yield in Steel

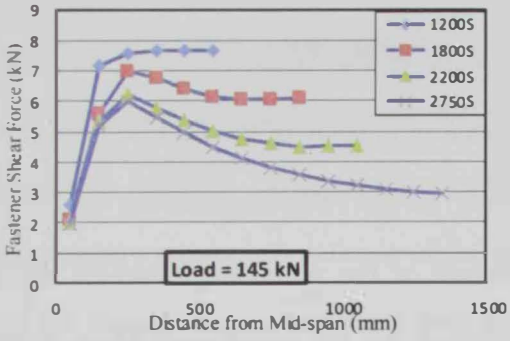

(c) At Load 145 kN

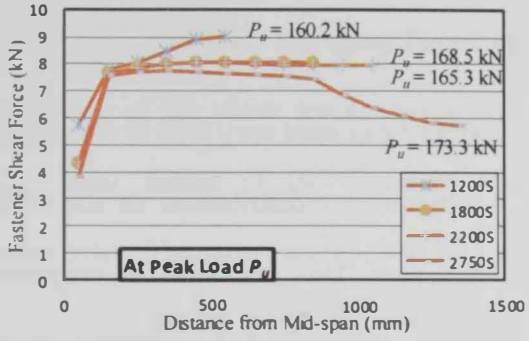

(d) At Peak Load

Figure 4.26: Forces Carried by Fasteners in Steel-FRP Beams at Different Loading Levels

Figure 4.26 shows the forces carried by fasteners in different steel-FRP beams at different levels of the mid-span loads. The observed tend in the figure reflects the increase in the fasteners' shear forces in the elastic range when the length of the FRP laminate decreases significantly (e.g., case of composite beam 1200S compared to 2750S). The is mainly due to the fact that the tensile load developed in the FRP is distributed over fewer fasteners. As the mid-span load increases, the longitudinal

This increase starts from the mid-span and spreads towards the support; exactly similar to the trend of spread of the plasticity.

As discussed earlier, the slip is the difference between the movement of the points at the bottom steel flange relative to the points on the FRP laminate. It is important to note that yielding of the steel and the formation of a plastic hinge at the mid-span significantly increases the slope of the composite beam leading to a significant movement of the steel points at the fasteners relative to the FRP points and consequently increase in the slip and shear forces in the fasteners is realized.

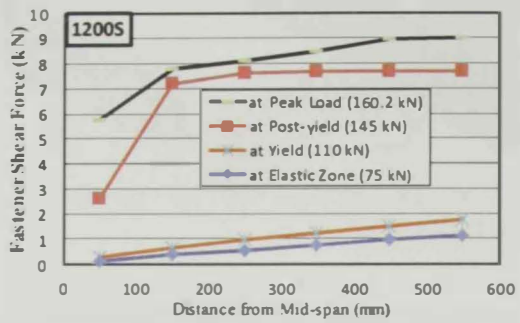

(a) Composite Beam 1200S

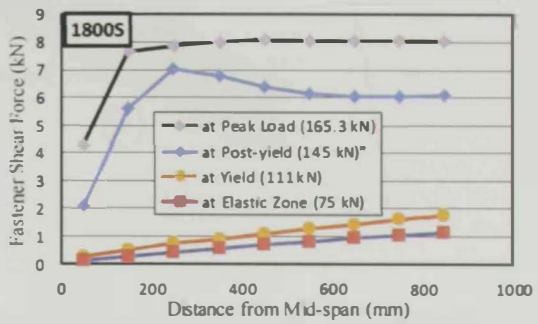

(b) Composite Beam 1800S

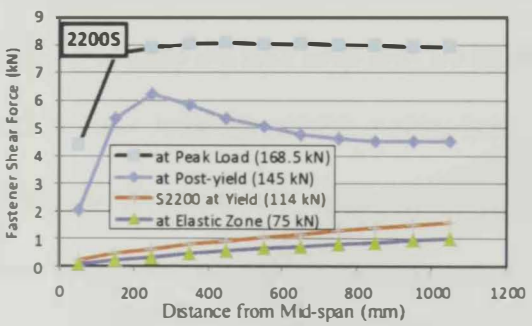

(c) Composite Beam 2200S

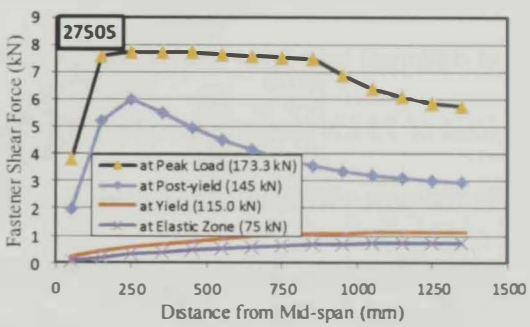

(d) Composite Beam 2750S

Figure 4.25: Forces Carried by Fasteners in Steel-FRP Beams With Different Lengths of FRP Laminate

Figure 4.27 shows the experimental load-deflection results at mid-span of the composite beam. Tracing the development of the numerical shear forces in the fasteners indicates that failure of the edge fastener takes place when the induced shear force in the fastener reaches the critical value of 10.6 kN. Figure 4.28 shows the distribution of the shear forces in the steel fasteners at the experimental peak applied load of 152 kN. It can be seen that at this particular applied load value, the shear force in the edge fastener reaches the maximum shear capacity of the fastener (i.e., 10.6 kN). The shear failure of the edge fastener leads to instantaneous redistribution of the shear forces among the remaining fasteners resulting in a progressive shear failure of the fasteners and consequently a complete collapse of the composite beam. Therefore, a mid-span load of 152 kN represents the maximum load the composite beam can carry before collapse. This explains the premature experimental failure of the composite beam 1200D at an applied load of 152 kN as shown in Fig. 4.27.

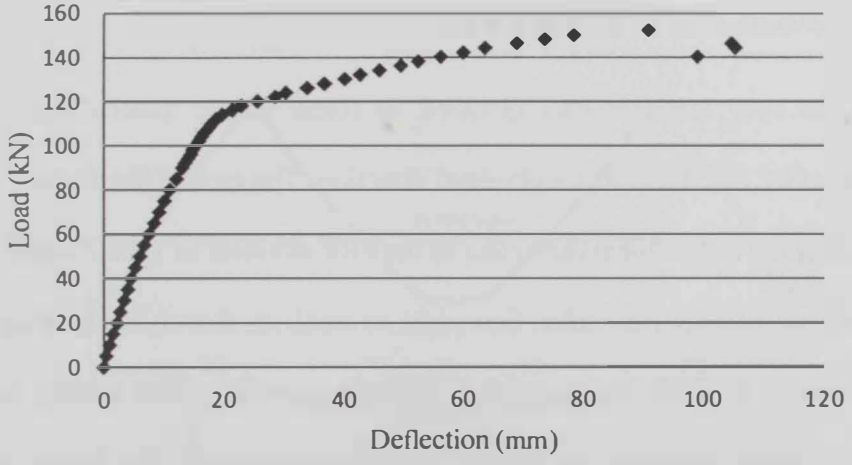

Figure 4.27: Experimental Load-Deflection Curve of 1200D Composite Beam at Mid-span [After Alhadid (2007)]

movements of the steel points around the yielded zone (i.e., mid-span) and away towards the supports are dominated by the increase in the slope of the composite beam due to the formation of plastic a hinge at the mid-span and therefore the shear forces tend to become constant for the fasteners located away from the mid-span (e.g., for the cases of 1800S and 2200S, Fig. 4.26c). For long FRP laminates (e.g., for the case of 2750S, Fig. 4.26c), the movement in the FRP becomes significant and the shear forces in the fasteners are reduced.

It is important to note that the increase in the fasteners' shear forces due to yielding in steel may lead to a sudden shear failure in some of the fasteners resulting in a subsequent redistribution of the tensile force in the FRP laminate on the remaining fasteners. This may lead to progressive failure of the remaining fasteners leading to sudden failure of the composite beams. Although the FE model used is not capable of simulating such shear failure in the fasteners, the load at which the first fastener fails in shear is still predictable.

To shed more light on such behavior, a FE analysis of the previously tested composite beam 1200D is conducted where two layers of FRP are intentionally used to allow for high shear forces in the fasteners. Similar to all beams tested by Alhadid (2011), fasteners used in 1200D beam are M6x258 made of high tensile steel Class 8.8 according to DIN ISO 4017 (2011) with shear strength of 375 MPa (BSI 5950-1:2000). The maximum shear force F_{shear} that can be carried by one fastener is estimated as:

$$F_{shear} = \left(\frac{\pi}{4}\right) \times 6^2 \times 375 = 10.6\,\text{kN} \tag{4.5}$$

Figure 4.30 presents the normal stress distribution across the width of the FRP laminate at the mid-span of the composite beam. The two peaks shown in the plot are due to the stress concentration around the steel fasteners. It is important to note that these peaks differ by about 4% from the average stress. The contour plot in Fig. 4.31 confirms the same stress concentration at the location of the fasteners.

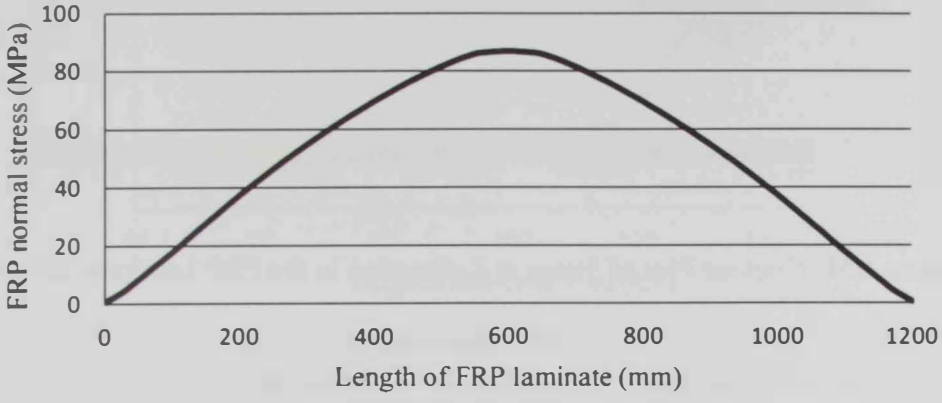

Figure 4.29: Longitudinal Normal Stress Distribution in the FRP Laminate in the 1200D Beam at a Mid-span Applied Load of 121 kN

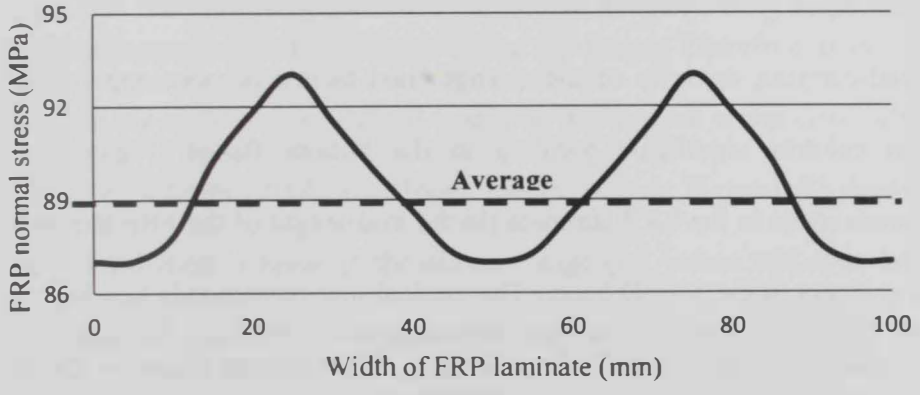

Figure 4.30: Normal Stress in the Cross-section of the FRP Laminate Located at the Mid-span of the 1200D Beam at a Mid-span Applied Load of 121 kN

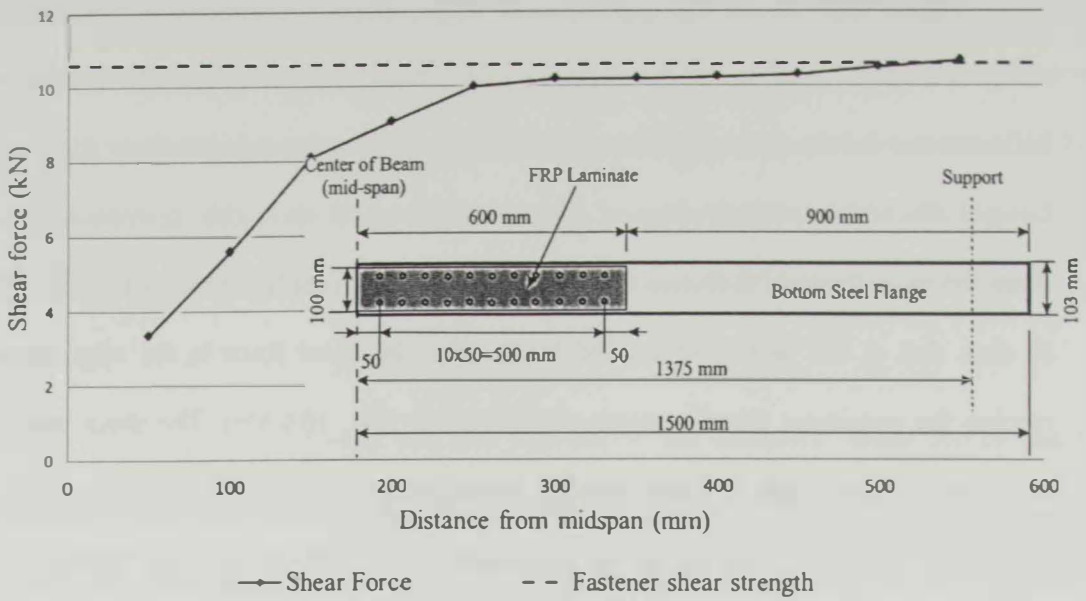

Figure 4.28: Distribution of Fasteners' Numerical Shear Forces in 1200D beam at a Mid-span Load of 152 kN

Stress distribution in the FRP laminate:

The FRP laminate was modeled as linear elastic material having an elastic modulus of 62.19 GPa in its longitudinal direction. The typical distribution of the normal stress along the longitudinal centerline of the FRP laminate in 1200D beam due to a mid-span load of 121 kN (i.e., after first yield in steel) is shown in Fig. 4.29. The stress distribution in the FRP laminate follows the same profile of the bending moment in the composite beam regardless of the FRP thickness or length. The figure shows that, as expected, the maximum stress occurs at the mid-span of the beam.

the shear forces in the fasteners leading to an inevitable shear failure in the fasteners at an applied load of 152 kN (Fig. 4.28).

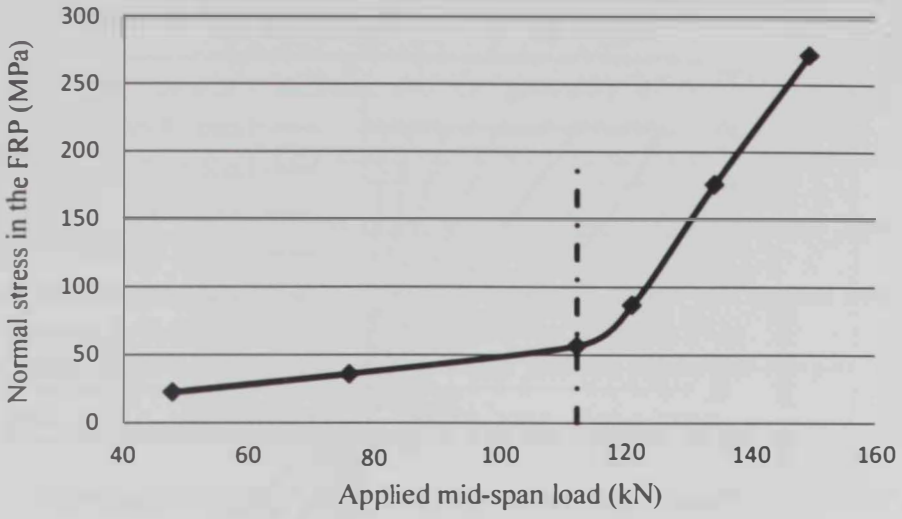

Figure 4.32: Maximum Longitudinal Stress in the FRP Laminate in the 1200D Beam at Different Loading Stages

Stress distribution in the steel section:

The point load acting at the mid-span of the composite beam produces a concentration of stresses around this region of the top flange. Therefore, a location away by 100 mm from the mid-span is selected to display the normal strain distribution in the steel cross-section of beam 2200D at different loading stages. Figure 4.33 shows that the normal strain distribution is linear in the elastic range (i.e., when mid-span load is less that first yield load of 112.5 kN). The strain distribution becomes nonlinear at load value of 115.4 kN that exceeds the first yield load. This is mainly due to the geometrical non-linearity introduced by the large mid-span deformation that significantly changes the initial geometry of the beam. Figure 4.33 shows also that at a mid-span load of 115.4 kN

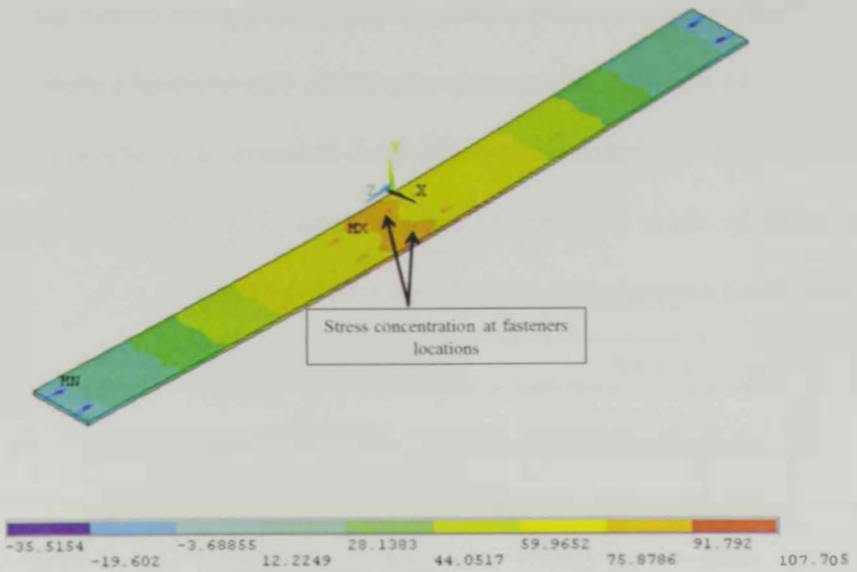

Figure 4.31: Contour Plot of Stress in Z-direction in the FRP Laminate of 1200D Beam at a Mid-span Load of 121 kN

As mentioned earlier, the drillable hybrid FRP laminates used by Alhadid (2011) have an elastic modulus of (62.19 GPa) which is about one third of the elastic modulus of the steel beam (190 GPa). Therefore, the contribution of the FRP laminate in improving the load-carrying capacity of the strengthened beams is more apparent after the steel section exhibits significant yielding in the bottom flange. Figure 4.32 shows the maximum stress in the FRP laminate (in the mid-length of the FRP laminate) at different loading stages in the 1200D beam. The vertical line corresponds to a load value of 112.5 kN at which the steel exhibits first yielding at the bottom flange in the mid-span. It is obvious that a substantial increase in the normal stress carried by the FRP laminate takes place directly after yielding of the steel section associated with a significant increase in

4.4 Parametric Study – Phase II

As indicated earlier, the first phase of the parametric study focused on studying the effect of the fastener's stiffness and the geometry of the FRP laminate on the mechanical behavior of steel-FRP composite beams. In addition to the previously stated aspects, the second phase targets studying the effect of geometrical and material parameters of the steel cross-section and FRP laminate on the mechanical behavior and response of composite beams. Those parameters include the height-to-span ratio of the steel beam, the thickness of FRP laminate, the distribution of the steel fasteners, the length of FRP relative to the span of the beam and the elastic modulus of the FRP laminate. In this phase the same finite element and material models and boundary conditions used earlier in the first phase are utilized.

4.4.1 Description of Steel Cross-Sections

Three steel beams with a span of 7000 mm and different cross-sections are considered in the numerical study namely; W8x48, W10x39 and W14x30. These three sections are selected such that they have very close elastic and plastic section moduli values (i.e., S_{xx} and Z_{xx}) with less than 2% and 3% variation, respectively, which should lead to having very close values of the mid-span loads at first and full yielding of the steel cross-section. Table 4.3 shows the geometrical properties of the three cross-sections while Fig. 4.34 presents the main parameters defining the geometry of the steel sections.

the neutral axis is clearly shifted downward. This is expected due to noticeable increase in the contribution of the FRP laminate in carrying the load after yielding of steel is initiated as indicated in Fig. 4.32.

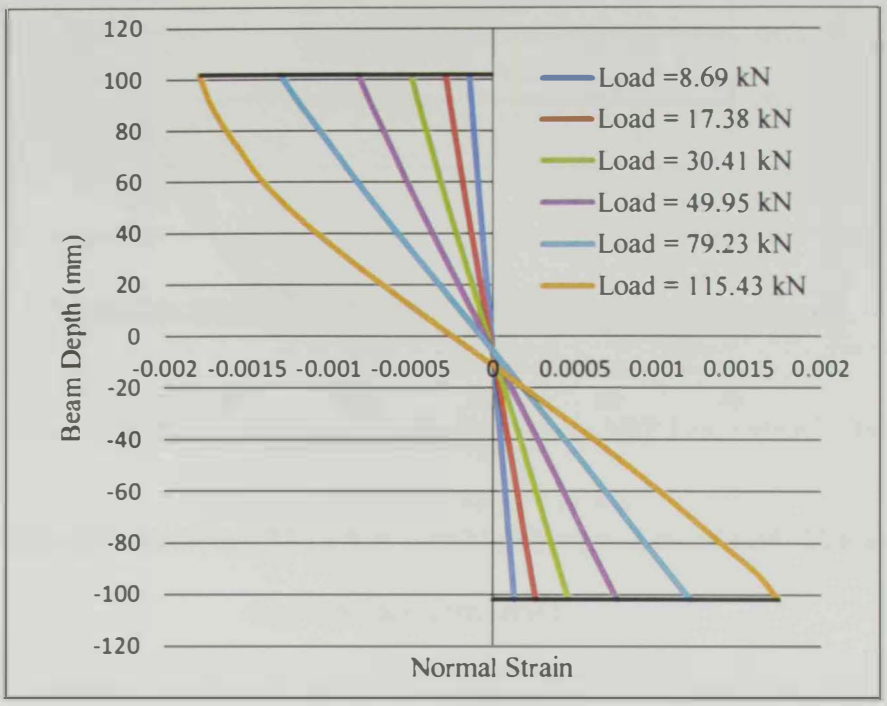

Figure 4.33: The normal strain distribution in the cross-section of the steel beam in 2200D at 100 mm away from the mid-span at different loading stages

yielding and extend to the strain hardening stage as per stress-strain relationship in Fig. 4.10.

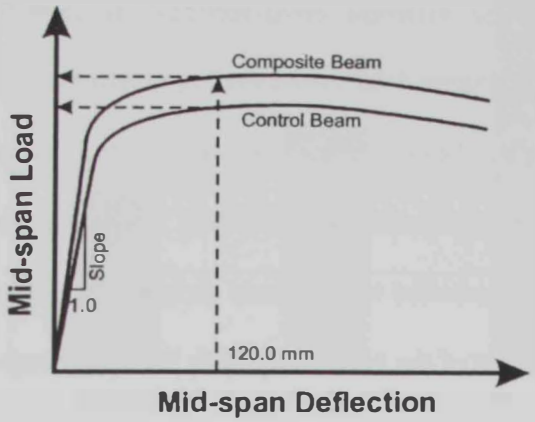

Figure 4.35: Measures Used in the Comparison Between the Mechanical Behaviors of the Control and Composite Beams

The resulting loads at the 120 mm deflection and the initial slopes of the beams' load-deflection curves at the mid-span, as defined in Fig. 4.35, are used as indices to evaluate the influence of the considered parameters on the mechanical behavior of composite steel-FRP beams. These indices are defined as

$$\% \text{ improvement} = \frac{\left(\text{Result}_{composite} - \text{Result}_{control} \right)}{\text{Result}_{control}} \% \qquad (4.6)$$

where *Result* is either the initial slope of the load-deflection curve or the mid-span load at deflection of 120 mm. The following sections consider the effect of each parameter at a time while keeping the others parameters unchanged.

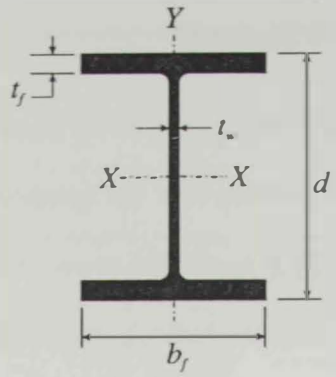

Figure 4.34: General Cross-sectional Parameters of the Wide Flange I-Sections

Table 4.3: Cross-sectional Geometrical Properties of Analyzed Steel Beams (AISC, 2005)

Section	d	b_f	t_f	A_f	t_w	I_{xx}	S_{xx}	Z_{xx}	$\lvert S_{xx}$ - Average $S_{xx} \rvert$ / (Average S_{xx})	$\lvert Z_{xx}$ - Average $Z_{xx} \rvert$ / (Average Z_{xx})
	(in)	(in)	(in)	(in^2)	(in)	(in^4)	(in^3)	(in^3)	%	%
W14×30	13.8	6.73	0.385	2.59	0.27	291	42	47.3	1.02	0.84
W10×39	9.92	7.99	0.53	4.23	0.315	209	42.1	46.8	0.79	1.89
W8×48	8.5	8.11	0.685	5.56	0.4	184	43.2	49	1.81	2.73

The rest of the geometry is typically defined by FRP laminate width of 100 mm, FRP thickness t_{frp} of 3.175 mm, fastener diameter of 6 mm, fastener pitch P of 100 mm and FRP length L_{frp} of 85% of the span, unless otherwise noted. The steel, FRP, and fasteners properties are as defined in Table 4.2, Fig. 4.10, and Fig. 4.11, respectively.

The control steel beam and composite steel-FRP beams are subjected to incremental mid-span downward displacement and the corresponding mid-span loads are determined. A maximum deflection of about (span / 60 ≈ 120 mm), is found to be enough to create normal stresses in the mid-span steel section that significantly exceed

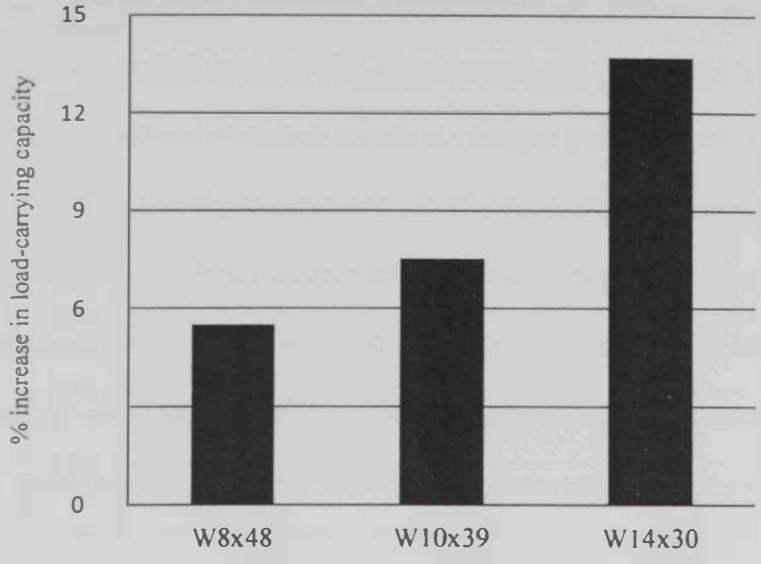

Figure 4.36: Percentage Increase in Mid-span Load, at 120 mm Deflection

4.4.3 FRP Thickness

As reported by Alhadid (2011), the steel-FRP interfacial behavior of the 3.175-mm thick STRONGWELL FRP laminate and 6-mm diameter steel bolts, is mainly controlled by bearing in the FRP laminates. In other words, the load-slip model presented in Chapter 3 and in Fig. 4.11 for a single layer of FRP (thickness of 3.175-mm) can be simply extended to other FRP thicknesses by scaling the load by (t_{frp} / 3.175).

In order to examine the influence of FRP thickness on the load-carrying capacity of the composite steel-FRP beams, two different FRP thicknesses are considered; namely 3.175 mm which corresponds to one layer of FRP and 6.35 mm that corresponds to two FRP layers. The other parameters are kept fixed and the fastener pitch size of 50 mm is used to avoid possible shear failure in the fasteners. Figure 4.37 shows the percentage

4.4.2 Section Height

The strengthening effect of increasing the height of the steel cross-section (i.e., through using the three different cross-sections) is explored while keeping other parameters unchanged. Figure 4.36 shows the improvement in the load-carrying capacity of composite steel-FRP beams relative to the control beam at 120 mm mid-span deflection for the three considered cross-sections. The improvement due to increasing the steel section height is attributed to two main simultaneous effects. Firstly, the increased longitudinal displacement of the bottom points in the steel flange at the fastener locations. This increase is due to having almost the same beam slope θ (since S_x and Z_x of the three sections are very close) that is multiplied by a bigger half-height of the steel cross-section (i.e., $\theta h / 2$) which leads to higher slip and consequently higher shear forces in the fasteners. Secondly, the increased moment arm of the shear forces in the fasteners amplifies their bending moments that counteract the effect of the applied mid-span load (as shown earlier in Fig. 4.3). The two effects together significantly reduce the bending moment carried by the steel section leading to a better strengthening effect.

Figure 4.38 shows a trend for the initial slope of the load deflection curve which is similar to the trend shown for the load-carrying capacity. This is mainly due to the increase in the cross-sectional moment of inertia of the composite beam with thicker FRP laminates.

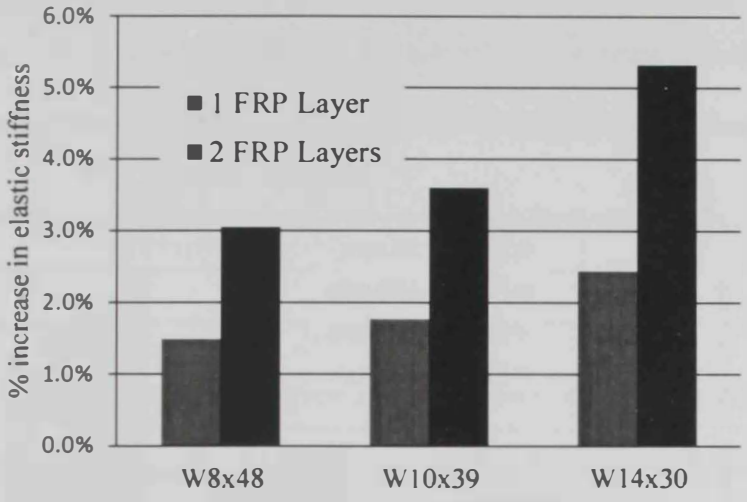

Figure 4.38: Percentage Increase in the Initial Slope of Load-Deflection Curve of Composite Beams for One and Two Layers of FRP

4.4.4 Distribution of the Steel Fasteners

The effect of the fasteners' pitch size (distance between fasteners) is examined in this section. Fastener pitch sizes of 50 mm, 100 mm, 150 mm and 200 mm and FRP thickness of 6.35 mm are considered while all the other parameters are kept fixed. Figure 4.39 shows the percentage increase in the load-carrying capacity over the control beam for different pitch sizes at a mid-span deflection of 120 mm. In general, reducing pitch size increases the load-carrying capacity of composite beams. This increase is more

increase in the load-carrying capacity over the control beam for the case of one and two layers of FRP laminates. The figure shows that the contribution of the FRP laminates in increasing the load-carrying capacity is almost doubled when two layers of FRP are used. This observation is in agreement with the outcomes of phase-I of the study and is mainly due to the increase in the shear forces in the fasteners in the case of thicker FRP laminate relative to the case of thinner FRP. This behavior is due to the increased slip resulting from two factors; almost unchanged slope of the composite beam in the two cases and decreased longitudinal movement of the thick (or stiff) FRP laminate at the fasteners locations.

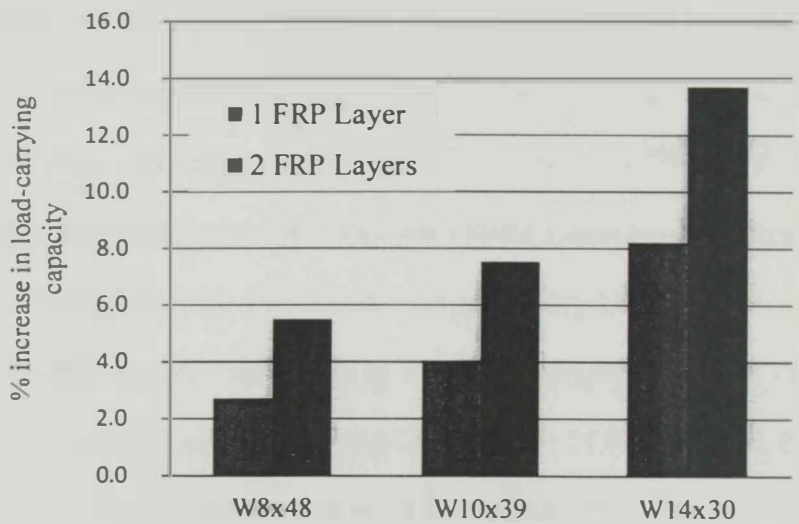

Figure 4.37: Percentage Increase in the Load-Carrying Capacity of Composite Beams at 120 mm Mid-span Deflection for One and Two Layers of FRP

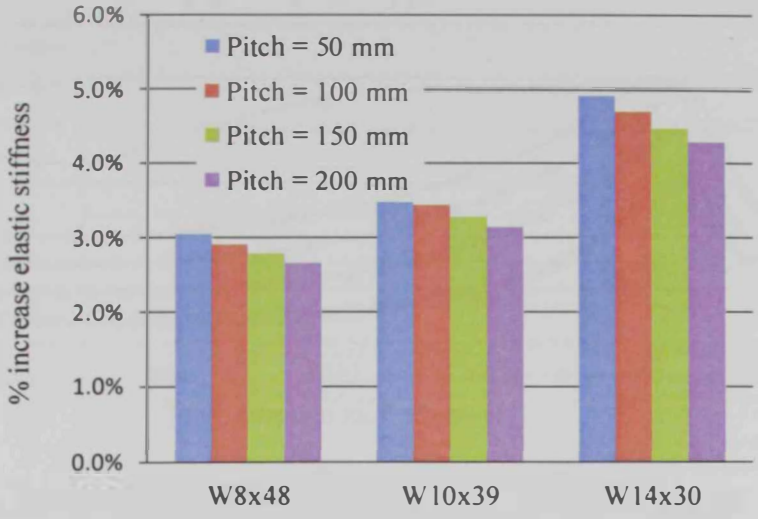

Figure 4.40: Effect of Pitch Size on the Slope of Load-Deflection Curve of Composite Beams

Figure 4.41 shows the distribution of the fasteners' shear forces for the pitch sizes of 50, 100, 150 and 200 mm for the case of W14x30. It is clear that fewer fasteners (i.e., bigger pitch size), results in higher shear forces (maximum of 9.92 kN for pitch size of 200 mm and 6.0 kN for 50 mm) which may exceed, in some situations, the shear strength of the fasteners leading to brittle shear failure. This indicates that the pitch sizes considered do not affect the overall mechanical behavior significantly, but it, evidently, affects the distribution of the shear forces in the fasteners.

pronounced for deeper steel sections for the same reason discussed in section 4.4.2 (e.g. 13.5% increase relative to the control beam for W14x30 and pitch size of 50 mm). Reducing the pitch size from 200 mm to 50 mm increases the improvement in the load-carrying capacity by about 3.3% for the beam W14x30. Meanwhile, the increase in the capacity improvement becomes about 0.9% for W8x48. A small change (less that 1%) in the improvement is noticed in the initial slope of the load deflection curve as shown in Fig. 4.40 which is attributed to the negligible effect of changing the number of fasteners on the interfacial slip and the cross-sectional inertia of the composite beam.

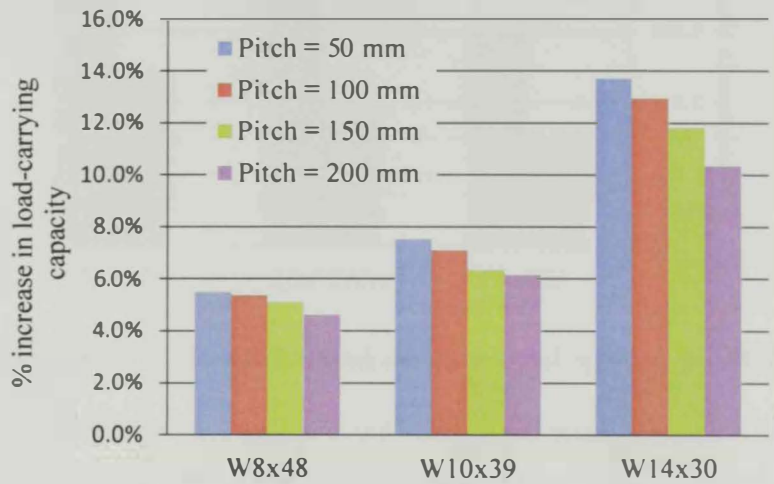

Figure 4.39: Effect of Pitch Size on the Load-Carrying Capacity of Composite Beams

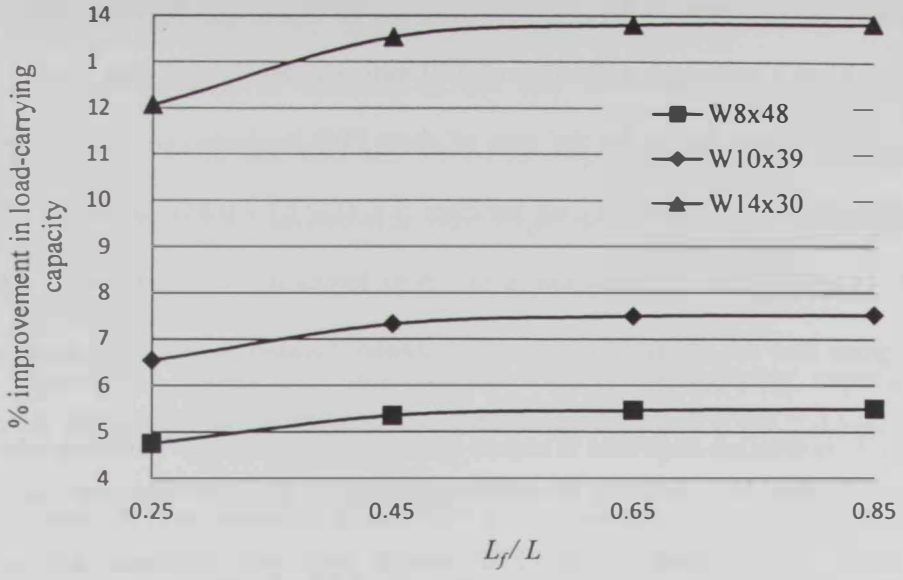

Figure 4.42: Effect of (L_f/L) Ratio on the Improvement of Load-Carrying Capacity at 120 mm Mid-span Deflection (2 Layers of FRP, P=50 mm)

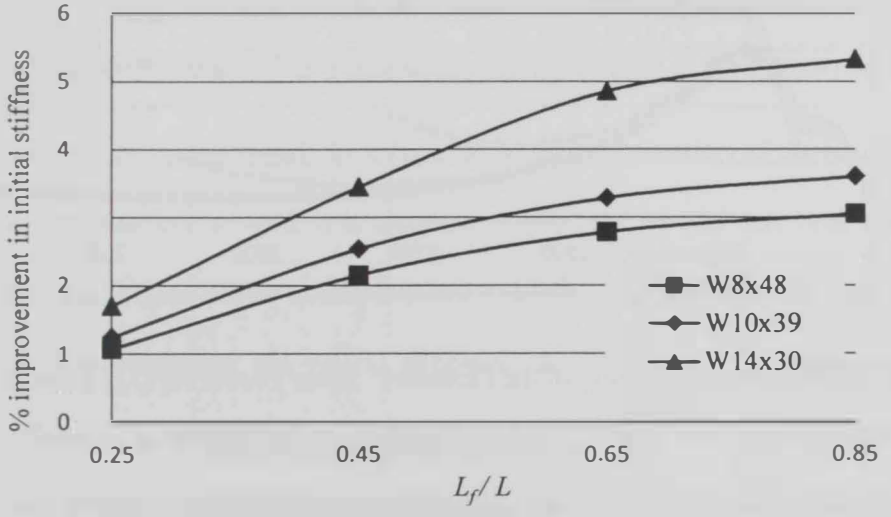

Figure 4.43: Effect of (L_f/L) Ratio on the Initial Slope of Load-Deflection Curve Relative to that of Control Beam at 120 mm Mid-span Deflection (2 Layers of FRP, P=50 mm)

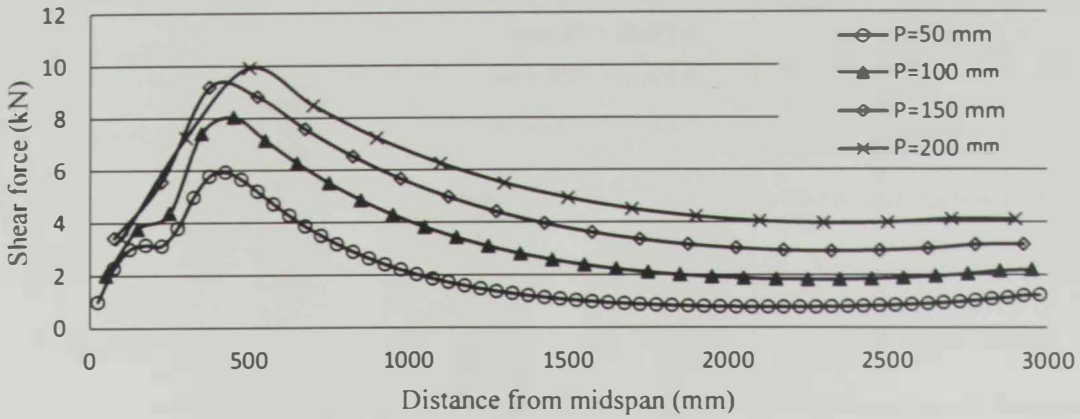

Figure 4.41: Distribution of the Fasteners' Shear Force for Different Pitch Sizes in Beam W14x30

4.4.5 FRP Length to Beam Span Ratio

The effect of the ratio between the length of the FRP laminate (L_f) and the span of the beam (L) is investigated. Four values of (L_f / L) are considered; namely 0.25, 0.45, 0.65 and 0.85. The pitch size of 50 mm and the FRP thickness of 6.35 mm are used while fixing all the other geometrical and material parameters of the composite beams. Figures 4.42 and 4.43 show the effect of (L_f / L) on the percentage improvement in the load-carrying capacity and initial slope of the load-deflection curve of the composite steel-FRP beams over the control beam, respectively. At (L_f / L) = 0.25, Fig. 4.42 and 4.43 show a rate of improvement that decreases as (L_f / L) increases towards 0.85. In general, increasing (L_f / L) over 0.65 does not introduce significant improvement in the mechanical behavior although it distribute the tensile force in the FRP laminate on more number of fasteners.

assumed that the load-slip model of the steel fasteners (Fig. 4.11) will not change due to the variation of modulus of elasticity of the FRP material. This assumption can be justified in view of the fact that the steel-FRP slip depends mainly on the bearing deformations in the GFRP layers with very slight dependency on the stiffness of the sandwiched CFRP layer.

Figure 4.45 shows the improvement in the load-carrying capacity of the composite steel-FRP beams over the control beams at mid-span deflection of 120 mm for the two cases of low modulus (LM-FRP) and ultrahigh modulus (UHM-FRP) FRP laminates. In the case of LM-FRP, the percentage increase in load-carrying capacity ranges from 6% for the shallow section (W8x48) to 14% for the deep section (W14x30). Meanwhile, this improvement ranges from 14% for W8x48 to 23% for W14x30 in the case of UHM-FRP. This is due to the significant increase in the fasteners' shear forces at UHM-FRP due to the small relative displacements in the FRP at the fastener locations.

The increase in the initial slope (i.e., in the elastic behavior) of the load-deflection curves are depicted in Fig. 4.46. It is clear that while the LM-FRP has little contribution (increasing the initial slope from 3% to 5% for sections W8x48 and W14x30, respectively) in increasing the elastic stiffness, the UHM-FRP provides considerably higher stiffness (e.g., increasing the initial slope from 15% to 23% over the control beam for sections W8x48 and W14x30, respectively). The increase in the initial slope when using UHM-FRP is mainly due to the increase in the overall stiffness of the composite system.

The distributions of the fasteners' shear forces, for the cases of (L_f / L) = 0.25 through 0.85 at a mid-span deflection of 120 mm, are depicted in Fig. 4.44. The figure shows that the shear forces for the case of short FRP laminate (i.e. (L_f / L) = 0.25) are higher than those of the case of long laminate (i.e. (L_f / L) = 0.85). In general, increasing the (L_f / L) ratio results in reduction in the shear forces induced in the fasteners. Figure 4.44 implies that the shear forces in the fasteners located in the FRP zone extending beyond (L_f / L = 0.65) decrease significantly. This observation, along with the outcomes of Figs. 4.42 and 4.43, indicate an optimum length of the FRP laminate (L_f / L= 0.65) after which any increase in the FRP length will not introduce any significant improvement in the behavior.

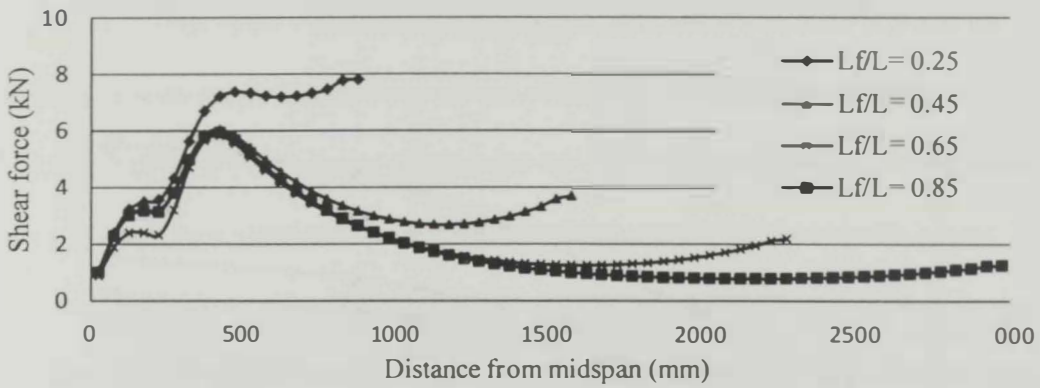

Figure 4.44: Effect Distribution of the Fasteners' Shear Forces for (L_f / L)=0.25 Through 0.85 at 120 mm Mid-span Deflection

4.4.6 Young's Modulus of FRP Laminate

In this section, low and ultrahigh Young's moduli of the FRP laminate are considered while all other geometrical and material properties are kept unchanged. It is

Figures 4.47, 4.48 and 4.49 show the load deflection curves of beams W14x30, W10x39 and W8x48, respectively, when strengthened with LM-FRP and UHM-FRP. These figures confirm the observations described earlier as they imply that the beams strengthened with UHM-FRP have gained significant increase in their stiffness and load-carrying capacity compared to the LM-FRP.

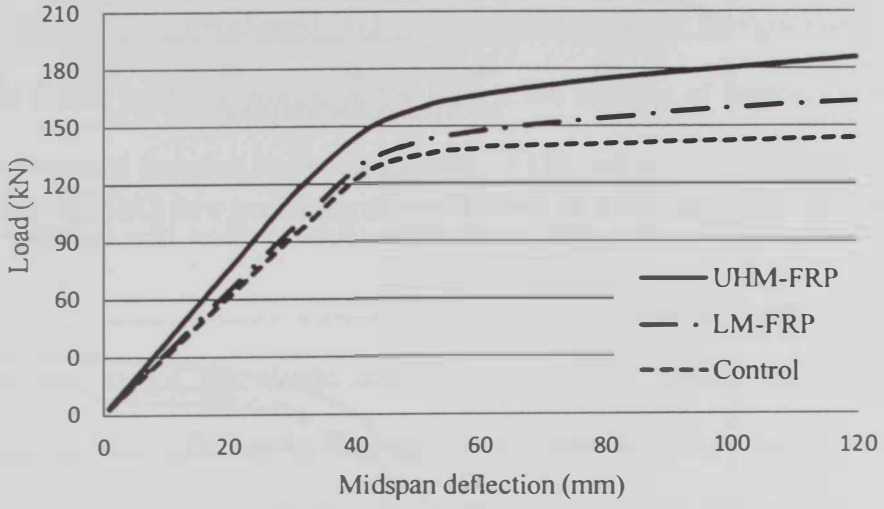

Figure 4.47: Response of the W14x30 Beam Strengthened with LM-FRP and UHM-FRP

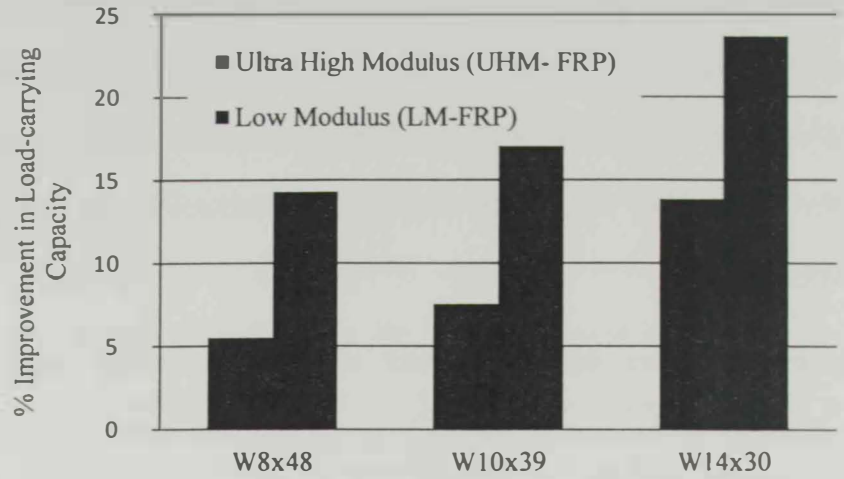

Figure 4.45: Improvement in Load-Carrying Capacity of the Composite Steel-FRP Beams for LM-FRP and UHM-FRP Laminates

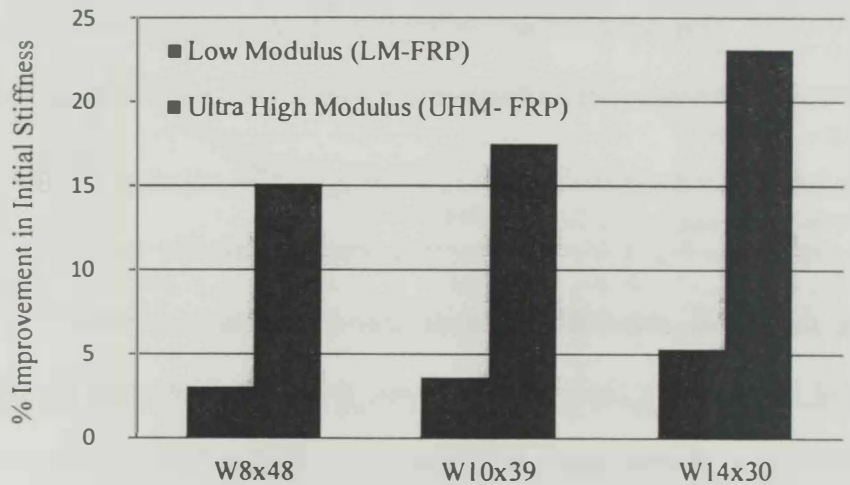

Figure 4.46: Improvement in the Elastic Stiffness of the Composite Steel-FRP Beams for LM-FRP and UHM-FRP Laminates

4.5 Conclusions

Several composite steel-FRP beams have been investigated numerically where the focus is put on understanding the mechanical behavior of the composite beams along with estimating the capacity and stress distribution through the different components of the composite system. The following items could be concluded from the numerical study:

1- The steel beams strengthened with mechanically fastened FRP laminates have a ductile failure mode by bearing in the FRP at the location of fasteners if sufficient number of steel fasteners and enough length of FRP are used. Insufficient number of steel fasteners will result in unfavorable brittle failure due to shear rupture in the fasteners.

2- The ratio between the elastic modulus of FRP and that of steel affects the contribution of the FRP in the load-carrying capacity of the composite beam. If the FRP modulus is significantly less than that of the steel, the FRP laminate does not provide significant contribution in carrying the loads except after the steel section exhibits significant yielding at the extreme fibers of the bottom flange. The contribution of the FRP is expected to increase and become more significant even before yielding of steel if the modulus of FRP is close or higher than that of the steel section.

3- The I-shaped steel beams with larger cross-sectional height exhibit relatively high contributions of the mechanically fastened FRP laminates in improving their flexural capacities. This is attributed to the increase in developed resisting bending moment

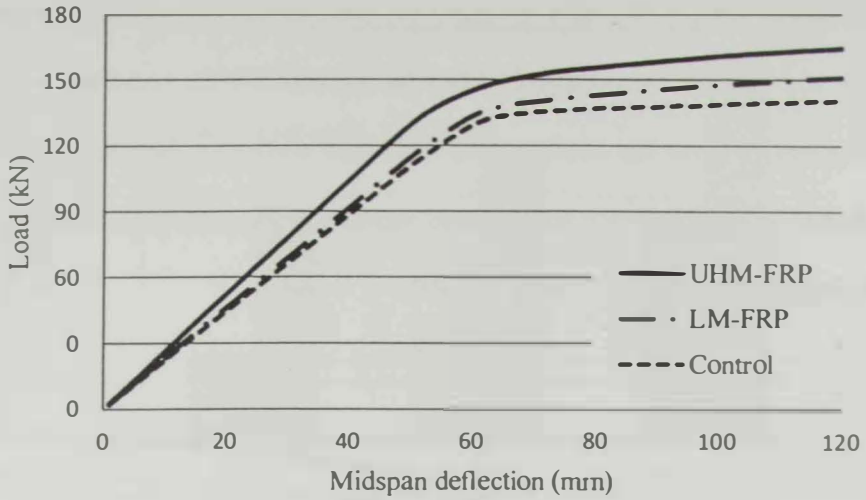

Figure 4.48: Response of the W10x39 Beam Strengthened with LM-FRP and UHM-FRP

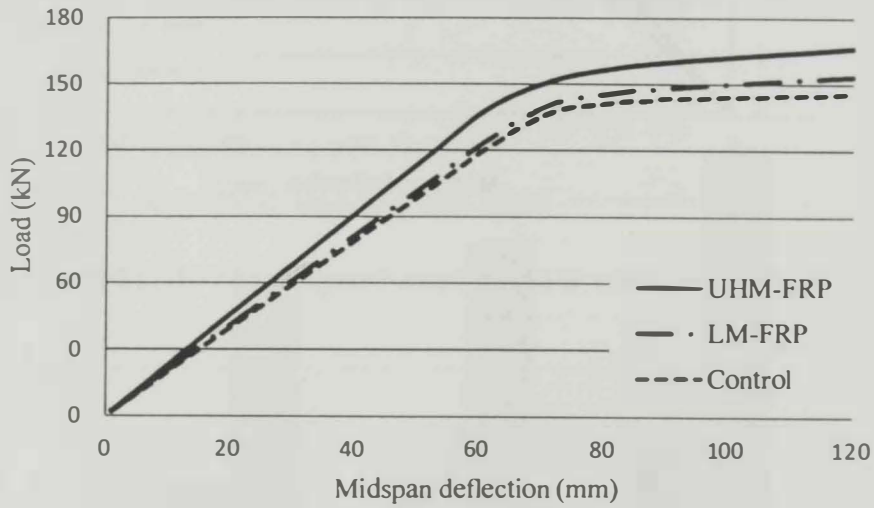

Figure 4.49: Response of the W8x48 Beam Strengthened with LM-FRP and UHM-FRP

CHAPTER 5

ANALYTICAL ELASTIC SOLUTION FOR THE RESPONSE OF COMPOSITE STEEL-FRP SYSTEMS

5.1 Introduction

There are two main structural design philosophies in current engineering practice; the Working Stress Design (WSD) and the Limit State Design (LSD). The WSD method requires that stresses in any structural element, under normal service loads, to be less than a maximum value defined by the material strength reduced by a factor of safety. Additionally the deflections should not to exceed certain limit to ensure good service to the occupants of the structure. On the other hand, the LSD method implies that any structure should be designed to fulfill its intended purpose and ensure that certain limits are not exceeded. Two main important limits are usually considered; namely the strength and serviceability limit states. To satisfy the strength limit, the ultimate load-carrying capacities of the structural elements at the state of impending collapse are analyzed and compared to the effects of the expected extreme effects of the loads (i.e., at ultimate or factored loads). The calculation of the nominal moment capacity is therefore essential for the design of beams. Unfortunately, there is no available analytical method to evaluate

in the steel beam due to the increased shear forces in the steel fasteners whose effect is amplified by the increase in the section height.

4- Increasing the thickness of the FRP laminate significantly improves the load-carrying capacity of the composite steel-FRP beams but at the same time increases the shear forces in the fasteners.

5- For the considered pitch sizes (i.e., 200-mm $\leq$ pitch $\leq$ 50-mm), increasing the number of steel fasteners, or reducing the pitch distance does not have significant improvement on the load-carrying capacity of the steel-FRP beam.

6- Increasing the length of FRP laminate beyond ($L_f / L = 0.65$) does not contribute significantly in enhancing the load-carrying capacity of the composite beam.

7- In general, for a fixed pitch size any increase in the length of the FRP laminate distributes the tensile force in the FRP on more fasteners. This may be required in some cases to ensure ductile bearing failure (in the composite beam) and avoid brittle shear failure in the fasteners.

8- The experimentally tested composite steel-FRP beams tend to fail by bearing at the fasteners' holes in the FRP laminate. At the bearing stage of the FRP laminate, the longitudinal carbon fibers exhibit low normal stresses relative to the tensile strength of the FRP laminate. In order to optimize the use of the FRP laminates in strengthening steel beams it is recommended to device a way to increase the bearing strength of the FRP laminate.

5.2 Background

The analysis of composite- or more specifically the partially composite beam requires the consideration of the interlayer contact and slip between its different subcomponents. Girhammar and Pan (2007) have studied the mechanical behavior of a composite beam with interlayer slip, made of two subcomponents (referred to as 1 for the top subcomponent and 2 for the bottom subcomponent) made of two different materials and connected by an adhesive layer that allows for interfacial shear and slip at the interface between the top and bottom subcomponents (Fig. 5.1).

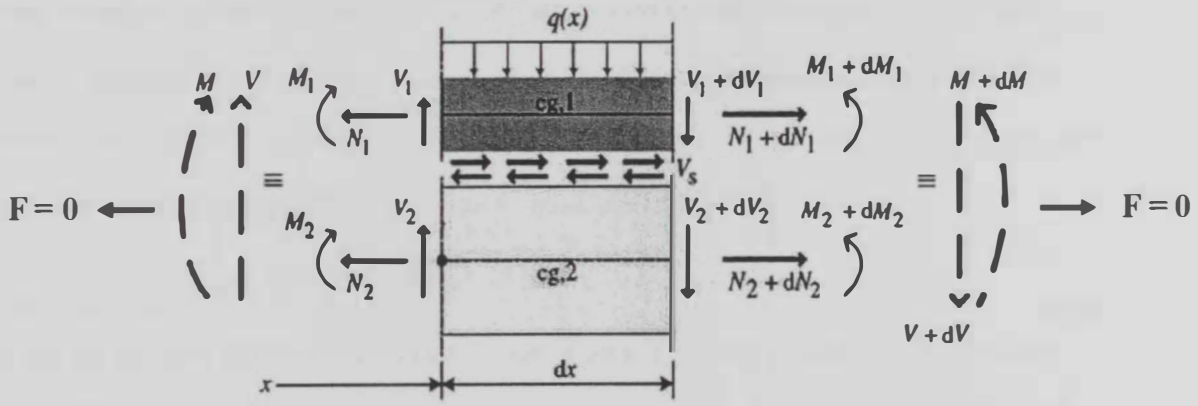

Figure 5.1: Forces Acting on an Infinitesimal Segment of a Beam Made of Two Different Subcomponents with Adhesive In-Between (After Girhammar and Pan, 2007)

Figure 5.1 shows an infinitesimal segment of the composite beam, of length dx, loaded with a distributed transverse load $q(x)$. The figure shows also the normal forces, shear forces, and moments acting on each subcomponent (e.g., N_1, V_1 and M_1 acting on subcomponent 1 and N_2, V_2, and M_2 acting on subcomponent 2) in addition to their

the nominal moment capacity of steel beams strengthened with mechanically fastened FRP laminates.

It is worth pointing out that satisfactory strength performance at ultimate loads does not guarantee satisfactory serviceability performance (e.g., acceptable deflection) at normal service loads. Since the adopted strengthening technique used in this study is characterized by a considerable reserve of strength in plastic region, this gives rise to excessive deformation which may have undesirable impact on the serviceability considerations. For a structural member such as a steel beam, the most important serviceability condition is the beam deflection under service loads, where the steel beam should not undergo excessive deflection. The deflection due to applied service loads is typically computed under the assumption of linear elastic behavior [Punmia *et al.* (2007)].

In this chapter a brief background about the partial interaction theory is firstly presented. Afterwards, the governing equations for the non-composite and the partially composite beam found in literature, are introduced and used to model the linear elastic behavior of the composite steel-FRP beams under static loading. The solution for the deflected shape is then presented followed by the prediction of the first yielding point of the composite steel-FRP beams and the distribution of the shear forces developed in the steel fasteners. Finally, the analytical results will be used to verify the FE model that was developed in chapter 3 to simulate the linear elastic behavior of the composite steel-FRP beams.

$$EI_{\infty} = EI_{o} + \frac{EA_{p} r^{2}}{EA_{o}} \tag{5.5}$$

where the $EA_0 = E_1 A_1 + E_2 A_2$, and $EA_p = (E_1 A_1)(E_2 A_2)$.

The general solution for Eqn. 5.2 is given by Girhammar and Gopu (1993) as:

$$w = a_1 \sinh(\alpha x) + a_2 \cosh(\alpha x) + a_3 x^3 + a_4 x^2 + a_5 x + a_6 + w_{ps} \tag{5.6}$$

where a_1 to a_6 are constants that can be evaluated after applying the boundary conditions of the composite steel-FRP beam. In addition, the term w_{ps} represents the particular solution of the differential equation which is a function of the distributed load $q(x)$ and is written as:

$$w_{ps} = \frac{1}{\alpha^5 EI_{\infty}} \int_{\frac{L-L_f}{2}}^{x} \left[\alpha^2 q(s) - \frac{EI_{\infty}}{EI_0} \frac{d^2 q(s)}{ds^2} \right] \left[\alpha(x-s) + \frac{\alpha^3}{6}(x-3)^3 - \sinh[\alpha(x-s)] \right] ds \tag{5.7}$$

where s is a dummy variable. The bending moment, shear force and axial force in the partially composite steel-FRP beam, can be evaluated by:

$$M = M_1 + M_2 + N_1 r = \frac{EI_{\infty}}{\alpha^2} \left[-\frac{d^4 w}{dx^4} + \alpha^2 \frac{d^2 w}{dx^2} + \frac{q}{EI_0} \right] \tag{5.8}$$

$$V = \frac{EI_{\infty}}{\alpha^2} \left[\frac{d^5 w}{dx^5} - \alpha^2 \frac{d^3 w}{dx^3} - \frac{1}{EI_0} \frac{dq}{dx} \right] \tag{5.9}$$

$$F = N_1 + N_2 = 0 \tag{5.10}$$

where

$$N_1 = -N_2 = \frac{EI_{\infty}}{\alpha^2 r} \left[-\frac{d^4 w}{dx^4} + \alpha^2 \left(1 - \frac{EI_0}{EI_{\infty}} \right) \frac{d^2 w}{dx^2} \right] \tag{5.11}$$

summations V and M that represent the shear force and moment acting on the full composite beam segment. The slip force V_s is assumed to be uniform and is related to the relative slip s through a linear elastic relationship having a slip modulus of K per unit length. This relation can be written as:

$$V_s = K s \tag{5.1}$$

Girhammar and Pan (2007) have derived the governing differential equation in terms of the vertical downward displacement (or deflection) function w as follows:

$$\frac{d^6 w}{dx^6} - \alpha^2 \frac{d^4 w}{dx^4} = \frac{-\alpha^2}{E I_\infty} q + \frac{1}{E I_o} \frac{d^2 q}{dx^2} \tag{5.2}$$

where α^2 is a parameter that expresses the degree of composite action between the top and bottom subcomponents and is found to be proportional to the slip modulus K, and is defined as:

$$\alpha^2 = K \left(\frac{1}{E_1 A_1} + \frac{1}{E_2 A_2} + \frac{r^2}{E I_o} \right) = K \left(\frac{E_1 A_1 + E_2 A_2}{(E_1 A_1)(E_2 A_2)} + \frac{r^2}{E I_o} \right) \tag{5.3}$$

where E_1, E_2, A_1 and A_2 are the Young's moduli and cross-sectional areas of the top and bottom beam subcomponents, respectively. In addition, r represents the distance between the centroids of the cross-sections of the top and bottom subcomponents, and the term EI_0 represents the flexural stiffness of the non-composite section (i.e., with no interfacial shear V_s between the two subcomponents) and is given by:

$$E I_o = E_1 I_1 + E_2 I_2 \tag{5.4}$$

The term EI_∞ represents flexural stiffness of the fully composite section (i.e., with no interlayer slip) and is defined as:

and area) are denoted as E_s, I_s, and A_s for the steel beam and E_f, I_f, and A_f for the FRP laminate, respectively. The differential equation governing the behavior of each zone along with the corresponding boundary conditions are discussed herein.

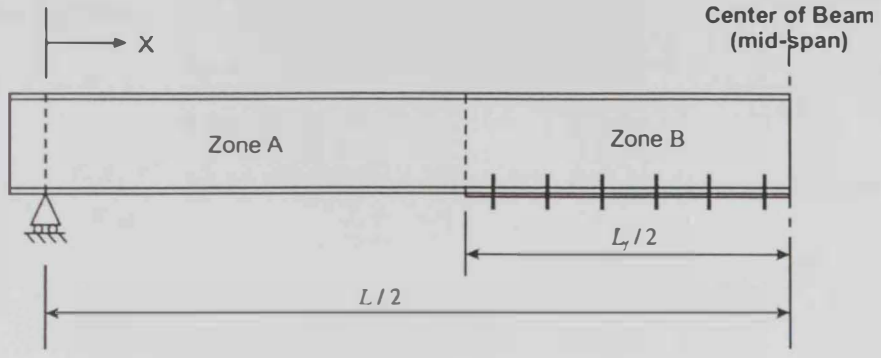

(a) Front View

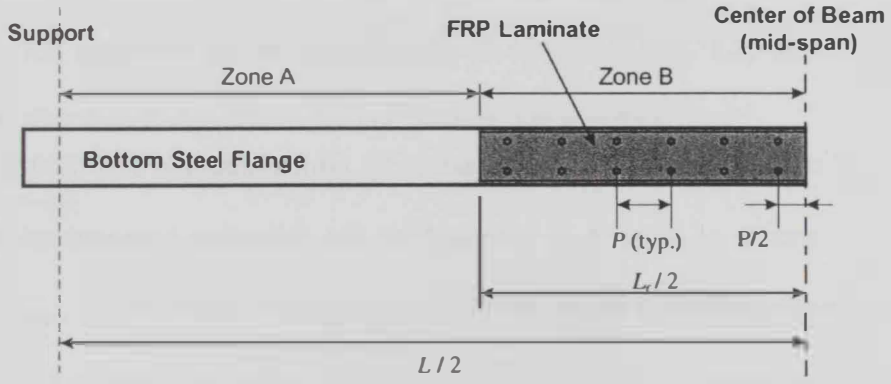

(b) Bottom View

Figure 5.2: The Zones of Different Governing Differential Equations in a Typical Composite Steel-FRP Beam

Zone A

The governing equation is the conventional Euler–Bernoulli beam equation defined by:

5.3 Deflection of Composite Steel-FRP Beams

In this section the deflection of a simply supported composite steel-FRP beam, subjected to a mid-span point load, is analyzed under the assumptions of linear elastic behavior for the steel and FRP materials and small deformations scheme. In the first sub-section, partial composite action theories developed by Girhammar and Pan (2007), in addition to Euler–Bernoulli beam theory, are revisited to derive the mathematical model of the beam's deflection. Knowing that the considered beams in this study are slender with isotropic material across the beam height, which makes the Euler–Bernoulli beam theory applicable. An example of deflection calculation is presented for a sample composite steel-FRP beam. Application of the analytical model is then explained in sub-section 5.3.2.

5.3.1 Derivation of the Analytical Solution

Figure 5.2 shows a typical composite steel-FRP beam made of two subcomponents namely; top steel I-shaped beam and bottom FRP laminate. The FRP laminate is covering a central portion of the bottom flange of the beam with length L_f. The beam can be subdivided into two different zones according to the mechanical behavior; the steel beam zone A (i.e, with no FRP) and the composite steel-FRP zone B. Due to the symmetry of the composite beam, only the left half is shown in Fig. 5.2. According to the figure, zone A is defined by $0 \le x \le (L-L_f)/2$ while zone B covers the region defined by $(L-L_f)/2 \le x \le L/2$. The mechanical and geometrical properties of the two different subcomponents (i.e., Young's modulus, cross-sectional moment of inertia

$$\alpha = \sqrt{K\left(\frac{1}{E_s A_s} + \frac{1}{E_f A_f} + \frac{r^2}{EI_o}\right)} \tag{5.17}$$

in which:

K is the slip modulus

$$EI_o = E_s I_s + E_f I_f \tag{5.18}$$

$$EI_\infty = EI_o + \frac{EA_p r^2}{EA_o} \tag{5.19}$$

$$EA_0 = E_s A_s + E_f A_f \tag{5.20}$$

$$EA_p = (E_s A_s)(E_f A_f) \tag{5.21}$$

For the case of composite steel-FRP beams where the discrete fasteners are used to connect FRP laminates to the steel flange, as shown in Fig. 5.2, the corresponding uniformly distributed slip modulus K may then be approximated as:

$$K = \frac{2K_{fastener}}{P} \tag{5.22}$$

where $K_{fastener}$ is the elastic slip modulus of one fastener discussed earlier in Chapters 3 and 4, and P is the pitch size representing the uniform longitudinal spacing between fasteners as presented in Fig. 5.2. It should be noted that this modulus is multiplied by 2 since there are two longitudinal gauge lines of fasteners along zone B as shown in Fig. 5.2b.

Boundary conditions

Table 5.1 summarizes the boundary conditions used to obtain the eight constants c_1 to c_8 in Eqns. (5.14 and (5.16. In Table 5.1 M_A is the moment at the end of zone A (i.e.,

$$\frac{d^2 w_A}{dx^2} = \frac{M}{E_s I_s} \tag{5.12}$$

For the case of simply supported beam with a point load F at the mid-span, Eqn. 5.12 becomes:

$$\frac{d^2 w_A}{dx^2} = \frac{F x}{2 E_s I_s} \tag{5.13}$$

Therefore, the general solution of the differential Eqn. 5.13 is:

$$w_A = \frac{F x^3}{12 E_s I_s} + c_1 x + c_2 \tag{5.14}$$

where w_A is the deflection function in zone A and c_1 and c_2 are constants that can be obtained after applying the boundary conditions pertaining to Zone A.

Zone B

In view of the differential equation proposed by Girhammar and Pan (2007) (i.e., Eqn. 5.2), the response of zone B is governed by the following homogenous differential equation for the particular case of $q(x)$=0:

$$\frac{d^6 w}{dx^6} - \alpha^2 \frac{d^4 w}{dx^4} = 0 \tag{5.15}$$

The general solution of Eqn. 5.15can be expressed as:

$$w_B = c_3 \sinh(\alpha x) + c_4 \cosh(\alpha x) + c_5 x^3 + c_6 x^2 + c_7 x + c_8 \tag{5.16}$$

where w_B is the deflection function in zone B, c_3 to c_8 are constants that depend on the boundary conditions and α the composite action parameter defined by

$$c_3\left(\frac{EI_o}{EI_\infty}\right)\sinh\left(\frac{\alpha(L-L_f)}{2}\right)+c_4\left(\frac{EI_o}{EI_\infty}\right)\cosh\left(\frac{\alpha(L-L_f)}{2}\right)+\left(\frac{EI_o}{EI_\infty}\right)\left(\frac{3c_5(L-L_f)}{\alpha^2}+\frac{2c_6}{\alpha^2}\right)=1 \quad (5.23d)$$

$$-c_1+\alpha c_3\cosh\left(\frac{\alpha(L-L_f)}{2}\right)+\alpha c_4\sinh\left(\frac{\alpha(L-L_f)}{2}\right)+\frac{3}{4}c_5(L-L_f)^2 + c_6(L-L_f)+c_7=\frac{F(L-L_f)^2}{16\,EI_\infty} \quad (5.23e)$$

$$\alpha\, c_3\cosh\left(\frac{\alpha L}{2}\right)+\alpha\, c_4\sinh\left(\frac{\alpha L}{2}\right)+\frac{3}{4}c_5L^2+c_6L+c_7=0 \quad (5.23f)$$

$$c_3\cosh(\alpha\frac{L}{2})\left(\frac{EI_o}{EI_\infty}\right)+c_4\sinh(\alpha\frac{L}{2})\left(\frac{EI_o}{EI_\infty}\right)+\left[\frac{6c_5}{\alpha^3}\right]\left(\frac{EI_o}{EI_\infty}\right)=1 \quad (5.23g)$$

$$c_5=\frac{-F}{12EI_\infty} \quad (5.23h)$$

There are eight unknowns c_1, c_2 ... c_8, whose values may be obtained by solving the eight equations (i.e., Eqn. 5.23) after being organized in a matrix form as follows:

$$[A]_{8x8}\ \{c\}_{8x1}=\{B\}_{8x1} \quad (5.24)$$

where matrix [A], vector $\{c\}$, and vector $\{B\}$ are defined as:

at $x = (L - L_f) / 2$) and M_B is the moment at the beginning of zone B (i.e., at $x = (L - L_f) /$ 2), while N_1 is the normal force induced in the FRP laminate.

Table 5.1: Boundary Conditions for the Composite Steel-FRP Beam

Boundary Condition #	Location	Imposed Condition	Justification
1	$x = 0$	$w_A = 0.0$	support (no vertical deflection)
2	$x = (L - L_f) / 2$	$w_A = w_B$	continuity of displacement between zone A & B
3	$x = (L - L_f) / 2$	$\frac{dw_A}{dx} = \frac{dw_B}{dx}$	continuity of rotation between zone A & B
4	$x = (L - L_f) / 2$	$M_A = M_B$	continuity of bending moment at zone's junction
5	$x = (L - L_f) / 2$	$N_1 = 0$	no normal force in the FRP at its edges
6	$x = L / 2$	$\frac{dw_B}{dx} = 0$	rotation at mid span is zero due to symmetry
7	$x = L / 2$	$\frac{dN_1}{dx} = 0$	slope of normal force function at mid span is zero due to symmetry
8	$x = L / 2$	$V = \frac{F}{2}$	value of shear force just before the mid span

Using the boundary conditions 1 to 8 shown in Table 5.1, the eight following equations are obtained.

$$c_2 = 0 \tag{5.23a}$$

$$\alpha^2 c_3 \sinh\left(\frac{\alpha(L-L_f)}{2}\right) + \alpha^2 c_4 \cosh\left(\frac{\alpha(L-L_f)}{2}\right) + 3c_5(L-L_f) + 2c_6 = \frac{F(L-L_f)}{4\,EI_\infty} \tag{5.23b}$$

$$-c_1\left(\frac{L-L_f}{2}\right) + c_3 \sinh\left(\frac{\alpha(L-L_f)}{2}\right) + c_4 \cosh\left(\frac{\alpha(L-L_f)}{2}\right) + c_5\left(\frac{L-L_f}{2}\right)^3 + c_6\left(\frac{L-L_f}{2}\right)^2 + c_7\left(\frac{L-L_f}{2}\right) + c_8 = \frac{F(L-L_f)^3}{96\,EI_\infty} \tag{5.23c}$$

$$w = \begin{cases} \dfrac{Fx^3}{12E_s I_s} + c_1 x + c_2 & 0 \le x \le \dfrac{L - L_f}{2} \\ c_3 \sinh(\alpha x) + c_4 \cosh(\alpha x) + c_5 x^3 + c_6 x^2 + c_7 x + c_8 & \dfrac{L - L_f}{2} \le x \le \dfrac{L}{2} \end{cases} \quad (5.25)$$

5.3.2 Application of Analysis Procedure

The mathematical solution derived in the preceding sub-section is applied to a simply supported composite steel-FRP beam with a span L=4.1 m. The beam cross section is UB 203x102x23. The FRP laminate is of 100 mm wide and 3.175 thick. The beam is subjected to a point load (F=30 kN) at the mid-span as shown in Fig. 5.3. The FRP laminate covers part of the bottom flange with a length L_f=2.7 m and is anchored to the steel flange by two parallel lines of 6 mm diameter fasteners spacing at a pitch size P=100 mm. Table 5.2 summarizes the values of geometrical and material properties of the considered steel-FRP composite beam.

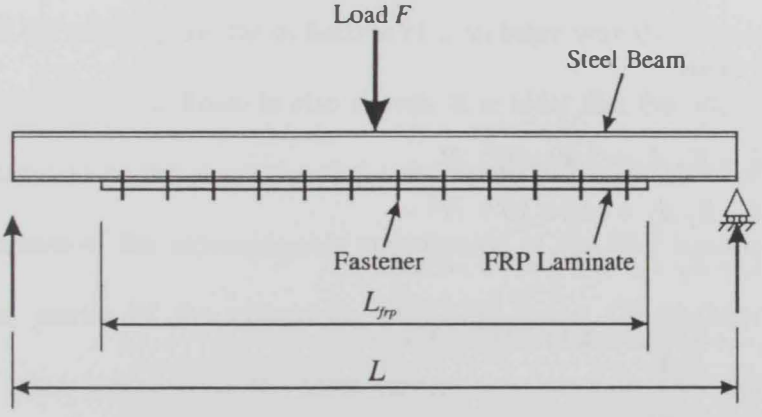

Figure 5.3: Simply Supported Composite Steel-FRP Beam Subjected to Mid-span Point Load

$$[A]=\begin{bmatrix}
0 & 1 & 0 & 0 & 0 & 0 & 0 & 0 \\
0 & 0 & \alpha^2 \sinh\left(\frac{\alpha(L-L_f)}{2}\right) & \alpha^2 \cosh\left(\frac{\alpha(L-L_f)}{2}\right) & 3(L-L_f) & 2 & 0 & 0 \\
\left(\frac{L_f-L}{2}\right) & 0 & \sinh\left(\frac{\alpha(L-L_f)}{2}\right) & \cosh\left(\frac{\alpha(L-L_f)}{2}\right) & \left(\frac{L-L_f}{2}\right)^3 & \left(\frac{L-L_f}{2}\right)^2 & \left(\frac{L-L_f}{2}\right) & 1 \\
0 & 0 & \left(\frac{EI_o}{EI_\infty}\right)\sinh\left(\frac{\alpha(L-L_f)}{2}\right) & \left(\frac{EI_o}{EI_\infty}\right)\cosh\left(\frac{\alpha(L-L_f)}{2}\right) & \frac{3}{\alpha^2}\left(\frac{EI_o}{EI_\infty}\right)(L-L_f) & \frac{2}{\alpha^2}\left(\frac{EI_o}{EI_\infty}\right) & 0 & 0 \\
-1 & 0 & \alpha\cosh\left(\frac{\alpha(L-L_f)}{2}\right) & \alpha\sinh\left(\frac{\alpha(L-L_f)}{2}\right) & 0.75(L-L_f)^2 & (L-L_f) & 1 & 0 \\
0 & 0 & \alpha\cosh(\alpha L/2) & \alpha\sinh(\alpha L/2) & 0.75L^2 & L & 1 & 0 \\
0 & 0 & \left(\frac{EI_o}{EI_\infty}\right)\cosh(\alpha L/2) & \left(\frac{EI_o}{EI_\infty}\right)\sinh(\alpha L/2) & \frac{6}{\alpha^3}\left(\frac{EI_o}{EI_\infty}\right) & 0 & 0 & 0 \\
0 & 0 & 0 & 0 & 1 & 0 & 0 & 0
\end{bmatrix}$$

$$\{c\}=\begin{bmatrix} c_1 \\ c_2 \\ c_3 \\ c_4 \\ c_5 \\ c_6 \\ c_7 \\ c_8 \end{bmatrix} \quad \text{and} \quad \{B\}=\begin{bmatrix} 0 \\ \frac{F(L-L_f)}{4EI_\infty} \\ \frac{F(L-L_f)^3}{96EI_\infty} \\ 1 \\ \frac{F(L-L_f)^2}{16EI_\infty} \\ 0 \\ 1 \\ \frac{-F}{12EI_\infty} \end{bmatrix}$$

The deflection w at any point along the considered beam is evaluated as:

$\alpha L = 7.059$

The values of $\{c_1, c_2 \ldots c_8\}$ for this particular case are obtained by using MS-Excel to solve Eqn. 5.24. The values of the constants $\{c_1, c_2 \ldots c_8\}$, having consistent units, are reported below:

$$\{c\} = \begin{bmatrix} -0.00859 \\ 0 \\ -0.146477 \\ 0.1491 \\ 6.66x10^{-10} \\ 5.914x10^{-12} \\ -0.00847 \\ -0.1203 \end{bmatrix}$$

Using Eqn. 5.25, the deflection functions are obtained as:

$$w = \begin{cases} 7x10^{-10}x^3 - 0.00859x & 0 \le x \le 700 \\ -0.146\sinh(0.00172x) + 0.149\cosh(0.00172x) + 6.66x10^{-10}x^3 + 5.91x10^{-12}x^2 - 0.0085x - 0.12 & 700 \le x \le 2050 \end{cases}$$

The deflection versus distance from the left support to the mid-span of the particular composite steel-FRP beam with the properties shown in Table 5.2 is presented in Fig. 5.4. On the same figure, the deflection of steel beam with the same dimensions but without the use of FRP laminate is also shown. It is clear that the addition of the FRP laminate contributed to the decrease of the deflection although, as expected, it is not significant because of the inconsiderable contribution of the FRP laminate to the gross cross-sectional inertia of the composite steel-FRP beam. On the same figure, the deflection of steel beams with the same dimensions but with two different fastener stiffness (K) values of 500,000 and 500 N/mm are also shown. The high K value (500,000 N/mm) represents the full composite action where no slip occurs between the steel and FRP laminate. This special case implies a reduction in the beam deflection as shown in

Table 5.2: The Geometrical and Material Properties for the Composite Steel-FRP Beam

Parameter	Value	Unit	Description
E_s	190000	N/mm^2	Young's modulus of steel
E_f	62000	N/mm^2	Young's modulus of FRP in the longitudinal direction
σ_y	300	N/mm^2	Yield stress of steel
A_s	2889.24	mm^2	Cross sectional area of steel beam UB 203x102x23
A_f	317.5	mm^2	cross sectional area of FRP laminate (100 mm wide and 3.175 mm thick)
I_s	20595941	mm^4	Moment of inertia of steel section around the major x- axis
I_f	266.7	mm^4	Moment of inertia of FRP laminate about minor axis
P	100	mm	Pitch size
L	4100	mm	Beam span
L_f	2700	mm	Length of FRP laminate
r	103	mm	Distance between the centroids of the two subcomponents
$K_{fastener}$	2700	N/mm	Slip modulus of the 6 mm diameter fastener
h	203	mm	Total height of steel cross-section
F	30	kN	Point load applied at the mid-span

Calculation Steps:

$$E A_o = E_s A_s + E_f A_f = 5.69 \times 10^8 \quad N$$

$$E A_p = E_s A_s . E_f A_f = 1.08 \times 10^{16} \quad N^2$$

$$E I_o = E_s I_s + E_f I_f = 3.91 \times 10^{12} \quad N.mm^2$$

$$E I_\infty = E I_0 + \frac{E A_p r^2}{E A_0} = 4.11 \times 10^{12} \quad N.mm^2$$

$$K = \frac{2K_{Bolt}}{P} = 54 \quad N/mm^2$$

$$\alpha = \sqrt{K\left(\frac{1}{E_s A_s} + \frac{1}{E_f A_f} + \frac{r^2}{EI_o}\right)} = 0.00172 \quad mm^{-1}$$

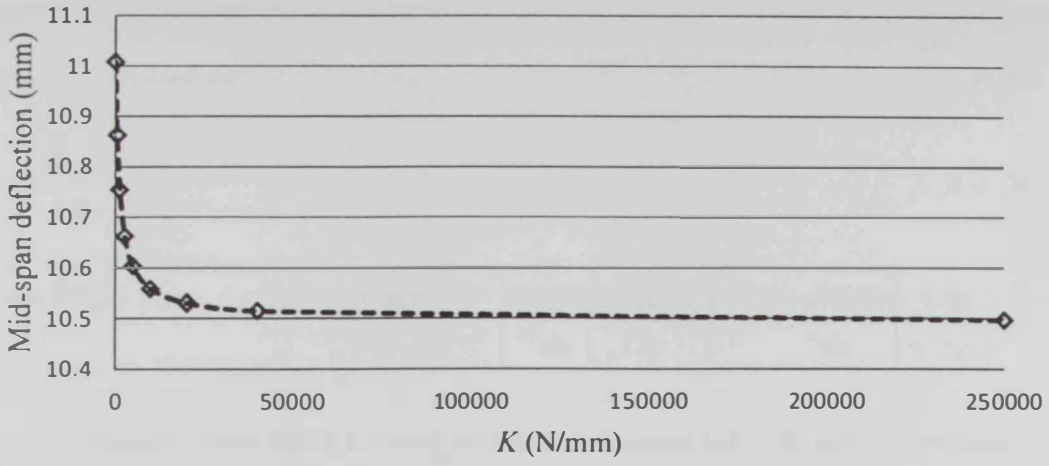

Figure 5.5: Mid-span Deflection of Composite Steel-FRP Beam with Different K Values

Figure 5.5 shows the variation of the mid-span deflection for the considered composite steel-FRP beam, with properties shown in Table 5.2, versus the different slip modulus (K) values. It is clear that the use of stiffer steel fasteners leads to higher reduction in beam deflection. The rate of reduction in beam deflection is relatively remarkable for K values ranging between (0) and (5000) N/mm. The enhancement in deflection values becomes much less apparent for slip modulus values higher than 5000 N/mm up to the full composite action status.

5.4 Yielding Load Prediction

The analytical solution developed in section 5.3 is extended to evaluate the load at which yielding of the steel section (as part of the composite steel-FRP beam) starts. The internal normal stress at the top fibers of the steel section is evaluated as:

Fig. 5.4. Meanwhile, the beam with low K value (500 N/mm) experienced more deflection than the composite steel-FRP beam having a K value of 2700 N/mm. This is attributed to the higher interfacial slip between the steel and FRP laminate associated with lower slip modulus values.

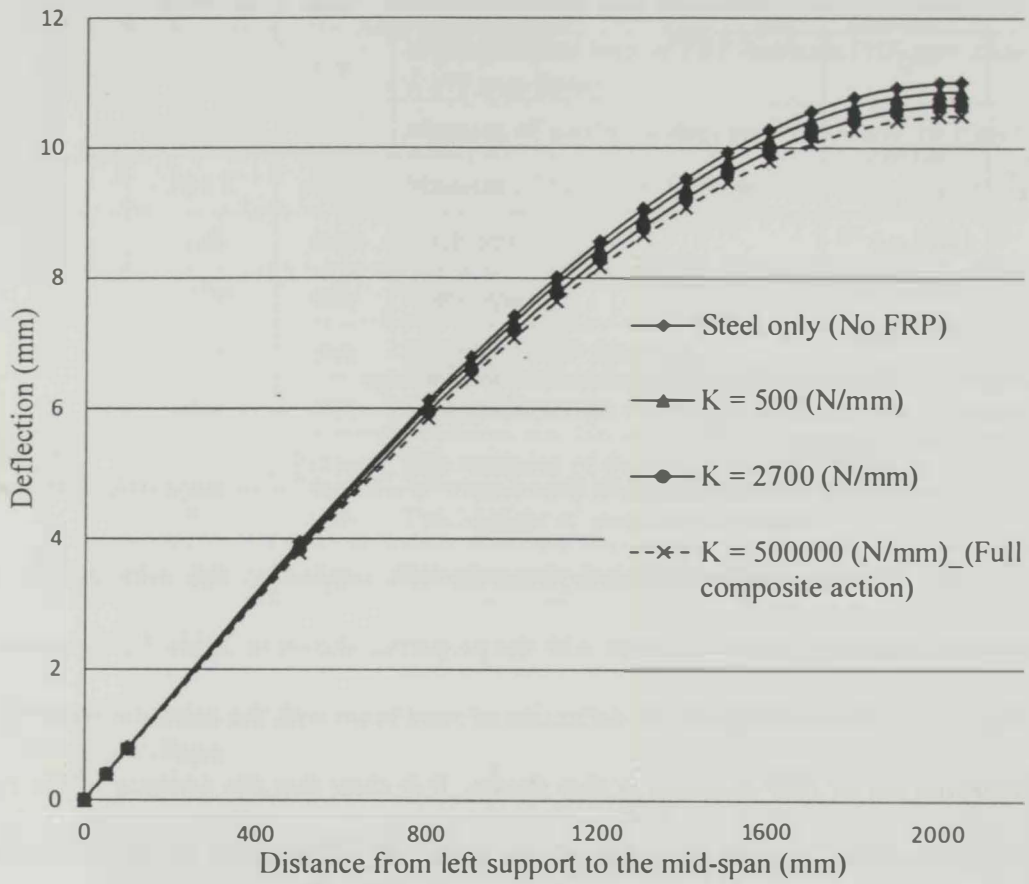

Figure 5.4: The Deflection of Composite Steel-FRP Beams with Different Fastener Stiffness (K) Values and Steel Beam Calculated Analytically

expected to be induced at the top flange of the steel section. The normal stress at the top flange is evaluated as:

$$\sigma_s = \frac{M_s\, h}{2\, I_s} + \frac{N_s}{A_s}$$

where h=203 mm, A_s= 2889.24 mm^2, I_s= 20595941 mm^4, and the yielding stress of the steel equals to 300 N/mm^2.

$$300 = \frac{M_s(203)}{2(20595941)} + \frac{N_s}{2889.24} = \frac{M_s}{202915.7} + \frac{N_s}{2889.24}$$

Knowing that both M_s and N_s are functions of the applied load F: (show them as function of F)

$$M_s = E_s\, I_s \left[\alpha^2 c_3 \sinh(\alpha x) + \alpha^2 c_4 \cosh(\alpha x) + 6c_5 x + 2c_6\right] \tag{5.27}$$

$$N_s = \frac{EI_\infty}{\alpha^2 r}\left[-\left(\alpha^4 c_3 \sinh(\alpha x) + \alpha^4 c_4 \cosh(\alpha x)\right) + \alpha^2\left(1 - \frac{EI_0}{EI_\infty}\right)\left(\alpha^2 c_3 \sinh(\alpha x) + \alpha^2 c_4 \cosh(\alpha x) + 6c_5 x + 2c_6\right)\right] \tag{5.28}$$

The yield load values that satisfies Eqn. 5.27 and Eqn. 5.28 is found to be 60 kN.

5.5 Shear Forces Distribution in the Fasteners

Referring to Eqn.5.11, the slip force V_s at a distance x from the left support of the composite steel-FRP beam can be evaluated as the following:

$$V_s = \frac{dN_1}{dx} = \frac{EI_\infty}{\alpha^2 r}\left[-\frac{d^5 w}{dx^5} + \alpha^2\left(1 - \frac{EI_0}{EI_\infty}\right)\frac{d^3 w}{dx^3}\right] \tag{5.29}$$

Knowing the slip modulus K and using Eqn. 5.1, the slip s is:

$$\sigma_s = \frac{M_s h}{2I_s} + \frac{N_s}{A_s} \tag{5.26}$$

where

$$M_s = E_s I_s \frac{d^2 w}{dx^2}$$

$$N_s = \frac{E I_\infty}{\alpha^2 r}\left[-\frac{d^4 w}{dx^4} + \alpha^2 \left(1 - \frac{E I_0}{E I_\infty}\right) \frac{d^2 w}{dx^2} \right]$$

In these equations M_s is the moment in the steel beam, h is the overall height of the steel section, I_s is the moment of inertia of the steel cross-section, N_s is the normal force acting at the centroid of the steel section (which is of equal magnitude and opposite direction to the normal force N_l carried by the FRP laminate), A_s is the cross-sectional area of the steel beam. w is the deflection function given by Eqn.5.25, EI_o and EI_∞ are bending stiffness parameters as provided by Eqns. 5.18 and 5.19, respectively. Given that both M_s and N_s are function of the applied load F, the load value that results in a specific stress value σ_s can be evaluated. It should be noted that the proposed procedure should not be used to predict stress values beyond the yield point since the adopted deflection function is valid within the elastic response range only.

5.4.1 Illustrative Example

Composite system analyzed in section 5.3.2 is considered to evaluate the load value F_y which will initiate yielding of the steel section. Table 5.2 and Fig. 5.3 show the properties and configuration of the considered beam. The maximum stress value is

The shear force developed in the steel fastener located at 150 mm from the mid-span is calculated according to Eqn.5.31 As the following:

$$F_{fastener} = sK_{fastener} = 0.0376 * 2700 = 101.52 \text{ N} = 0.102 \text{ kN}$$

A similar procedure is used to calculate the shear forces in the other fasteners. Figure 5.6 shows the distribution of shear forces in the fasteners at the loading of 30 kN.

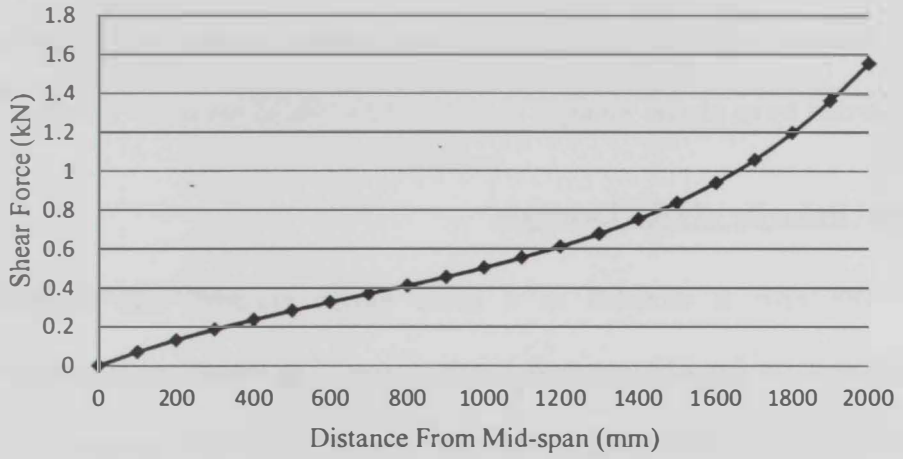

Figure 5.6: Shear Forces Carried by the Steel Fasteners at Mid-span Load of 30 kN

5.6 Comparison Between Analytical Results and FE Predictions

A three dimensional (3D) finite element modeling is conducted using the general purpose finite element software package ANSYS to simulate the linear elastic behavior of composite steel-FRP beams. The FE model has similar features to the one presented earlier in Chapter 3 and Chapter 4 except for the material models of the steel and fasteners. In this section these material models are briefly described and then the results

$$s = \frac{V_s}{K} \tag{5.30}$$

For a composite steel-FRP beam with a pitch size P and a fastener elastic stiffness $K_{fastener}$, the shear force carried by each fastener can be calculated as shown below:

$$F_{fastener} = s\ K_{fastener} \tag{5.31}$$

5.5.1 Illustrative Example

The composite system analyzed in section 5.3.2 is considered to evaluate the shear forces developed in the steel fasteners. Table 5.2 and Fig. 5.3 show the properties and configuration of the considered beam. To evaluate the shear force carried by the steel fastener at a distance 150 mm from the mid-span, the slip force at the same location is first calculated using Eqn.5.31:

$$V_s = \frac{EI_\infty}{\alpha^2 r}\left[-\frac{d^5 w}{dx^5} + \alpha^2\left(1 - \frac{EI_0}{EI_\infty}\right)\frac{d^3 w}{dx^3}\right]$$

$$V_s = \frac{4.115x10^{12}}{2.99x10^{-6} * 103}\left[-4.02x10^{-16} + 2.99x10^{-6}\left(1 - \frac{3.9132x10^{12}}{4.115x10^{12}}\right)3.779x10^{-9}\right] = -2.03 \quad N/mm$$

To calculate the slip s, Eqns. 5.22 and 5.30 are used to calculate the stiffness modulus and slip, respectively:

$$K = \frac{2K_{fastener}}{P} = \frac{2 * 2700}{100} = 54 \ N/mm^2$$

$$s = \frac{V_s}{K} = \frac{-2.03}{54} = 0.0376 \ mm$$

The shear force developed in the steel fastener located at 150 mm from the mid-span is calculated according to Eqn.5.31 As the following:

$$F_{fastener} = sK_{fastener} = 0.0376 * 2700 = 101.52 \text{ N} = 0.102 \text{ kN}$$

A similar procedure is used to calculate the shear forces in the other fasteners. Figure 5.6 shows the distribution of shear forces in the fasteners at the loading of 30 kN.

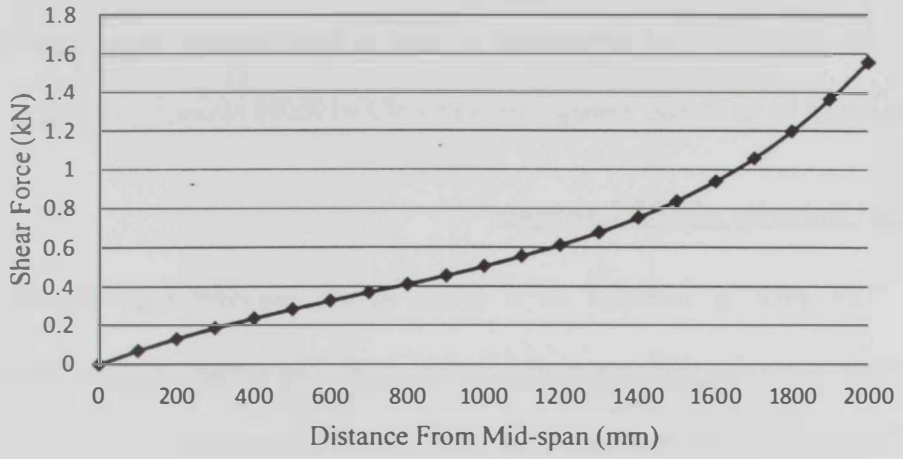

Figure 5.6: Shear Forces Carried by the Steel Fasteners at Mid-span Load of 30 kN

5.6 Comparison Between Analytical Results and FE Predictions

A three dimensional (3D) finite element modeling is conducted using the general purpose finite element software package ANSYS to simulate the linear elastic behavior of composite steel-FRP beams. The FE model has similar features to the one presented earlier in Chapter 3 and Chapter 4 except for the material models of the steel and fasteners. In this section these material models are briefly described and then the results

$$s = \frac{V_s}{K} \tag{5.30}$$

For a composite steel-FRP beam with a pitch size P and a fastener elastic stiffness $K_{fastener}$, the shear force carried by each fastener can be calculated as shown below:

$$F_{fastener} = s\ K_{fastener} \tag{5.31}$$

5.5.1 Illustrative Example

The composite system analyzed in section 5.3.2 is considered to evaluate the shear forces developed in the steel fasteners. Table 5.2 and Fig. 5.3 show the properties and configuration of the considered beam. To evaluate the shear force carried by the steel fastener at a distance 150 mm from the mid-span, the slip force at the same location is first calculated using Eqn.5.31:

$$V_s = \frac{EI_\infty}{\alpha^2 r}\left[-\frac{d^5 w}{dx^5} + \alpha^2\left(1 - \frac{EI_0}{EI_\infty}\right)\frac{d^3 w}{dx^3}\right]$$

$$V_s = \frac{4.115x10^{12}}{2.99x10^{-6} * 103}\left[-4.02x10^{-16} + 2.99x10^{-6}\left(1 - \frac{3.9132x10^{12}}{4.115x10^{12}}\right)3.779x10^{-9}\right] = -2.03 \quad N/mm$$

To calculate the slip s, Eqns. 5.22 and 5.30 are used to calculate the stiffness modulus and slip, respectively:

$$K = \frac{2K_{fastener}}{P} = \frac{2*2700}{100} = 54 \ N/mm^2$$

$$s = \frac{V_s}{K} = \frac{-2.03}{54} = 0.0376 \ mm$$

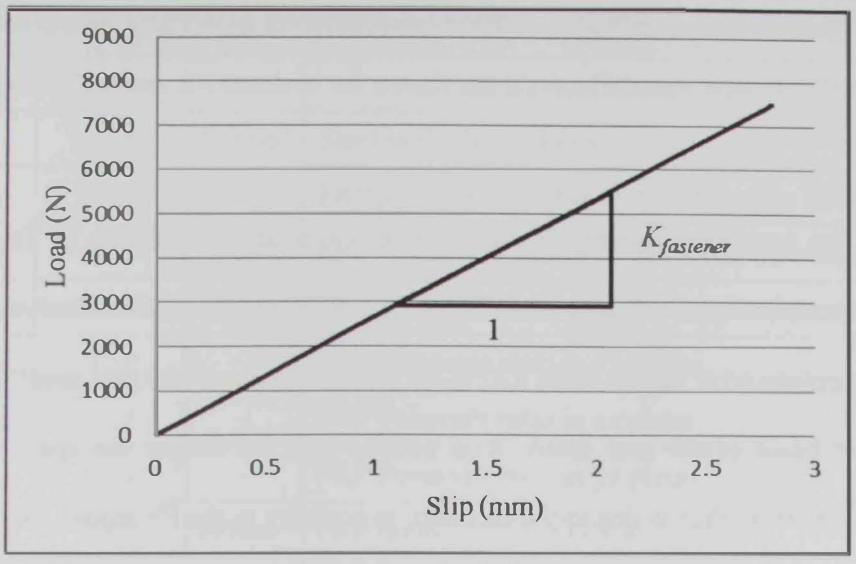

Figure 5.7: Simplified Material Model for the Spring Element Used to Simulate the Fasteners

5.6.2 Comparative Study

The FE model described in the preceding section is employed to evaluate the linear elastic behavior with small deformations of composite steel-FRP beams under a point mid-span load. The load-deflection behavior, the load at first yielding in the steel cross-section, and the distribution of the shear forces developed in the steel fasteners are obtained from the FE results and compared to the analytical values obtained based on the procedures outlined in sections 5.3 and 5.4. Table 5.3 shows the basic material properties and geometric configuration considered in the comparative study.

Beam deflection

The deflection at the mid-span of composite steel-FRP beam with different spans and FRP lengths at different load stages are presented in Table 5.4. The table reports on

of the FE model are verified against the analytical solution presented in the preceding sections.

5.6.1 Material Models

All materials used in the FE model are assumed to be of linear elastic characteristics. The simplified material models adopted in this chapter are listed herein:

Material Behavior of Steel Beam:

The steel material is assumed to have a linear elastic stress-strain relationship characterized by an elastic Young's modulus of E=190000 N/mm^2 = 190 GPa.

Material Behavior of FRP Laminate

The FRP is modeled as a linear elastic material with different material characteristics in the different working directions. The elastic modulus, shear modulus and Poisson's ratio values are given in Table 3.1.

Material Behavior of Steel Fasteners

As discussed earlier in Chapter3 and Chapter 4, each steel fastener is modeled using a ANSYS spring element COMBIN39. The spring element stiffness in the Z-direction (the longitudinal direction of interfacial slip between the steel beam and the FRP laminate) is assigned a single value of $K_{fastener}$ = 2700 N/mm as shown in Fig. 5.7. This value corresponds to the elastic fastener stiffness specified in Chapter 3.

Table 5.3: Material and Geometrical properties used in the Comparative Study

Parameter		Value	Unit	Description
E_s		190000	N/mm^2	Steel young's modulus
E_f	E_{fx}	4800	N/mm^2	FRP young's modulus in the transverse direction
	E_{fy}	4800	N/mm^2	FRP young's modulus in the vertical direction
	E_{fz}	62000	N/mm^2	FRP young's modulus in the longitudinal direction
v_f	v_{fxy}	0.30	-	FRP Poisson's ratio in xy plane
	v_{fxz}	0.22	-	FRP Poisson's ratio in xz plane
	v_{fyz}	0.22	-	FRP Poisson's ratio in yz plane
G_f	G_{fxy}	1967	N/mm^2	FRP modulus of rigidity in xy plane
	G_{fxz}	3270	N/mm^2	FRP modulus of rigidity in xz plane
	G_{fyz}	3270	N/mm^2	FRP modulus of rigidity in yz plane
σ_y		300	N/mm^2	Yield stress of steel
A_s		2889.24	mm^2	The steel section cross sectional area
A_f		317.5	mm^2	FRP laminate cross sectional area
I_s		20595941	mm^4	Moment of inertia of the steel section about its centroid
I_f		266.7	mm^4	Moment of inertia of the FRP laminate about its centroid
P		100	mm	Pitch size
r		103.0875	mm	Distance between the centroids of the two subcomponents
$K_{fastener}$		2678.57	N/mm	Slip modulus of the steel fastener
h		203	mm	The height of the steel cross section

composite steel-FRP beams with spans/FRP lengths of 8100/4100 mm, 6100/3700 mm, and 4100/2700 mm. The deflections are shown for both the FE and analytical methods of analysis.

The percentage errors for the different cases are also shown in Table 5.4. The results show an excellent agreement between the FE model and the analytical solution. The percentage error ranges from 0.31% for the long beam (8100 mm span) to 2.52% for the short beam (4100 mm span). It is noticed that the longer the span, the less the percentage error. That is due to the fact that, in contrary to the FE model, Girhammar and Pan (2007) in the partial composite action theory, did not consider the effect of transverse shear strains on the deflection. The contribution of the shear deformation to the deflection at the mid-span of the beam is higher at smaller span-to-height ratios, and vanish at span-to-height ratios more than 20 [Lowe, P. G. (1971)].

Yielding point prediction

The first yield in the steel beam typically starts at the top subcomponent of the top flange of the composite steel-FRP beam and the yield stress in steel is assumed to be σ_y = 300 N/mm^2. In the FE model, the Von Mises stress at the top flange are obtained and at any mid-span load then the load is scaled to produce a value for Von Mises stress that is equal to σ_y = 300 N/mm^2. The mid-span load at this stress level represents the load at first yield F_y.

Table 5.5 shows the comparison between the FE and the analytical solutions for the three different cases described earlier in the preceding section. The FE results, the results show a good agreement between the two models with percentage error ranges from 0.47% for the 4100 mm span beam to 3.61% for the 8100 mm span beam.

Table 5.5: The Load Value (F_y) Corresponds to First Yield in the Composite Steel-FRP Beam Calculated Using FE Model and the Analytical Solution

Case #	L (mm)	L_f (mm)	F_y (kN)		% error
			FE model	Analytical Solution	
1	8100	4100	31.56	30.46	**3.61%**
2	6100	3700	39.30	40.41	**2.75%**
3	4100	2700	60.29	60.01	**0.47%**

The shear force distribution in the fasteners

The distribution of the shear forces developed in the steel fasteners is obtained analytically for some of Alhadid's beams presented in Chapter 4. The analytical results

Table 5.4: The Deflection Values Obtained from the FE Model and the Analytical Model for the Composite Steel-FRP Beam

L = 8100 (mm) & L_f = 4100 (mm)			
Load kN	Mid-span deflection (mm)		% Error
	FE model	**Analytical Solution**	
0.73	2.00	2.006	**0.300%**
1.47	4.00	4.012	**0.300%**
2.20	6.00	6.018	**0.300%**
5.14	14.00	14.043	**0.307%**
8.08	22.00	22.068	**0.309%**
9.54	26.00	26.08	**0.308%**
11.01	30.00	30.092	**0.307%**
L = 6100 (mm) & L_f = 3700 (mm)			
Load kN	Mid-span deflection (mm)		% Error
	FE model	**Analytical Solution**	
1.709	2.00	1.991	**0.450%**
3.418	4.00	3.982	**0.450%**
8.544	10.00	9.956	**0.440%**
13.670	16.00	15.93	**0.438%**
18.797	22.00	21.904	**0.436%**
25.632	30.00	29.869	**0.437%**
L = 4100 (mm) & L_f = 2700 (mm)			
Load kN	Mid-span deflection (mm)		% Error
	FE model	**Analytical solution**	
5.486	2.00	1.95	**2.500%**
10.971	4.00	3.899	**2.525%**
16.457	6.00	5.849	**2.517%**
21.942	8.00	7.799	**2.513%**
27.428	10.00	9.749	**2.510%**
32.914	12.00	11.698	**2.517%**

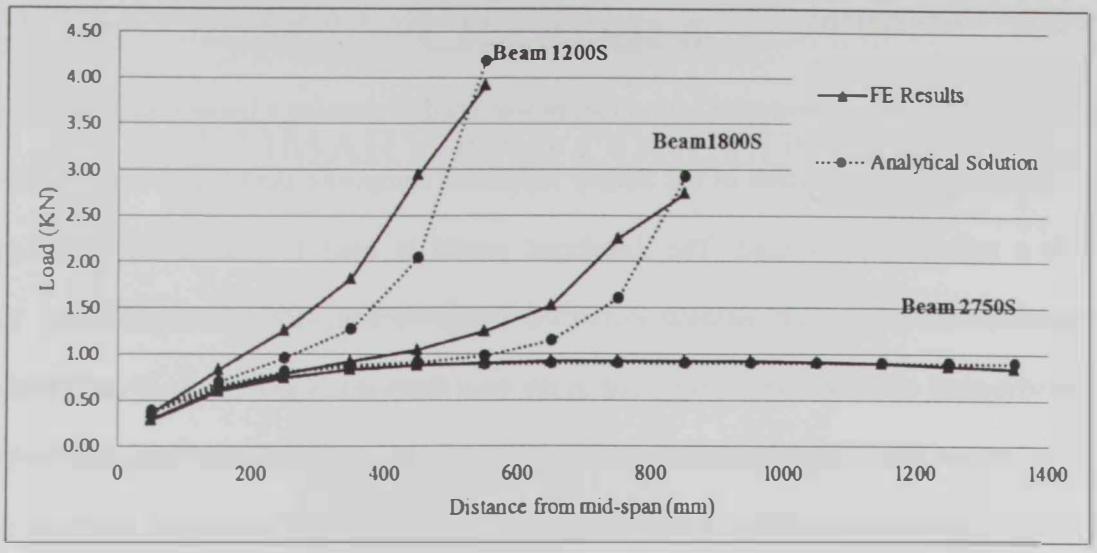

Figure 5.9: FE and Analytical Results for the Distribution of the Fasteners' Shear Forces in Three Different Beams Due to a Mid-span Point Load of 75 kN and $K_{fastener}$ of 100,000 N/mm

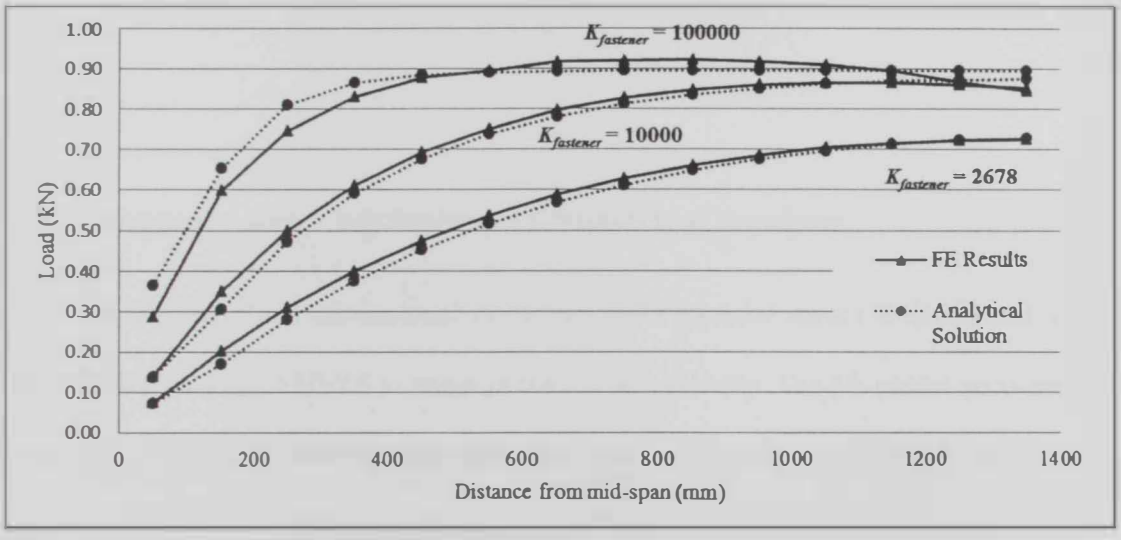

Figure 5.10: FE and Analytical Results for the Distribution of the Fasteners' Shear Forces in Beam 2750S Due to a Mid-span Point Load of 75 kN with Three Different $K_{fastener}$ values

are compared to the FE results for different fastener stiffness values ($K_{fastener}$). Figure 5.8 Shows the distribution of the fasteners' shear forces in three different beams due to a mid-span point load of 75 kN and $K_{fastener}$ of 2,678 N/mm. Figure 5.9 shows the distribution of shear forces in the steel fasteners at the same load but with a higher stiffness value ($K_{fastener}$ = 100,000 N/mm) which represents a case that is very close to that of the fully composite steel-FRP beam. Figure 5.10 shows the distribution of shear forces in the steel fasteners in the beam 2750S with different $K_{fastener}$ values. The figures show very good agreement between the FE and analytical results especially for long spans (e.g., 2750S). For the cases of 1200S and 1800S, where $K_{fastener}$ is high, there is a small difference which is attributed to the shear deformations being neglected in the partial composite action theory considered by Girhammar and Pan (2007).

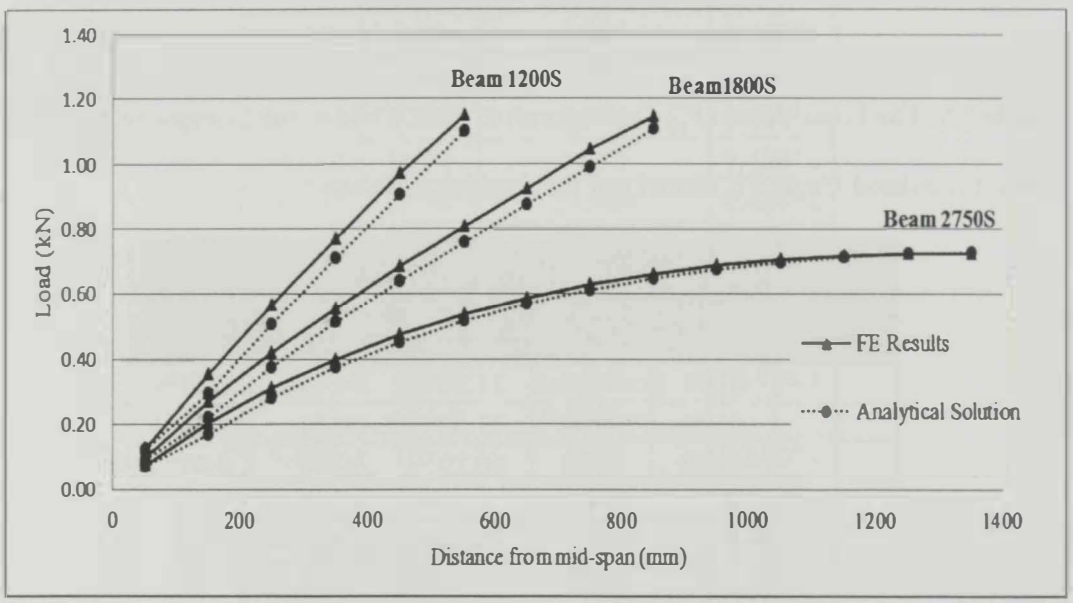

Figure 5.8: FE and Analytical Results for the Distribution of the Fasteners' Shear Forces in Three Different Beams Due to a MID-span Point Load of 75 kN and $K_{fastener}$ of 2,678 N/mm

CHAPTER 6

SUMMARY AND CONCLUSIONS

The research work presented in this thesis is devoted to studying the mechanical behavior of I-shaped steel beams strengthened with mechanically fastened FRP laminates. Both numerical and analytical techniques are employed to achieve this task. Numerical analysis is used to explore the effects of the different geometrical and/or material parameters on the composite behavior. Meanwhile, a closed form analytical solution is derived to identify the linear elastic behavior of the considered composite beams. The current chapter presents a brief summary of the conducted research, main outcomes of both the numerical and analytical studies, and recommendations for future research.

6.1 Summary and Conclusions of Numerical Analysis

A detailed three dimensional nonlinear finite element model is developed using the software package ANSYS to conduct the numerical study. The FE model accounts for both geometrical and material non-linearities and is intended to simulate the flexural behavior of the steel-FRP composite beams. A linear elastic material is used for the FRP laminate while a multi-linear elasto-plastic model is implemented for the steel material. The load-slip model developed by Ahadid (2011) is used to model the nonlinear behavior of the fasteners. To ensure that the behavior of simulated beams is dominated by overall

5.7 Conclusions

The partial composite action theory was used to develop a linear elastic analytical solution for the deflection of the simply supported composite steel-FRP beam subjected to a mid-span point load. The developed model is used to predict the load value corresponds to the first yielding in the top flange of composite steel-FRP beam. The distribution of shear forces developed in the steel fasteners is also obtained analytically. The results obtained from the linear elastic finite element model are compared to the analytical solution results and a good agreement is observed. This ensures that both the analytical and FE models are reliable for deflection calculation in the linear elastic analysis of composite steel-FRP beams and similar composite beams.

behavior of the fasteners controls significantly the mechanical behavior and ultimate load-carrying capacity of the steel-FRP beam.

- Regarding the behavior of composite beam before yielding of steel, the contribution of the FRP becomes significant if the modulus of elasticity of FRP is close or higher than that of the steel material.
- In the elastic stage (i.e., at small mid-span loading and when the fasteners and steel materials behave elastically), the distribution of the shear forces in the steel fasteners starts with very small values in the vicinity of the mid-span where the beam slope is zero due to symmetry. Then, fastener forces increase gradually as the fastener's location becomes closer to the supports. This is mainly derived by the increase in the slope of the deformed steel beam.
- In the elastic stage and as the fastener stiffness increases, the shear forces in the fasteners increase; especially for short FRP laminates. For the case where FRP covers most of the span of the steel beam, and as the fastener stiffness increases, the maximum shear force in the fasteners increases and approaches the value that corresponds to the case of a fully composite steel-FRP beam. In such a case, the distribution tends to follow the distribution of the shear force diagram along the span of the beam.
- In the post-yielding stage, yielding followed by the formation of a plastic hinge at the mid-span of the steel section leads to a considerable increase in the slope of the composite beam leading to significant longitudinal movements of the steel points at the fasteners relative to the FRP points. As a result the interfacial slip increases as

flexural response, steel stiffeners are added at the locations of stress concentration (i.e., at mid-span and supports) to prevent local buckling. Additionally, lateral supports are employed at specific locations along the span of the beams to avoid premature failure by lateral torsional buckling. Comparisons between the experimental mid-span load-deflection curves of Alhadid (2011) and their numerical counterparts show a very good agreement indicating the accuracy of the developed FE model.

The numerical study is composed of two phases. The first phase is conducted in the context of the experimental study performed by Alhadid (2011) to shed more light on the experimental outcomes and explain them in view of the FE results. In addition, other steel-FRP beams having the same steel and FRP materials and cross-sections but with different fastener stiffness and FRP lengths are also examined. The second phase of the numerical study deals with three simply supported steel-FRP composite beams having span of 7.0 m and similar steel and FRP materials but with different beam cross-sections. These cross-sections, although different, are intentionally selected to provide similar plastic moduli (i.e., Z_{xx}) to represent three equally possible flexural designs for the same applied bending moments. The main outcomes of the numerical study, based on the considered geometries and materials of the steel-FRP beams, are listed below:

- In the case of providing insufficient number of steel fasteners in a steel-FRP beam, it will have unfavorable brittle failure due to shear rupture in the fasteners. On the contrary, when adequate number of fasteners is used, the steel-FRP beams will exhibit a ductile flexural mode of failure accompanied by significant bearing deformations in the FRP at the fastener locations. In the latter case, the load-slip

stiffness of the steel bottom flange ($E_s A_{flange} / pitch$) or that of the FRP laminate ($E_{FRP} A_{FRP} / pitch$).

6.2 Summary and Conclusions of Analytical Study

The partial composite action theory developed by Girhammar and Pan (2007) in addition to Euler–Bernoulli beam theory is used to derive a linear elastic analytical solution for the deflection of the simply supported partial composite steel-FRP beam subjected to a point load at the mid-span. The analytical model accounts for the relative slip between the steel and the FRP laminate at the fastener locations and is used to evaluate the deflection of the beam. Moreover, the same model is used to predict the mid-span load that corresponds to the first yielding in the top flange of composite beam. In addition, the distribution of shear forces induced in the steel fasteners is also obtained analytically. The results obtained from the linear elastic finite element model (as part of the numerical phase of this research) are compared to the analytical counterparts and a close agreement is found. This model is expected to help the designers in predicting the elastic behavior of the composite steel-FRP beams by evaluating deflection, yielding load and distribution of the interfacial shear forces in the fasteners.

6.3 Recommendations for Future Research

The positive experimental findings reported by Alhadid (2011) on the strengthening of steel beams with mechanically fastened FRP laminates and the promising numerical and

well as the shear forces in the fasteners. This increase starts from the mid-span and spreads towards the supports in a manner similar to the spread of plasticity.

- If the pitch size is kept fixed, the shear forces in the fasteners decrease as the length of the FRP increases (or number of fasteners increases). This is attributed to distributing the tensile force in the FRP on a more fasteners in the long FRP laminate.
- Increasing the height of the steel section in a composite steel-FRP beam, while keeping S_x and Z_x almost unchanged, increases the load-carrying capacity of the beam as a result of increasing the tension in the FRP laminate and shear forces in the fasteners. That is due to the increase in the slip at the fastener locations.
- Increasing the thickness of the FRP laminate significantly improves the load-carrying capacity of composite steel-FRP beams. However, this increases the interfacial slip and consequently increases the shears forces in the fasteners.
- Increasing the number of steel fasteners, or reducing the pitch distance, increases very slightly the load-carrying capacity of steel-FRP beams, while helping to avoid the brittle shear failure in the fasteners.
- As the length of the FRP laminate increases relative to the span of the beam, the index of composite action increases indicating higher efficiency of the FRP laminate; especially at low fastener stiffness. As the fastener stiffness increases the effect of the length of the FRP becomes less significant. The low efficiency of the composite action in the beams tested by Alhadid (2011) is mainly due to the small value of the elastic spring stiffness K relative to the elastic axial longitudinal

REFERENCES

[1] Abdel Baky, H., Ebead, U., & Neale, K., (2007). *"Flexural and interfacial behavior of FRP-Strengthened reinforced concrete beams"*. Composite for Construction, Vol. 11, No. 6, 629-693.

[2] ACI Committee 440, (2002). *"Guide for the design and construction of externally bonded FRP systems for strengthening concrete structures"*. American Concrete Institute, ACI Committee 440, 118pp.

[3] Achillides Z.& Pilakoutas K. (2006). *"FE modeling of bond interaction of FRP bars to concrete"*. Structural Concrete, 7(1): 7-16.

[4] ADINA R&D, Inc. (2004). *"Automatic dynamic incremental nonlinear analysis: Finite-element software"*. Version 8.2, Watertown, Mass.

[5] Ahmed, O., Van Gemert, D. & Vandewalle, L. (2001). *"Improved model for plate-end shear of CFRP strengthened RC beams"*. Cement and Concrete Composites, 23, 3-19.

[6] Alhadid, M. (2011). *"Strengthening of steel beams using mechanically anchored carbon fiber reinforced polymers laminates"*. Master's thesis, United Arab Emirates University, Abu Dhabi, United Arab Emirates.

analytical results obtained in the current research should motivate the researchers to investigate more issues related to the same research area. Below are some suggestions for future research work:

1. The load-slip behavior of the fasteners is a key issue that affects significantly the mechanical behavior of the steel-FRP beams. Therefore, it is recommended to devise a way to improve such load-slip behavior. This may be achieved by increasing the bearing strength of the FRP laminate.
2. The load-slip model still needs broader investigations to develop a generalized model that takes into account several design parameters including fasteners arrangements, strength of the fasteners, and fastener's diameter and spacing.
3. The development of a closed form (or semi-analytical) solution for the inelastic behavior of composite steel-FRP beams is of great importance since it will provide an accurate and handy tool to designers.
4. The study of the mechanical behavior of composite steel-FRP beams under different loading patterns and supporting conditions, in both static and dynamic schemes, is of high importance and requires both experimental and numerical investigations.
5. It is essential to study the behavior of steel beams strengthened with mechanically fastened FRP laminates under various environmental conditions especially at elevated temperature.

[14] Bank, LC., & Arora, D. (2007). "Analysis of RC beams strengthened with mechanically fastened FRP (MF-FRP) strips". Composites for Structures, 79(2), 180-191.

[15] Barnes, R., & Mays, G. (1999). *"Fatigue performance of concrete beams strengthened with CFRP plates"*. Composites for Construction, 3(2), 63–72.

[16] Benachour, A., Benyoucef, S., Tounsi, A., & Adda bedia EA. (2008). *"Interfacial stress analysis of steel beams reinforced with bonded prestressed FRP plate"*. Engineering Structures, Vol. 30, 3305-3315.

[17] Bizindavyi, L., & Neale, W. (1999). *"Transfer lengths and bond strengths for composites bonded to concrete"*. Journal of Composites for Construction, Vol. 3, No. 4, 153-160.

[18] Bonacci JF, & Maalej M., (2001). *"Behavioral trends of RC beams strengthened with externally bonded FRP"*. Journal of Composites for Construction, Vol. 5, No. 2, 102-113.

[19] Brena, S. F., Bramblett, R. M., Wood, S. L., & Kreger, M. E., (2003) *"Increasing flexural capacity of reinforced concrete beams using carbon fiber-reinforced polymer composites"*. ACI Structural Journal, 100, 1, 36–46.

[20] Bridge Program Group, National Bridge Inventory: "*Count of Deficient Highway Bridges*". The Federal Highway Administration, Washington, DC, 2002.

[7] American Concrete Institute (ACI 440.2R). (2002). *"Guide for the design and construction of externally bonded FRP systems for strengthening concrete structures"*. Farmington Hills, MI.

[8] American Concrete Institute (ACI). (1999). *"Building code requirements for structural concrete (318-99) and commentary (318R-99)"*. Committee 318, Farmington Hills, Mich.

[9] American Institute of Steel Construction (AISC). (1998). *"Manual of steel construction, Load and resistance factor design"*. Vol. 1. Second edition.

[10] ANSYS, Release 13.0 (2011). User's Manual Guide, Canonsburg, Pennsylvania, USA.

[11] Arduini, M. & Nanni, A. (1997). *"Behavior of precracked RC beams strengthened with carbon FRP sheets"*. Composites for Construction, ASCE, Vol. 1, No. 2, 63-70.

[12] Bakay, R. (2003). *"Midspan Shear Debonding of CFRP Laminated Reinforced Concrete Beams"*. MSc Thesis, Department of Civil Engineering, University of Calgary, Calgary, Alberta, Canada.

[13] Bank, LC., & Borowicz, DT. (2004). *"Mechanically fastened FRP strengthening of large scale RC bridge T-beams"*. Advanced Structural Engineering, 7(6), 525-537.

[28] Deng, J., Lee, MK., & Moy, S., (2004). *"Stress analysis of steel beams reinforced with a bonded CFRP plate"*. Composite structures 65, 205-215.

[29] Ebead, U., (2011). *"Behavior of RC beams strengthened with mechanically fastened FRP systems"*. 1st Middle East Conference on Smart Monitoring, Assessment and Rehabilitation of Civil Structures. Dubai, UAE.

[30] Edberg, W., Mertz, D., & Gillespie, J., (1996). *"Rehabilitation of steel beams using composite materials"*. Materials Engineering Conference, Materials for the New Millenium, ASCE, New York, NY, Nov 10-14, 1996, 502-508.

[31] El Damatty, AA., Abushagur, M., & Youssef MA., (2003a). *"Experimental and analytical investigation of steel beams rehabilitated using GFRP sheets"*. Steel and Composite Structures, 3(6), 421-438.

[32] El Damatty, AA., & Abushagur, M., (2003b). *"Testing and modeling of shear and peel behavior for bonded steel/FRP connections"*. Thin-Walled Structures. Volume 41, Issue 11, 987–1003.

[33] El Damatty, AA., Abushagur, M., & Youssef MA., (2005). *"Rehabilitation of composite steel bridges using GFRP plates"*. Applied Composite Materials 12, 309-325.

[34] El-Mihilmy, M., & Tedesco, J., (2001). *"Prediction of anchorage failure for reinforced concrete beams strengthened with fiber-reinforced polymer plates"*. ACI structural Journal, 98(3), 301-314.

[21] Buyle-Bodin, F., David, E., & Ragneau E, (2002). *"Finite element modeling of flexural behavior of externally bonded CFRP reinforced concrete structures"*. Engineering Structures, 24, 1423-1429.

[22] Buyukozturk, O., Gunes, O., & Karaca, E., (2004). *"Progress on understanding debonding problems in reinforced concrete and steel members strengthened using FRP composites"*. Construction and Building Materials 18, 9-19.

[23] Chajes, J., Thomson, A., Januszka, F., & Finch, W., (1994). *"Flexural strengthening of concrete beams using externally bonded composite materials"*. Construction and Building Materials. Vol. 8, No. 3, 191-201.

[24] Chen, F., & Teng G., (2001). *"Anchorage strength model for FRP and steel plates attached to concrete"*. Journal of Structural Engineering, ASCE, 127(7):784-791.

[25] Colombi, P., & Poggi, C., (2006). *"An experimental, analytical and numerical study of the static behavior of steel beams reinforced by pultruded CFRP strips"*. Composites Part B 37. 64-73.

[26] CRC construction innovation (2002). *"Review of strengthening techniques using externally bonded fiber reinforced polymer composites"*. Report 2002-005-C-01.

[27] Crisfield, M. A., (1981). "*A Fast Incremental-Iterative Solution Procedure That Handles Snap-Through.*", Computer and Structures, Vol 13, pp. 55-62.

[41] Girhammar, U. A., & Pan, D. H., (2007). "*Exact static analysis of partially composite beams and beam-columns*". Int. Journal of Mechanical Science, 49, 239-255.

[42] Hamoush, S., & Ahmad, S., (19901). "*Debonding of steel plate-strengthened concrete beams*". Journal of Structural Engineering ASCE, 116(2), 356–371.

[43] Hearing, B., (2000). "*Delamination in reinforced concrete retrofitted with fiber reinforced plastics*". Ph.D. thesis, Massachusetts Institute of Technology, Cambridge, MA.

[44] Hilti., (2001). "*Hilti North America product guide*". Hilti Corp., Tulsa, OKla., Chapter 3.

[45] Hosny, A., Sayed-Ahmed, Y., Abdelrahamn, A., & Alhlaby, A. (2006). "*Strengthening precast-prestressed hollow core slabs to resist negative moments using CFRP strips: an experimental investigation and a critical review of CSA 806-02*". Canadian Journal of Civil Engineering, 33(8), 955-967.

[46] Jun, D., & Marcus, MK., (2007). "*Behavior under static loading of metallic beams reinforced with a bonded CFRP plate*". Composite for Construction, 78, 232-242.

[47] Kadhim, M., (2012). "*Effect of CFRP plate length strengthening continuous steel beam*". Construction and Building Materials, Vol. 28, 648-652.

[35] Elsayed, W., Ebead, U.A., & Neale, K.W., (2005). *"Modelling of debonding failures in FRP-strengthened two-way slabs Fiber Reinforced Polymer Reinforcement for Reinforcement Concrete Structures"*. Shield, C.K., Busel, J.P., Walkup, S.L. and Gremel, D.D., Eds., ACI SP-230, Vol. 1, pp. 461–479.

[36] Esfahani, R., Kianoush, R., & Tajari, R., (2007). *"Flexural behavior of reinforced concrete beams strengthened by CFRP sheets"*. Engineering Structures, vol. 29, pp. 2428-44.

[37] Garden, H., Hollaway L., & Thorne, A., (1997). *"A preliminary evaluation of carbon fiber reinforced polymer plates for strengthening reinforced concrete members"*. P I Civil Eng–Str B, 123, 127-142.

[38] Gerald, C. F., Gren, C. J., & Wealthy, P. O., (2003). *"Applied Numerical Analysis"*. 7th Ed., Addison Wesly Longman, California, USA.

[39] Gillespie, JW., Mertz, DR., Kasai, K., Edberg, WM., Demitz, JR., & Hodgson, I., (1996). *"Rehabilitation of Steel Bridge Girders: Large Scale Testing"*. Proceeding of the American Society for Composites 11th Technical Conference on Composite Materials, 1996, pp. 231-240.

[40] Girhammar, U. A., & Gopu V. K. A., (1993). *"Composite beam-columns with interlayer slip, exact analysis"*. Journal of Structural Engineering ASCE, 119, 1265-1270.

[54] Lee, JH., Lopez, MM., & Bakis, CE., (2009). "*Slip effect in reinforced concrete beams with mechanically fastened FRP strip*". Cement and Concrete Composites, 31, 496-504.

[55] Lenwari, A., Thepchatri, T., & Albrecht, P., (2005). *"Flexural response of steel beams strengthened with partial-length CFRP plates"*. Composites for Construction, Vol. 9, No. 4, 296-303.

[56] Liu, X., Silva, PF., & Nanni, A., (2001). *"Rehabilitation of steel bridge members with FRP composite materials"*. Proc., CCC200 I, Composites in Construction, Porto, Portugal, 2001, 613-617.

[57] Lowe, P. G., (1971). "*Classical theory of structures based on the differential equation*". London: Cambridge University Press.

[58] Lu, Z., Ye, P., Teng, G., Ye, P., & Jiang, J., (2005). *"Bond-slip models for FRP sheets/plates bonded to concrete"*. Engineering Structures, 27, 6, 920-937.

[59] Maalej, M., & Bian, Y., (2001). *"Interfacial shear stress concentration in FRP-strengthened beams"*. Composite Structures, 54, 417–426.

[60] Martin, JA., & Lamanna, AJ., (2008). "*Performance of mechanically fastened FRP strengthened reinforced concrete beams in flexure*". Journal of Composites for Construction, Vol. 12, No. 3, 257-265.

[61] Mathews, J. H., & Kurtis, F. D., (2004). *"Numerical Methods using Matlab"*. 4th Ed, Pearson Prentice Hall Publishers, Upper Saddle River, New Jersey, USA.

[48] Karam, G. N., (1992). *"Optimal design for prestressing with FRP sheets in structural members"*. Advanced Composite Materials in Bridges and Construction, CSCE Conference Proceedings, 277-285.

[49] Kotynia, R., Abdel Baky, H., Neale, K., & Ebead, U., (2008). *"Flexural Strengthening of RC Beams with Externally Bonded CFRP Systems: Test Results and 3D Nonlinear FE Analysis"*. Composite for Construction, Vol. 12, No. 2, 190-194.

[50] Lamanna AJ., (2002). *"Flexural strengthening of reinforced concrete beams with mechanically fastened fiber reinforced polymer strips"*. PhD thesis, University of Wisconsin: Madison.

[51] Lamanna, AJ., Bank, LC., & Scott DW., (2001). *"Flexural strengthening of reinforced concrete beams using fasteners and fiber-reinforced polymer strips"*. ACI Structural Journal, Vol. 98, No. 3, 368-376.

[52] Lamanna, AJ., Bank, LC., Borowicz, DT., & Arora, D., (2002). "*Strengtheneing of concrete beams with mechanically fastened FRP Strips*". 3rd International Conference on Composites in Infrastructures. San Francisco, USA.

[53] Lamanna, AJ., Bank, LC., & Scott, DW., (2004) *"Flexural strengthening of reinforced concrete beams by mechanically attaching fiber-reinforced polymer strips"*. Journal of Composites for Construction, ASCE. Vol. 8, No. 3,203-210.

[70] Roberts, T., & Haji-Kazemi H., (1989). *"A theoretical study of the behavior of reinforced concrete beams strengthened by externally bonded steel plates"*. Proceedings of the Institution of Civil Engineers Part 2, Research and Theory,87, 39–55.

[71] Saadatmanesh, H., & Ehsani M., (1990). *"Fiber composites can strengthen beams"*. Concrete International: Design and Construction, 12(3), 65–71.

[72] Saleem, MH., Sharaky, IA., & Sallam M., (2010). *"Flexural behavior of steel beams strengthened by carbon fiber reinforced polymer plates – Three dimensional finite element simulation"*. Materials and Design, Vol. 31, 1317-1324.

[73] Salmon, C. G., & Johnson, J. E., (1990). *"Steel structures, design and behavior"*. New York: Harper Collins.

[74] Sayed-Ahmed, E., Baky, R., & Shrive, N., (2009). *"Bond Strength of FRP Laminates to Concrete: State-of-the-Art Review"*. Electronic Journal of Structural Engineering, 9.

[75] Sayed-Ahmed, Y., Riad, H., & Shrive, G., (2004). *"Flexural strengthening of precast reinforced concrete bridge girders using bonded CFRP strips or external post-tensioning*". Canadian Journal of Civil Engineering. 31(3): 499-512.

[62] Meier, U., (1995). *"Strengthening of structures using carbon fibre/epoxy composites"*. Construction and Building Materials, Vol. 9, No. 6.

[63] Nardone, F., Lignola, GP., Prota, A., Manfredi, G., & Nanni, A., (2011). *"Modeling of flexural behavior of RC beams strengthened with mechanically fastened FRP strips"*. Composite Structures, 93, 1973-1985.

[64] Nguyen, D., Chan, T., & Cheong, H., (2001). *"Brittle failure and bond development length of CFRP-Concrete beams"*. Composites for Construction, Vol. 5, No. 1, Feb. 2001, 12-17.

[65] Pelosi, G., (2007). *"The finite-element method, Part I: R. L. "Courant: Historical Corner"*. IEEE Antennas and Propagation Magazine, Vol.49, W. 2.

[66] Photiou, NK., Hollaway, LC., & Chryssanthopoulos, MK., (2006). *"Strengthening of an artificially degraded steel beam utilizing a carbon/glass composite system"*. Construction and Building Materials, Vol. 20, 11-21.

[67] Punmia, B. C., Jain, Ashok K., & Jain, Arun K., (2007). *"Limit state design for reinforced concrete"*. New Delhi: Laxmi Publications.

[68] Rahimi, H., & Hutchinson, A., (2001). *"Concrete beams strengthened with externally bonded FRP plates"*. Composites for Construction, Vol. 5, No. 1, 44-56.

[69] Ramset, (1999). *"ITW Ramset/Read head product and resource book"*. Illinoise Tool Works, Inc., Wood Dale, Ill.

[83] Tavakkolizadeh, M., & Saadatmanesh, H., (2003b). *"Strengthening of Steel-Concrete Composite Girders Using Carbon Fiber Reinforced Polymers Sheets"*. Journal of Structural Engineering. ASCE, Vol. 129, No.l, pp. 30-40.

[84] Tawfik, Q., & Karunasena, W., (2010). *"Use of CFRP for Rehabilitation of Steel Structures: a Review"*. Unpublished paper presented at Southern Region Engineering Conference, Toowoomba, Australia.

[85] Teng, J.G., Yu, T., & Fernando, D., (2012). *"Review, Strengthening of steel structures with fiber-reinforced polymer composites"*. Journal of constructional steel research, Vol. 78, pp. 131-143.

[86] Ueda, T., Dai, G., & Sato, Y., (2003). *"A nonlinear bond stress-slip relationship for FRP sheet-concrete interface. Proceedings of international symposium on latest achievement of technology and research on retrofitting concrete structures"*. Kyoto, Japan, pp. 113-120.

[87] Youssef, MA., (2006). *"Analytical prediction of the linear and nonlinear behavior of steel beams rehabilitated using FRP sheets"*. Engineering Structures, Vol. 28, 903-911.

[88] Yuan, H., Teng, J.G., Seracino, R., Wu, Z.S., & Yao, J., (2004). *"Full-range behabiour of FRP-to-concrete bonded joints"*. Engineering Structures, 26(5), 553-564.

[76] Schnerch, D., (2005). *"Strengthening of steel structures with high modulus Carbon Fiber Reinforced Polymer (CFRP) materials"*. Doctoral dissertation, North Carolina State University, USA.

[77] Sen, R., Liby, L., & Mullins, G., (2001). *"Strengthening steel bridge sections using CFRP laminates"*. Composites, Part B 32. 309-322.

[78] Shaat, A., Schnerch, D., Fam, A., & Rizkalla, S., (2004). *"Retrofit of Steel Structures Using Fiber Reinforced Polymers (FRP): State-of-the-Art"*. In: Transportation research board (TRB) annual meeting, 2004. CD-ROM (04-4063).

[79] Shahawy, A., Arockiasamy, M., Beitelman, T., & Sowrirajan R., (1996). *"Reinforced concrete rectangular beams strengthened with CFRP laminates"*. Composites Part B: Engineering, Vol. 27, No. 3, 225-233.

[80] Spadea, G., Bencardino, F., & Swamy, N., (1998). *"Structural behavior of composite RC beams with externally bonded CFRP"*. Journal of Composites for Construction, ASCE, Vol. 2, No. 3, 132-137.

[81] Stein E., (2009). *"Olgierd C. Zienkiewicz, a pioneer in the development of the finite element method in engineering science"*. Steel Construction, 2 (4), 264-272.

[82] Tavakkolizadeh, M., & Saadatmanesh, H., (2003a). *"Repair of Cracked Steel Girders Using CFRP Sheets"*. Froc. ISEC-OJ, Hawaii, 24-27.

عائد إلى أن قوة القص المحمولة في المسامير الفولاذية تسبب عزماً دورانياً حول منتصف ارتفاع العارضة الفولاذية تتناسب طرديا مع ارتفاعها.

الدراسة اظهرت ايضا ان زيادة سمك الشرائح البلاستيكية المسلحة يحسن بشكل كبير قوة تحمل العوارض الفولاذية المركبة بشرط استخدام عدد كافي من المسامير المثبتة وطول كافي من الشرائح البلاستيكية المسلحة لتجنب الانهيار بفعل القص في المسامير الفولاذية، كما أنه لوحظ أن زيادة عدد المسامير الفولاذية أو تقليل المسافة بينها لا يؤدي إلى تحسن ملحوظ في أداء العوارض الفولاذية لكنه يضمن انهياراً مرنا لها.

الحل الرياضي المستخدم في هذه الدراسة يوفر وسيلة جيدة يمكن استخدامها لحساب مقدار الانحناء في العوارض الفولاذية المركبة مع الأخذ بعين الاعتبار الإنزلاق الحاصل بين الفولاذ والشرائح البلاستيكية المسلحة، هذا الحل أيضا يساعد في التنبؤ بالحمل الذي يسبب الخضوع في الفولاذ ويساعد في حساب توزيع الأحمال في المسامير الفولاذية.

كلمات ذات صلة: العوارض الفولاذية، تقوية، إعادة تهيئة، الشرائح البلاستيكية المسلحة، الأداء الإنحنائي، التحليل العددي، نموذج العناصر متناهية الضغر، الحل الرياضي، العوارض المركبة، العوارض المركبة جزئيا، الإنزلاق.

عن طريق إلصاقها بالسطح الخارجي – تميل إلى الإنهيار القصف بفعل انفكاك الشرائح البلاستيكية المسلحة عن القواطع الفولاذية.

مؤخرا كشفت الأبحاث أن ربط الشرائح البلاستيكية المسلحة ميكانيكيا بالعوارض الخرسانية المسلحة (عن طريق المسامير) اعطى نتائج مبشرة على صعيد فعالية التركيب ومقدار الزيادة في قوة التحمل وبشكل أهم منع انفكاك الشرائح البلاستيكية قبل تهشم الخرسانة. هذه النتائج فتحت الباب أمام إمكانية استخدام الشرائح البلاستيكية المسلحة المثبتة ميكانيكيا لتقوية العوارض الفولاذية.

دراسة تجريبية واحدة فقط تناولت تقوية العوارض الفولاذية باستخدام الشرائح البلاستيكية المسلحة المثبتة ميكانيكيا قام بها الحديد (2011). الدراسة كشفت أن العوارض الفولاذية المقواة بهذه الطريقة تميل للانهيار المرن اذا ما تم استخدام عدد كاف من المسامير. استخدام أطوال غير كافية من الشرائح البلاستيكية المسلحة نسبة إلى طول العوارض الفولاذية أو استخدام عدد غير كافي من المسامير قد يؤدي إلى انهيار قصف للعوارض الفولاذية المقواة عن طريق قص المسامير أو قطع شدّي في الشرائح البلاستيكية المسلحة.

الدافع لهذه الدراسة البحثية نابع من الحاجة لفهم الأداء الميكانيكي للعوارض الفولاذية المقواة بالشرائح البلاستيكية المسلحة والمثبتة ميكانيكيا. في هذه الدراسة تم استخدام كل من طريقة العناصر المتناهية الصغر ثلاثية الأبعاد بالإضافة إلى التحليل الرياضي . النموذج ثلاثي الأبعاد للعناصر متناهية الصغر الذي تم انشاءه في هذه الدراسة يأخذ بعين الاعتبار الأداء غير الخطي لمكونات العوارض الفولاذية بالإضافة للأداء غير الخطي لشكل هذه العوارض، تم التأكد من صحة أداء هذا النموذج من خلال مقارنته بدراسة تجريبية قام بها الحديد (2011)، حيث تم الحصول على توافق ممتاز بين نتائج الحالتين . طريقة العناصر المتناهية الصغر استخدمت في هذا البحث

لدراسة أداء مكونات العوارض الفولاذية المركبة (المقواة بالشرائح البلاستيكية المسلحة والمثبتة ميكانيكيا)، وقد شملت هذا دراسة توزيع القوى في المسامير الفولاذية وتوزيع الضغط وانتشار الخضوع في الفولاذ و قيم الشد فى الشرائح البلاستيكية . بالإضافة إلى ذلك فإن نموذج العناصر المتناهية الصغر تم استخدامه في دراسة تأثير بعض من العوامل على الأداء الميكانيكي للعوارض الفولاذية المركبة . هذه العوامل تشمل ارتفاع العوارض الحديدية و طول وسماكة الشرائح البلاستيكية المسلحة وطريقة توزيع المسامير الفولاذية المثبتة لهذه الشرائح. أما بالنسبة للحل الرياضي فقد تم تطويره من أجل التنبؤ بالأداء المرن للعوارض الفولاذية المركبة مع الأخذ بعين الاعتبار تأثير الانزلاق على السطح الفاصل بين الفولاذ وبين الشرائح البلاستيكية المسلحة، وقد تم استخدام الحل الرياضي لاحقا في حساب مقدار الانحناء وحساب الحمل المسبب للخضوع في الفولاذ بالإضافة إلى حساب الأحمال الموزعة على المسامير الفولاذية المثبة للشرائح البلاستيكية المسلحة.

هذه الدراسة كشفت أن مقدار مساهمة الشرائح البلاستيكية المسلحة في تقليل الانحناء في العوارض الفولاذية تزداد بازدياد معامل المرونة لهذه الشرائح ليعادل أو ليفوق معامل المرونة للفولاذ. كلما زاد طول الشرائح البلاستيكية المسلحة فإن معيار الأداء المركب يزداد ما يعني ازدياد فعالية هذه الشرائح في تقوية العوارض الفولاذية. بعد الخضوع (في السطح الخارجي للفولاذ والمتصل بالشرائح البلاستيكية المسلحة عن طريق المسامير) تصبح مساهمة الشرائح البلاستيكية المسلحة في تقوية العارضة الفولاذية أكثر فعاليةً لأن الشرائح تكون ما زالت مرنة وقادرة على حمل المزيد من قوة الشد.

الدراسة أيضا تشير إلى أن الشرائح البلاستيكية المسلحة تكون أكثر فاعليةً اذا ما استخدمت مع العوارض الفولاذية الأكثر ارتفاعا مقارنة بالعوارض الأقل ارتفاعة وبنفس قيمة الصلابة . هذا

ملخص الرسالة

لاقت عملية تقوية المنشآت الفولاذية اهتماما كبيرا خلال العقدين الماضيين وذلك بسبب الأعداد المتزايدة للمنشآت المتهالكة في مناطق مختلفة حول العالم ؛ حيث أن الطرق التقليدية لإعادة تهيئة أو تقوية المنشآت الفولاذية – والمتمثلة باستبدال المكونات الفولاذية الانشائية أو بتركيب مكونات جديدة فوق المكونات المتهالكة – تحتاج إلى وقت طويل وقابلة للصدأ بالإضافة الى صعوبة تركيبها . الكثير من المشاكل المرتبطة بالطرق التقليدية للتقوية يمكن تجنبها باستخدام شرائح الألياف البلاستيكية ؛ وذلك بفعل ما تتميز به من قوة شد عالية نسبة إلى وزنها الخفيف و مقاومتها للصدأ ، مما يجعلها أكثرا استدامةً خصوصا اذا كانت الظروف الجوية عاملا أساسيا في اختيار الطريقة المناسبة للتقوية أو إعادة إصلاح المنشآت الفولاذية .

تناولت الكثير من الدراسات البحثية فعالية تقوية عوارض الخرسانة المسلحة بشرائح الألياف البلاستيكية الملتصقة على السطوح الخارجية، وبعد النجاح الذي حققته هذه الطريقة مع العوارض الخرسانية المسلحة انتقل الباحثون لاستخدامها مع العوارض الفولاذية، على الرغم من أن هذه الفكرة عورضت في البداية من بعض الباحثين بسبب تدني معامل المرونة لمثل هذه الشرائح مقارنة بالفولاذ، لكن هذه الفكرة بدأت تطفو على السطح من جديد مع انتاج شرائح بلاستيكية مسلحة ذات معامل مرونة عالٍ يفوق في بعض الأنواع معامل المرونة الخاص بالفولاذ. حيث استخدم الباحثون في البداية الشرائح البلاستيكية المسلحة عن طريق إلصاقها بالسطح الخارجي للعوارض الفولاذية بنفس الطريقة التي كانوا يتبعونها مع عوارض الخرسانة المسلحة لتقوية الأداء الانحنائي لهذه العوارض. توصل الباحثون إلى أن العوارض الفولاذية - المقواة بالشرائح البلاستيكية المسلحة

جامعة الإمارات العربية المتحدة
United Arab Emirates University

UAEU

برنامج ماجستير الهندسة المدنية
قسم الهندسة المدنية والبيئية
كلية الهندسة
جامعة الإمارات العربية المتحدة

عنوان الرسالة:

دراسة الأداء الميكانيكي للعوارض الإنشائية الفولاذية على شكل حرف I والمقواة بواسطة شرائح الألياف المثبتة بـها ميكانيكيا

اسم الباحث:

حذيفة نايف رجوب

أسماء المشرفين:

د. خالد محمود الصاوي
الأستاذ المشارك في الهندسة الإنشائية
قسم الهندسة المدنية والبيئية بكلية الهندسة
جامعة الإمارات العربية المتحدة
الإمارات العربية المتحدة

د. عمرو محمود سويدان
الأستاذ المشارك في الهندسة الإنشائية
قسم الهندسة المدنية والبيئية بكلية الهندسة
جامعة الإمارات العربية المتحدة
الإمارات العربية المتحدة